Transparent Self-Cleaning Coatings on Polycarbonate Surfaces

Von der Naturwissenschaftlichen Fakultät

Der Gottfried Wilhelm Leibniz Universität Hannover

Zur Erlangung des Grades

Doktorin der Naturwissenschaften

Dr. rer. nat

genehmigte Dissertation

Razan Fateh, Mağstir

Geboren am 26.03.1978 in Damaskus, Syrien

2014

Referent: Prof. Dr. rer. nat. Detlef W. Bahnemann

Koreferent: Prof. Dr. rer. nat. Jürgen Caro

Tag der Promotion 15. Mai 2014

Erklärung zur Dissertation

Hiermit erkläre ich, dass ich die vorliegende Dissertation **,,Transparent Self-Cleaning Coatings on Polycarbonate Surfaces''** während meiner Tätigkeit als wissenschaftlichere Mitarbeiterin am Institut für Technische Chemie der Gottfried Wilhelm Leibniz Universität Hannover selbständig verfasst und alle benutzen Hilfsmittel sowie evtl. zur Hilfeleistung herangezogene Institutionen vollständig angegeben habe.

Die Dissertation wurde nicht schon als Diplom- oder ähnliche Prüfungsarbeit verwendet.

Hannover, den 15. Mai 2014

Razan Fateh

Acknowledgements

First of all, a huge "thank you" to my supervisor for these past years, Prof. Dr. Detlef Bahnemann, whose encouragement, guidance, inspiring reviews, and support from the initial to the final level enabled me to develop not only an understanding of the subject but also all aspects that the scientist dreams to learn.

My sincere thanks go to Prof. Dr. Jürgen Caro and Prof. Dr. Ursula Rinas for their very kind agreement to be the examiners of my PhD thesis.

I would like also to thank deeply Dr. Ralf Dillert for his advice, and scientific discussion during all the stage of this work. Department of chemistry, Damascus University is gratefully acknowledged to granting me the PhD scholarship.

I thank Prof. Claus Rücher and his team at Institut für Mineralogie, Leibniz Universität Hannover for their help in the FTIR and TGA measurements. I would like to thank Mrs. V. Becker and Dipl.-Chem. Ann-Christin Möller, Institut für Physikalische Chemie and Institut für Anorganische Chemie, respectively, Leibniz Universität Hannover, for the AFM and XRD measurements, respectively. I also thank Hella KG, Lippstadt, for providing the polycarbonate plates.

I want to gratitude my colleagues in the groups for the friendly and lovely atmosphere of work. I won't forget to thank all of my friends in Syria and in Germany for encouraging me to continue on and finish up my dissertation. I would also like to thank my parents, my brothers, and my sister for all of their love and support.

There really are no words to express gratitude for my husband, Amer for his helping and supporting. He is my most enthusiastic cheerleader, he is my best friend, and he is an amazing husband.

I would like to thank every person that deserves my gratitude and I didn't mention to him.

Finally, I would like to dedicate this dissertation to my parents: my father, who dreamed a lot in this moment and went away before realizing this dream and my mother, who made every effort in our upbringing and our education.

Abstract

Transparent hydrophilic photocatalytic TiO_2-based coatings have been applied to induce self-cleaning properties to polycarbonate surfaces. It was observed that the photocatalytic performance can be enhanced by improving the ability of surface adsorption by increasing the amount of hydroxyl surface groups, and by decreasing the rate of the photogenerated charge carrier recombination.

In the present work, transparent mesoporous TiO_2, nanocrystale TiO_2, TiO_2-ZnO, and TiO_2-SiO_2 thin films, respectively, have been successfully deposited on the surface of polycarbonate to provide these polymeric sheets with a self-cleaning, superhydrophilic, and photocatalytically active surface layer. In each case, the coating process was conducted in three consecutive steps. In the first process step, the polycarbonate sheets (PC) were irradiated by UV(C) light for 2 h to form hydroxyl groups on their surface enabling the covalent linkage of the polymer with the inorganic material of an interlayer. In the second step, a photocatalytically inert SiO_2 layer was deposited on the PC by dip-coating in order to enhance the binding between the organic polymer and the photocatalytically active layer and to protect the PC from the action of the photocatalytic layer that otherwise might induce the degradation of the polymer. In the last step, photocatalytically active films were deposited on the substrate by dip-coating. The films were characterized by UV/Vis spectrophotometry, ellipsometry, transmission electron microscopy (TEM), atomic force microscopy (AFM), X-ray diffraction analysis (XRD), Fourier transform infrared spectroscopy (FTIR), specific surface area measurements (BET) and water contact angle measurements. The mechanical strength of the prepared thin films was tested by felt-abrasion tests whereas their adhesion strength was defined quantitatively by carrying out a cross-cut test. The photocatalytic activity, expressed as photonic efficiency, of the coated surfaces was estimated from the kinetics of the photocatalytic degradation of three types of model pollutants in liquid, solid, and gas phases using methylene blue, methyl stearate, and acetaldehyde, respectively. The combination

between the superhydrophilic properties and the photocatalytic activity was determined by studying the change of water contact angle during the storage of the prepared films in the dark under ambient atmosphere and under an atmosphere containing either acetone or propan-2-ol followed by UV(A) irradiation. In addition, self-cleaning properties were examined by determining the changes of the contact angle during the irradiation time after applying oleic acid to the surface. Moreover, mechanisms explaining the relation between the structure and the photoinduced superhydrophilicity are discussed extensively in this work.

All prepared films are transparent with thicknesses in the range between 120 and 250 nm and possess superhydrophilic properties with good to perfect adhesion and mechanical strengths. Furthermore, the results show that meso- TiO_2 films exhibit the highest photocataytic activity for methylene blue degradation (photonic efficiency = 0.078%). However, these films suffer from their relatively low mechanical stability as evidenced by an activity decrease of 45% after the felt abrasion test. Modification of TiO_2 by SiO_2 leads to an improvement of the optical properties by a decrease of the light scattering. Moreover, introduction of SiO_2 to TiO_2 increases the mechanical stability and the photocatalytic activity of the prepared films reaching the highest values at molar ratios TiO_2-SiO_2 equal to 1:0.9 and 1:0.2 for acetaldehyde and methyl stearate degradation, respectively. In spite of the high photocatalytic activities of these films, they need quite long times to reach the superhydrophilic state.

On the other hand, modification of TiO_2 by ZnO with a molar TiO_2-ZnO ratio of 1: 0.05 is sufficient to get superhydrophilic coating exhibits the best self-cleaning properties combined with a good mechanical stability and a very good stability against UV(A) irradiation. Consequently, the thus prepared films can be used for the respective self-cleaning applications.

Keywords: self-cleaning; adhesion; mechanical stability; thin film; photocatalysis; superhydrophilicity.

Kurzzusammenfassung

Transparente hydrophile photokatalytisch aktive TiO₂-basierte Beschichtungen wurden hergestellt, um Selbstreinigungseigenschaften auf Polycarbonatoberflächen zu induzieren. Es wurde beobachtet, dass die photokatalytische Leistung durch die Verbesserung der Oberflächenadsorption, eine Erhöhung der Menge von Hydroxyloberflächengruppen, und eine Verringerung der Geschwindigkeit der photogenerierten Ladungsträgerrekombination verbessert werden kann.

In der vorliegenden Arbeit wurden transparente mesoporöse sowie nanokristalline TiO₂, TiO₂-ZnO und TiO₂-SiO₂ Dünnschichten erfolgreich auf der Oberfläche von Polycarbonat aufgebracht, um diesen Polymerträgern selbstreinigende, superhydrophile, photokatalytisch aktive Oberflächenschichten zu verleihen. In allen Fällen wurde das Beschichtungsverfahren in drei aufeinanderfolgenden Schritten durchgeführt. Im ersten Verfahrensschritt wurden die Polycarbonatträger (PC) durch UV (C) Licht für 2 h bestrahlt, um Hydroxylgruppen zu bilden, welche auf der Oberfläche die kovalente Verknüpfung des Polymers mit dem anorganischen Material der Zwischenschicht ermöglichen. Im zweiten Schritt wurde eine photokatalytisch inerte SiO₂ Schicht auf dem PC durch Tauchbeschichtung aufgebracht, um die Bindung zwischen dem organischen Polymer und der photokatalytisch aktiven Schicht zu verbessern und das PC von der Wirkung des photokatalytischen Schicht zu schützen, welche andernfalls den Abbau des Polymers induzieren würde. Im letzten Schritt wurden die photokatalytischen aktiven Schichten auf dem Substrat durch Tauchbeschichtung aufgebracht. Die Filme wurden durch UV/Vis Spektrophotometrie, Ellipsometrie, Transmissionselektronenmikroskopie (TEM), Rasterkraftmikroskopie (AFM), Röntgenbeugungsanalyse (XRD), Fourier -Transformations-Infrarot -Spektroskopie (FTIR), spezifische Oberflächen Messungen (BET) und Wasserkontaktwinkelmessungen charakterisiert. Die mechanische Festigkeit der hergestellten Dünnfilme wurde durch einen Filz-Abriebtests getestet, während die Haftfestigkeit quantitativ durch die sogenannte einer

Gitterschnittprüfung charakterisiert wurde. Die photokatalytische Aktivität, ausgedrückt als Photoneneffizienz, wurde aus der Kinetik des photokatalytischen Abbaus von drei verschiedenen Modell-Schadstoffen in flüssiger, fester und gasförmiger Phase (Methylenblau, Methylstearat und Acetaldehyd) ermittelt. Der Zusammenhang zwischen den superhydrophilen Eigenschaften und der photokatalytischen Aktivität wurde durch die Untersuchung der Veränderung des Wasserkontaktwinkels während der Lagerung der hergestellten Filme im Dunkeln und unter Umgebungsatmosphäre sowie unter einer Aceton- oder Propan-2-ol-Atmosphäre, sowie einer anschließende UV(A)-Bestrahlung bestimmt. Außerdem wurden die selbstreinigenden Eigenschaften durch die Bestimmung der Änderungen des Kontaktwinkels während der Bestrahlungszeit nach dem Aufbringen von Ölsäure auf die Oberfläche untersucht. Zudem werden die Mechanismen, die die Beziehung zwischen der Struktur und der photoinduzierten Superhydrophilie darstellen, in dieser Arbeit diskutiert.

Alle hergestellten Beschichtungen sind transparent mit Schichtdicken im Bereich zwischen 120 und 250 nm und besitzen superhydrophile Eigenschaften mit guter bis perfekter Haftung und überzeugende mechanischen Festigkeiten. Darüber hinaus zeigen die Ergebnisse, dass mesoporöse TiO_2 Filme die höchsten photokatalytischen Aktivitäten für den Methylenblauabbau (Photoneneffizienz = 0,078 %) besitzen. Allerdings zeigen diese Filme eine relativ geringe mechanische Stabilität, welche sich durch eine Verringerung ihrer photokatalytische Aktivität um 45 % nach einem durchgeführten Abriebtest manifestiert. Mischungen von TiO_2 mit SiO_2 führen zu einer Verbesserung der optischen Eigenschaften was sich durch eine Abnahme der Lichtstreuung zeigt. Außerdem erhöht sich dadurch die mechanische Stabilität sowie die photokatalytische Aktivität der hergestellten Filme. Die höchsten Aktivitätswerte wurden bei TiO_2-SiO_2 Molverhältnissen von 1:0,9 und 1:0,2 für den Acetaldehyd- und Methylstearat- Abbau gefunden. Trotz der hohen photokatalytischen

Aktivitäten dieser Filme benötigen sie eine lang Bestrahlungszeit, um ihren superhydrophilen Zustand zu erreichen.

Andererseits führt die Mischung von TiO$_2$ mit ZnO bei Molverhältnissen von 1:0,05   zu superhydrophilen Beschichtung, die die besten Selbstreinigungseigenschaften verbunden mit einer guten mechanischen Stabilität und eine sehr gute Stabilität gegenüber UV(A) Bestrahlung manifestiert. Folglich können die so hergestellten Folien für die jeweiligen Selbstreinigungsanwendungen verwendet werden.

Stichworte: Selbstreinigung; Haftfestigkeit; mechanische Festigkeit; Dünnschicht; Photokatalyse; Superhydrophilie.

Index

Figures

Tables

1   Theoretical Background

1.1   A General Overview

For over 50 years it has been known that titanium dioxide has the ability to oxidize a wide range of organic compounds upon UV light irradiation. This phenomenon, which is further called the photocatalytic effect of the titanium dioxide, is due to the reactions of the photogenerated electron-hole pairs created upon excitation by UV light with an energy larger or equal to its band gap energy ($E_g = 3.2$ eV in the case of anatase TiO_2, corresponding to $\lambda \leq$ 380nm). In addition to the photocatalytic effect, changes of the wettability of the surface of titanium dioxide by water or organic liquids are usually observed. Under irradiation by UV light, the contact angle of water on the titanium dioxide surface decreases and water begins to spread over the surface. This phenomena, which is called photo-induced superhydrophilicity, is important from the technical point of view for the production of so-called self-cleaning surfaces [1].

The first self-cleaning windows were produced in 2001 by a major glass manufacturing company, i.e., by Pilkington Glass, called Pilkington Activ™. The transparent coating on Pilkington Activ^{TM} (comprising of a film of nanocrystalline titanium dioxide as the active photocatalyst layer) is just 40 nm thick, and is applied to the glass by chemical vapor deposition during the manufacturing process at temperatures of 600°C [2]. This layer is applied to clear float glass to produce a hard, thin, transparent, mechanically-robust, photoactive coating of titanium dioxide. This material appears to be the ideal, readily available titanium dioxide photocatalyst film. Afterwards, Pilkington Activ™ has been used as a benchmark for all other photocatalyst films currently being produced by research groups in academia and industry alike for light-driven air and water purification and for self-cleaning purposes [3].

However, in the near future rigid plastic optical components will replace parts made from glass whenever improved properties and/or lower costs can be achieved. In recent years [4] polycarbonate (PC) has become a very attractive material for a range of industrial applications. The global polycarbonate market in 2009 was 2.9 million tons, whereas the global demand for polycarbonate is predicted to grow at a compound annual growth rate of 6% up to 2015 [5]. The European production of polycarbonate reaches about 66% of the total bisphenol A production (Figure 1.1)[6].
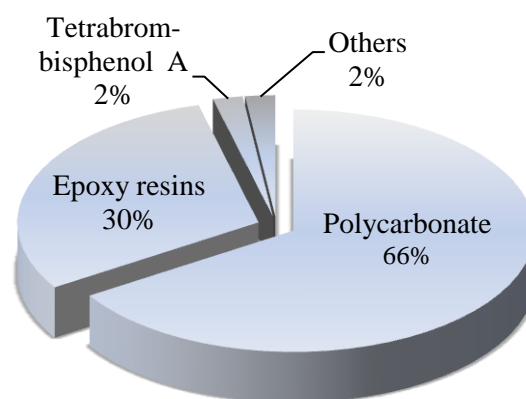
Figure 1.1: Global bisphenol A production.

The name of "polycarbonate" is derived from the carbonate group existent in its structure (c.f. Figure 1.2) [7].
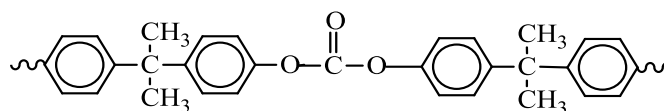
Figure 1.2: The chemical structure of polycarbonate and its properties.

The unique properties of polycarbonate; including high transparency, break resistance, weather resistance, non-flammability, and safety; make it an amazing candidate for a lot of applications. The applications of polycarbonates range from plastic vessels and machine parts to optical grades for compact discs and optical fibres. Figure 1.3 presents the consumption of polycarbonates in different industries in Europe by sectors [8].

However, the properties of polycarbonate have to be improved in order to match the enhancement in the materials quality to meet the future demand of industries especially the automotive one.

This can be achived by providing the material, i.e., the polycarbonate sheets, with a self-cleaning superhydrophilic and photocatalytically active surface layer. Demands such as high transparency, low reflectivity, and high mechanical stability of the applied layers have to be taken into consideration.
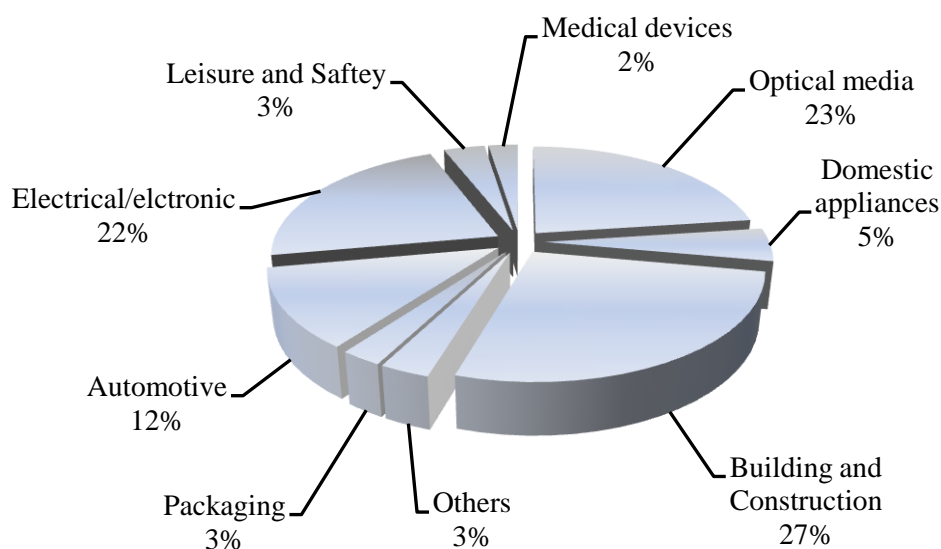
Figure 1.3: The European consumption of polycarbonates in different industries.

Ideally, a self-cleaning surface must comply with two essential criteria: (1) High photo-induced superhydrophilic properties, (2) uninterrupted performance in the absence of UV light [9]. The superhydrophilic property of the surface allows water to spread completely across the surface rather than to remain in droplet form which provides the surface with an additional important property besides the self-cleaning properties [10, 11].

1.2   Self-Cleaning Coatings

The self-cleaning technology is old as old as nature since numerous surfaces in nature show self-cleaning properties such as the wings of butterflies and the leaves of plants, e.g., cabbage or lotus [12].

Providing polymers with self-cleaning coatings is one of the research fields which have attracted the attention of a lot of scientists all over the world due to its industrial importance.

Superhydrophobic surfaces with a water contact angle higher than 150° and superhydrophilic surfaces with a water contact angle smaller than 5° have prompted extensive interests for both fundamental research and practical applications.
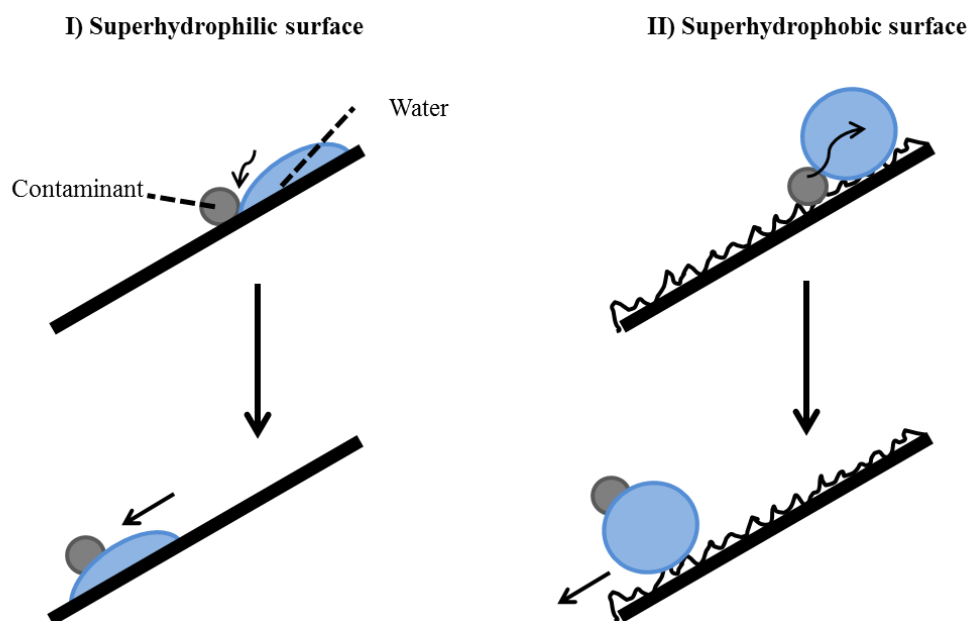
Figure 1.4: Schematic illustrations of self-cleaning processes on I) superhydrophilic surface, and II) superhydrophobic surfaces.

In general, self-cleaning coatings are divided into two types: hydrophobic and hydrophilic. The cleaning of the surface of these two categories is through the action of water; i.e., in the hydrophobic type by rolling droplets whereas the hydrophilic one functions by sheeting water that carries away dirt (Figure 1.4) [12].

Moreover, the hydrophilic coatings may also have an additional property, i.e., they can chemically break down adsorbed dirt upon illumination with suitable light sources such as sunlight [13, 14] as Figure 1.5 explains (this will be deeply discussed in section 1.4).
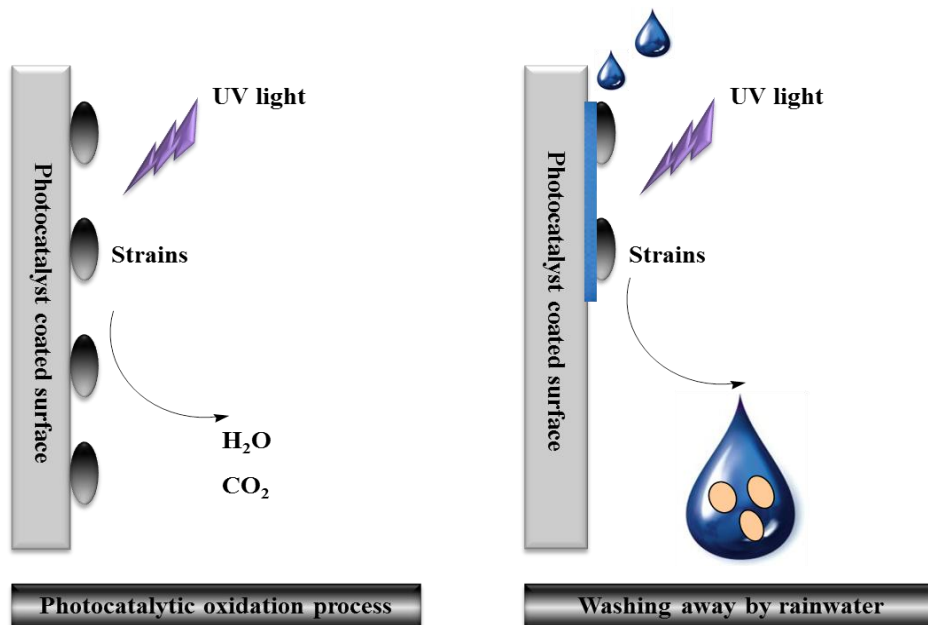
Figure 1.5: The self-cleaning process on the photocatalytically active surface: conventional photocatalytic oxidation process (left) and spreading of water droplets on the superhydrophilic surface (right)).

1.3   Wettability and Photoinduced Hydrophilicity
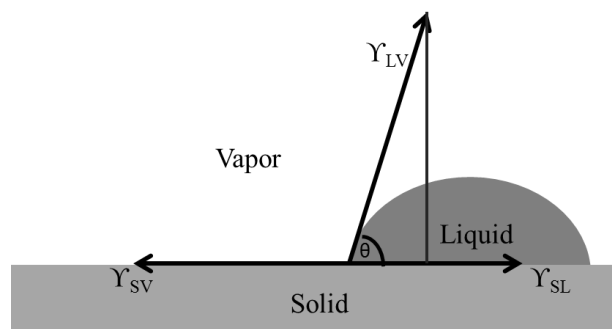
Figure 1.6: Relationship between the interfacial energies per unit area at the point of the three-phase equilibrium.

The wettability, that is, how liquids behave on a surface, is one of the fundamental properties of every solid and, thus, important for a wide range of natural systems as well as in many technical applications. It can be assessed using contact angle measurements[15].
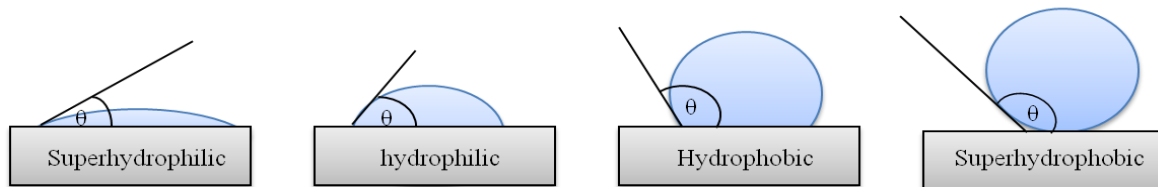
Figure 1.7: Schematic of the contact angle of a droplet on different surfaces.

The contact angle (θ) is defined as the angle between the tangent to the liquid-air interface and the tangent to the solid–air interface (Figure 1.6). In the special case of water being the wetting liquid, when the contact angle is less than 90°, the water droplet spreads out and the surface is called hydrophilic surface (when $\theta \approx 0°$, the surface is superhydrophilic). If the contact angle exceeds 90° and the water droplet drops the surface is called hydrophobic surface (when $\theta \approx 180°$, the surface is superhydrophobic) (Figure 1.7) [15].
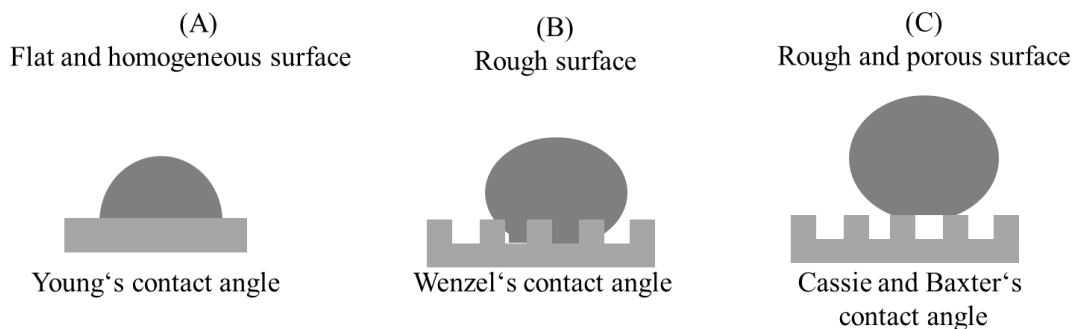
Figure 1.8: The contact angle models.

The contact angle (θ_w) on an ideal surface (flat and homogeneous) was firstly defined by Young's equation in 1805 [16].

$$cos\ \theta_w = (\Upsilon_{SV} - \Upsilon_{SL})/\ \Upsilon_{LV} \qquad\qquad Eq.\ 1.1$$

Here, Υ_{SV}, Υ_{SL}, and Υ_{LV} are the interfacial energy of the solid-vapor interface, the solid-liquid interface, and the liquid-vapor interface, respectively (cf. Figure 1.8, A).

However, the Young equation neglects the effect of the gravity and of the roughness of the surface. In reality, the contact angles are influenced by the specific kinds of atoms and surface terminations present at the liquid-solid-vapor interfaces. Nevertheless, surface roughness plays an equally important role for the wettability [16]. This means that Young's equation is not accurate.

Wenzel [16] assumed the complete penetration of the water droplet into the grooves of the rough surface and suggested the following equation

$$cos\ \theta_W = r\ cos\theta_Y \qquad\qquad\qquad Eq.\ 1.2$$

where θ_W is the predicted Wenzel contact angle and r defines the roughness of a solid surface. According to Wenzel's equation, increasing the surface' roughness of a hydrophilic surface enhances the wettability thus enhancing the hydrophibicity of a hydrophobic surface (cf. Figure 1.8, B).

On the other hand, Cassie and Baxter assumed that when a liquid spreads over a rough porous surface the solid–vapor interface is destroyed and two new interfaces, i.e., the solid-liquid and the liquid-vapor interface, are formed. Thus, the contact angle on this surface is given by:

$$cos\theta_{CB} = f\ cos\theta_W + (1\text{-}f)cos\theta_V \qquad\qquad\qquad Eq.\ 1.3$$

where θ_{CB} is the predicted Cassie–Baxter contact angle, and f is defined to be the fractional projected area of a material with smooth surface contact angle, θ, hence, the (1−f) term reflects the contribution of air remaining under the drop. In this case, the vapor pockets are trapped underneath the liquid, this means the droplet does not wet entirely as a results of the trapped superhydrophobic vapor pocket (cf. Figure 1.8,C) [17].

Moreover, the individual water droplets will form a film of water on the hydrophilic surfaces. The formation of this film provides the surfaces with new features, e.g., the surfaces will have an anti-fogging effect. Here the water forms a film on the surface and no small droplets, thus, it is not clouded in the field of view. A hydrophilic surface prevents fogging of

the glass, that is not in itself but only by the way in which water is reflected on the surface (Figure 1.9).
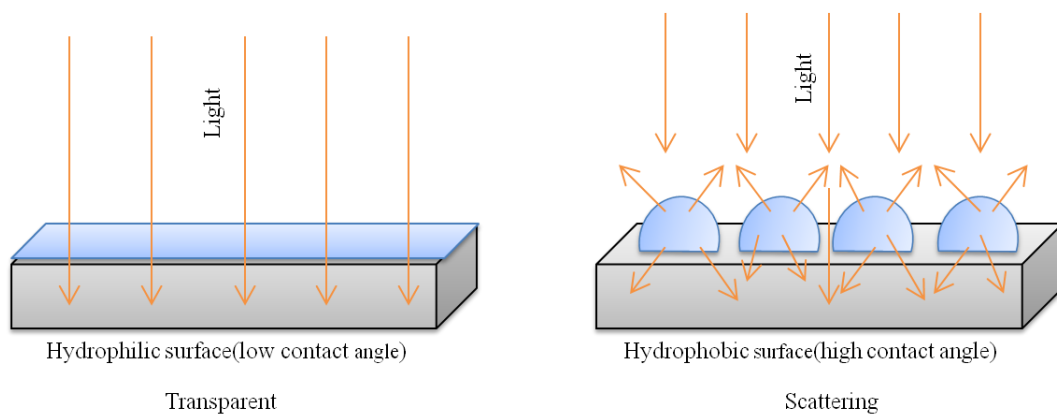
Figure 1.9: The difference between a hydrophilic and a hydrophobic surface.

1.4 Photocatalytically active coatings

1.4.1 Photocatalysts and Photocatalysis Mechanism

The photocatalysis mechanism has been extensively studied over the past 30 years [1]. Generally, when a semiconductor is irradiated by light of sufficient energy, electrons are excited from its valence band to the conduction band. The photogenerated charge carriers (conduction band electron and valence band hole) may migrate to the surface of the crystallite where they are able to reduce and oxidize, respectively, adsorbed electron acceptors and donors by interfacial charge transfer. However, this is not the only fate of these photogenerated charge carriers since they may also recombine and transform their energy to heat.

In order to be reduced, the relevant potential level of the acceptor species is thermodynamically required to lie below (i.e., less negatively on the electrochemical scale) the conduction band potential of the semiconductor. On the other hand, the potential level of the donor needs to be located above the valence band position of the semiconductor to be able to donate an electron to the vacant hole [13]. Actually, the energy level at the bottom of the conduction band is the reduction potential of the photogenerated electrons, whereas the

energy level at the top of valence band determines the oxidizing ability of the photogenerated holes, each value reflecting the ability of the system to promote reductions and oxidations.
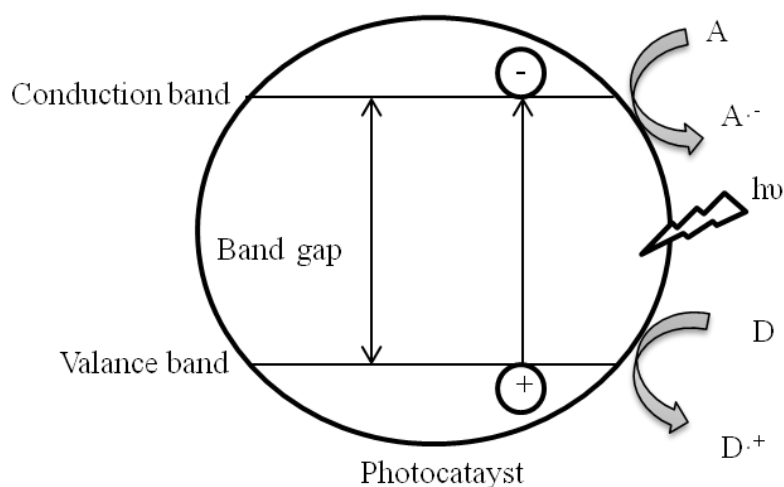
Figure 1.10: The mechanism of photocatalysis.

When the photocatalyst adsorbs photons the energy of which exceeds the band gap energy and which can be provided, e.g., from the ultraviolet radiation of the sunlight or from a suitable illuminating light source, it will produce pairs of electrons and holes. This occurs since an electron from the valance band from the photocatalyst becomes excited upon illumination by light (The valence band is the highest energy level containing an electron of the atoms comprising the semiconductor material in its ground state). The excess light energy thus promotes the electron to the conduction band of the photocatalyst consequently creating the pair consisting of the negatively charged electron (e^-) and the positively charged hole (h^+) pair (The conduction band is the band of LUMO (lowest unoccupied molecular orbitals) that are high in energy and are generally empty). The energy difference between the valance and the conduction band is the band gap energy. For example, the band gap energy of TiO_2 is 3.2 eV [18]. Excited-state electrons and holes can recombine and dissipate the input energy as heat or light, get trapped in metastable surface states, or react with electron donors and acceptors adsorbed at the semiconductor surface. For example, after their reaction with water,

the holes can produce hydroxyl radicals with high oxidation potential. Depending upon the exact conditions, the holes themselves, $^{\bullet}OH$ radicals, superoxide radicals $O^{\bullet}_2{}^-$, H_2O_2 and O_2 itself can play important roles in the photocatalytic reaction mechanism (Figure 1.10) [19]. The photocatalytic activity of a given system is usually tested by measuring the degradation of model pollutants. Due to the ease of the determination of the concentration of compounds such as stearic acid, methylene blue, and chlorophenol quantitatively by chromatography and spectroscopy, they are popular choices as model pollutants [13].

Titanium dioxide is the most famous photocatalyst and it has been used frequently for self-cleaning windows and hydrophilic self-cleaning surfaces due to its favorable physical and chemical properties. In addition to its high photocalytic activity under UV(A) illumination and its photoinduced superhydrophilicity, it is also non-toxic, chemically inert in the absence of light, inexpensive, relatively easy to handle and it can be conveniently be deposit into thin films [13].
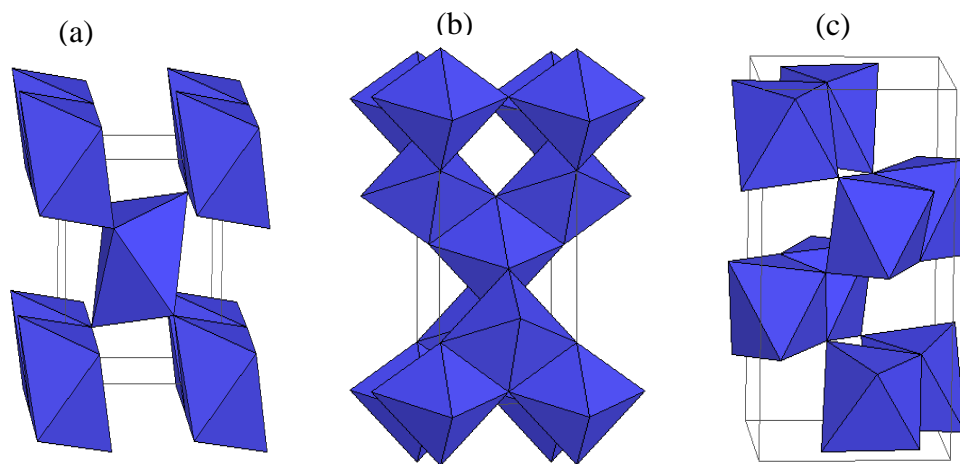
Figure 1.11: Crystal structures of TiO$_2$ (a) anatase, (b) rutile, and (c) brookite.

TiO$_2$ is an n-type semiconductor because of its oxygen vacancies. This material exists in nature in three crystal phases: anatase (tetragonal), rutile (orthorhombic), and brookite (tetragonal). Each crystal phase exhibits slightly different physical and chemical properties [19]. Figure 1.11 shows the crystal structure of the three types of TiO$_2$.

The differences in lattice structure of anatase and rutile TiO_2 cause different charge densities and electronic band structures, leading to different band gaps (for bulk materials: anatase 3.20 eV and rutile 3.02 eV) [19]. Therefore, the absorption thresholds correspond to wavelengths of 384 and 410 nm, respectively, for the two titania forms. The mentioned values have been determined for single crystals or at least well-crystallized samples. However, higher values of band gabs are usually obtained for weakly crystallized thin films or nanosized materials.

1.4.2 Photocatalytically Active Films

Recently, thin transparent layers containing TiO_2 have been intensively studied based upon their interesting application potential including photocatalytic water and air purification [20]. The self-cleaning properties of TiO_2 films derive from two unique light-induced properties: photocatalysis [19] and superhydrophilicity [21]. That is, organic pollutants adsorbed on the surface of a TiO_2 film can be decomposed under illumination with ultraviolet light (UV(A)), and dust is easily washed off, for example, by rainwater due to the spreading of the water on the superhydrophilic surface [22]. Table 1.1 summarizes the main self-cleaning applications of TiO_2 [23].

Table 1.1: Applications of self-cleaning TiO_2.

Function	Material	Application
Cleaning easiness	Material for road	Tunnel lighting
		Tunnel wall
	Material for house	Kitchen parts, bathroom and interior furnishing
	Materials for electric and electronic devices	Computer display, electronic wires
	Daily necessities and	Tableware, kitchenware

	consumer products	
Self-cleaning by rainfall	Materials for road	Traffic sign, lighting, soundproof wall, guardrail decorative laminate panel
	Materials for buildings	Exterior tiles, siding boards, curtain wall, painted steel plate, aluminium panel, building stone, crystallized glass, glass film, window, sash, screen door, gate door, sun parlous, veranda parts
	Materials for eclectic and electronic devices	Upper glass of a solar cell, insulator
	Materials for vehicles	Painting and coating of vehicles, outside of windows, headlight

1.4.2.1 Introducing porosity in TiO$_2$ film

The mesoporous material as characterized by IUPAC is the porous material having a pore diameter of $2.0 \leq d \leq 50$ nm [24]. Usually, mesoporous metal oxides are prepared by template-based methods using soft templates (surfactants and block polymers) [25] and/or hard templates (porous silica, polystyrene spheres, porous carbon) [26].The importance of this type of materials stem from their high specific surface areas and pore volumes, as well as from the usually narrow pore size distributions which offer more active sites for catalytic reactions to take place [27]. Since the adsorption of the molecules (electron acceptor and donor) on the surface of the photocatalyst is essential in the photocatalytic systems, enhancing the surface area of the photocatalyst is expected to increase it photocatalytic activity. Moreover, mesoporous TiO$_2$ is an interesting material for photocatalytic applications not only

because of its higher surface area but also due to its continuous particle framework, which may be beneficial compared to separate individual nanoparticles. The low number of studies which has been reported on ordered mesoporous TiO_2 as a photocatalyst is likely related to the difficulties in making it as an ordered material [28]. Moreover, the mechanical properties of coatings prepared using mesoporous metal oxides are relatively poor and need to be improved.

1.4.2.2   Modifying TiO_2 with other metal oxide

Mixed oxide composite materials can sometimes be more efficient photocatalysts than pure substances [29, 30]. This is due to the generation of new active sites as a result of interactions between the oxides. Furthermore, mixing of metal oxides may lead to an increased surface area, and to improved mechanical strength and thermal stability [31].

SiO_2 exhibits high thermal stability, excellent mechanical strength and supports the creation of new catalytically active sites due to the interaction between TiO_2 and SiO_2 [32]. A mixed metal oxide (TiO_2/SiO_2) can enhance the photocatalytic performance improving the ability of surface adsorption and increasing the amount of hydroxyl surface groups [33]. Simultaneously, SiO_2 acts as the carrier of TiO_2 leading to a large surface area as well as to a suitable porous structure [34, 35]. On the other hand, it is well known that the coupling of two semiconductors[31], in particular TiO_2 and ZnO [36], is useful in achieving a more efficient separation of photo-generated electron–hole pairs. The electron transfers from the conduction band of ZnO to the conduction band of TiO_2 under illumination and, conversely, the hole transfers from the valence band of TiO_2 to that of ZnO resulting in a decrease of the rate of electron-hole recombination. This, in turn, leads to an improvement in the photocatalytic activity.

1.4.3   Photoinduced Superhydrophylicity

The discovery of the phenomenon of photoinduced superhydrophylicity of TiO_2 thin films opens a lot of new aspects for industrial applications such as self-cleaning and anti-fogging. According to the photoinduced superhydrophilicity phenomenon, The TiO_2 surface becomes superhydrophilic with a water contact angle <5° [37]. To this day, the reasons behind the photoinduced superhydrophylicity are still an open question. But the three most proposed ones are: (I) generation of surface vacancies, (II) photoinduced reconstruction of Ti-OH bonds, and (III) photocatalytic decomposition of organic adsorbents.

1.4.3.1   Generation of surface vacancies

When electron–hole pairs are generated upon irradiation with UV-light, the holes diffuse to the surface and cause oxygen vacancies at the surface. This results in a reduction of Ti^{4+} to Ti^{3+}. These Ti^{3+} sites can cause water dissociation, resulting in adsorbed –OH species, which are hydrophilic [21].

Hashimoto and co-authors [38] further show that hydrophilicity closely depends on the crystal surface. The (110) surface shows better hydrophilic properties than the (001) surface since it has bridging oxygen atoms which are not found on (001) surface.

Although a lot of experimental results correspond with the proposed mechanism, there are also some results that disagree with this mechanism. White et al. [39] studied the hydrophilic effect on the TiO_2 (110) surfaces prepared with or without oxygen vacancies. They point out that the hydrophilic property is not influenced whether or not oxygen vacancies (up to 14%) are present, which is obviously contradicted with the current mechanism.

1.4.3.2   Photo-induced reconstruction of Ti–OH bonds

The reconstruction of hydroxyl groups of the TiO_2 surface is attributable to photo generated holes. As is explained in equations 1.4 and 1.5, the photo generated holes are trapped at surface lattice oxygen atoms, causing a dissociation of their bonds with titanium

atoms, followed by the adsorption of water molecules, which leads to appear hydroxyl groups on surface defects [40].

$$\text{Ti-O-Ti} + h^+ + H_2O \rightarrow [\text{Ti-O}^\bullet \text{ HO-Ti}] + H^+ \qquad\qquad Eq.\ 1.4$$

$$[\text{Ti-O}^\bullet \text{ HO-Ti}] + H_2O \rightarrow [\text{Ti-OH HO-Ti}] + {}^\bullet OH \qquad\qquad Eq.\ 1.5$$
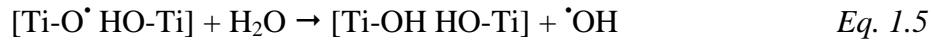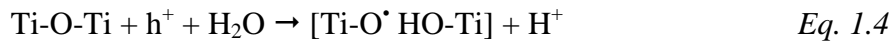
However, Anpo et al. [41] shows that vacuum can cause an immediate disappearance of superhydrophilicity of TiO_2. The authors argued that these results cannot be explained by the newly formed OH groups during UV-illumination, because those cannot be removed by evacuation at room temperature. Thus, the proposed reconstruction of the Ti–OH bond mechanism needs to be modified.

1.4.3.3   Photocatalytic decomposition of organic adsorbents

The photoinduced superhydrophylicity conversion was initially considered to be directly associated with its photocatalytic activity. When TiO_2 surface is contaminated it turns to hydrophobic (strictly, it has water contact angle smaller than 90°) due to the adsorption of certain gas (organic) components contained in the air. After UV irradiation, the organic adsorbents photocatalytically oxidized and removed from the TiO_2 surface [42].

As a matter of fact, it cannot be consider that the removal and adsorption of organic contaminate is the only reason causing the wettability change of TiO_2 surface. But also a preferential adsorption of water molecules with dissociation on the photo generated surface defective sites contributes to the formation of highly hydrophilic TiO_2 surfaces [42].

Hennessy et al. [43] found that the well-protected clean surface of rutile TiO_2 (110) still exhibits a large water contact angle, consistent with previously reported measurements by the Hashimoto group [38]. The mechanochemical treatment like ultrasonic treatment or cleaning the surface with NaOH should enhance hydrophilicity thus organic contaminants are decomposed in the same way as by photocatalysis. But the contact angle only decreases to values about 10°–20°and no superhydrophilic state is reached [42]. This leads to the

conclusion that photocatalytic decomposition of the adsorbed pollutants cannot be the only process to achieve superhydrophilicity.

1.5   Methods for Preparing Self-Cleaning Coatings on Polymer surfaces

Several routes are possible to apply self-cleaning coatings onto surfaces such as physical or chemical vapor deposition. However, while these techniques exhibit many advantages they are expensive and cumbersome [44]. In addition, the range and shape of materials that can be coated by these techniques is limited [44]. An alternative coating method is the sol-gel route allowing novel materials, such as organic-inorganic hybrids, to be deposited on various substrates from a solution at or near room temperature. Consequently, this technique is suitable for coating polymers, which usually have limited thermal stability [44]. It enables the coating of large surfaces and also the attainment of thin layers with good thermal and mechanical stabilities as well as high optical quality [45]. Furthermore, the sol–gel method is relatively simple and inexpensive.

1.5.1   The Sol-Gel Process

The sol-gel process can be defined as follows: the synthesis of an inorganic or organic network by a chemical reaction in solution at low temperature [46]. This solution, which is called a sol, is a colloidal suspension of solid particles in a liquid (a colloid is a suspension in which the dispersed phase is so small (~ 1 – 1000 nm) that the gravitational force is negligible and interactions are dominated by short range forces, such as Van der Waals attraction and surface charges [47]. The continuous solid skeleton made of colloidal particles is called a gel [18].

The sol-gel synthesis is realized via various process paths. By employing this method, it is possible either to generate small (nano) particles to coat parts or surfaces or even to form three-dimensional structures.

The sol-gel process is used in many different applications. Table 1.2 summarizes the applications of the sol-gel method [18].

Table 1.2: Applications of the sol-gel methods.

Applications of Sol-Gel Method	
Mechanical & Chemical	Protection with hard coats, catalysts, anticorrosion films.
Optics & Photonics	Solar cells, laser elements, waveguides, optical switching, antireflection coatings.
Electronics	Capacitors, non-volatile memories, transport electrodes.
Thermal	Refractory ceramics, fibres, low expansion ceramics.
Biomedical	Biocompatible films, entrapment of enzyme and cells, medical tests.

In Figure 1.12 different nanostructures produced sol-gel synthesis are shown. Starting point of the production route from the solution of precursors is always a sol, which evolves towards the formation of a gel containing both of liquid and solid phases whose morphologies range from discrete particles to continuous polymer networks. Dried gels, either Xerogels or Aerogels (Xerogels are dried by evaporation, whereas Aerogels are dried by supercritical extraction of solvent) are distinguished by their enormous surface area and correspondingly small pore sizes [18].

Upon removal of the solvent in the formation of Xerogel, the network is not completely linked and the resulting product has a porosity of about 50 percent. By a subsequent drying process at high temperatures, it is possible to obtain a solid ceramic with low porosity. Aerogels can also be produced directly from the gel stage by removing the solvent at high pressure and high temperature (supercritical extraction of solvent), thus the gel network formed retains its structure, and the resulting solid comprises up to 95 percent pores. It is also

possible to produce fibers obtained from the sol, which is then sintered at high temperatures [18].
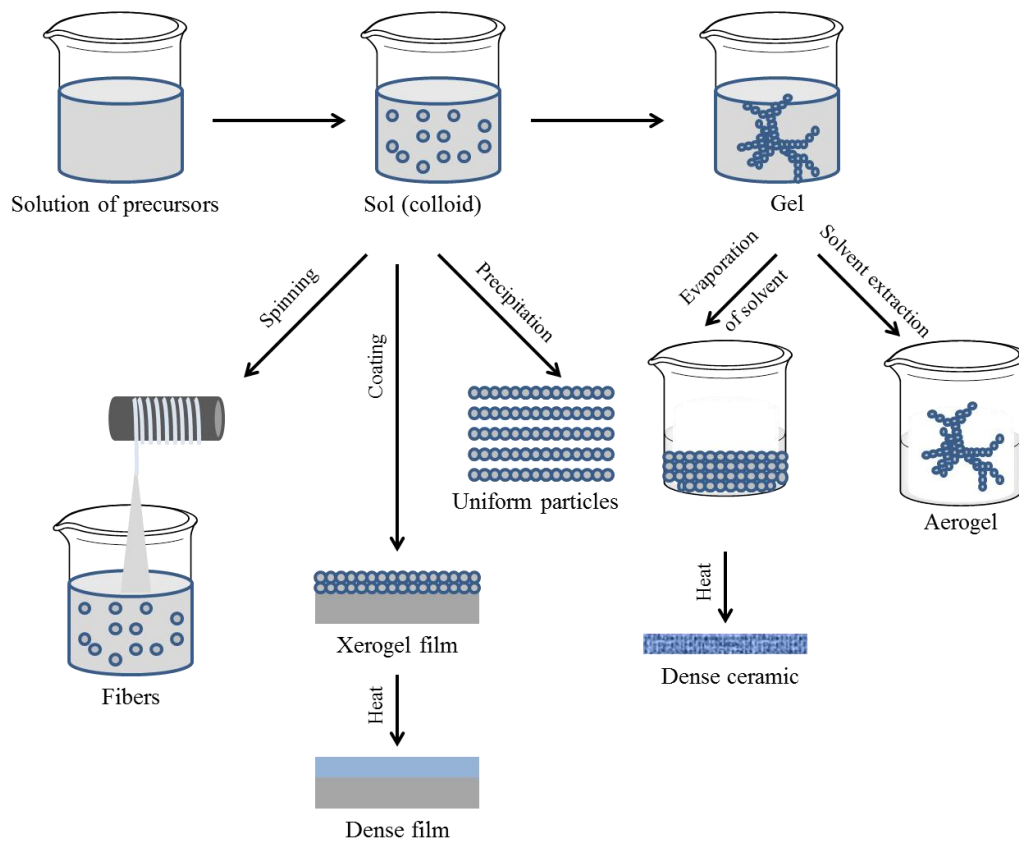
Figure 1.12: Sol gel process for preparation of different materials and devices.

In fact, one of the main sol-gel applications is the coating of surfaces. In this case, dip and spin coating procedures are used to deposit the sol onto the substrate to form the thin film. Actually, the following conditions have to be matched during the film formation:

- The solution must wet the substrate;

- The solution must remain stable during the aging process;

- The solution solidifies as homogeneous transparent film;

- The solution should have some tendency towards crystallization into a stable high temperature phase;

- For multiple layers the previous layer must be either insoluble or heat treated to make layers insoluble before subsequent depositions.

Alkoxide solutions and aqueous solutions of different metal salts (chloride, nitrate...) fulfill these conditions. Table 1.3 presents the substances used in the preparation of various sols and their roles [48].

Table 1.3: Substances used in the preparation of sols and their roles.

	Substance	Role	Example
Basis	Alkoxide	Ti – donor	Titanisopropylate
	Alcohol	Solvent	Propan-2-ol
	Water	Hydrolysis	
Additives	Chelator	Hydrolysis Controlling	Acetylaceton, acetic acid
	Acid, base	-	Acetic acid, HCl, HNO$_3$ NH$_4$OH
	Additional solvent	Drying control	Polyethylenglycol(PEG), dimethylformamid(DMF)
	Organic binder	-	Hydroxypropylcellulose

In general, the precursors used for the preparation of the coating sols can be divided into two groups: organic metallic compounds , i.e., the alkoxide, and inorganic salts [18].

With an alkoxide (M(OR)$_n$) as precursor, the sol-gel reactions can be described as follows:

Hydrolysis: -MOR   +   H$_2$O   →   -MOH   +   ROH   *Eq.1.6*

Condensation: -MOH   +   ROM-   →   -MOM-   +   ROH   *Eq.1.7*

                        -MOH   +   HOM-   →   -MOM-   +   H$_2$O   *Eq.1.8*
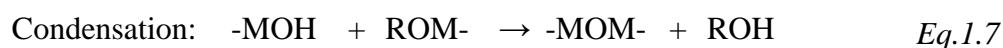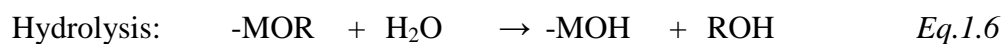
Equations 1.9-15 describe the reaction mechanisms for acid (Equations 1.9-12) and base (Equations 1.13-15) catalyzed hydrolysis condensation of alkoxy silane.

Acid catalyzed

$$Eq.1.9$$

$$Eq.1.10$$

$$Eq.1.11$$

$$Eq.1.12$$

Base catalyzed

$$Eq.1.13$$

$$Eq.1.14$$

$$Eq.1.15$$
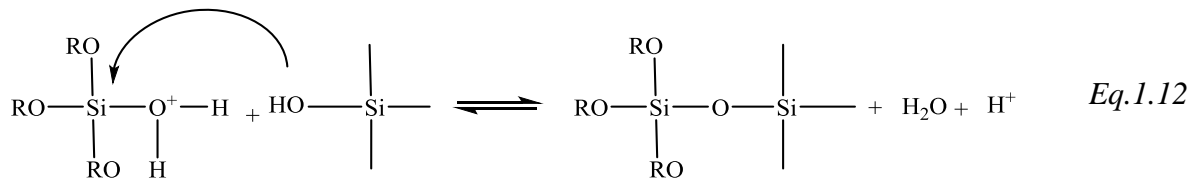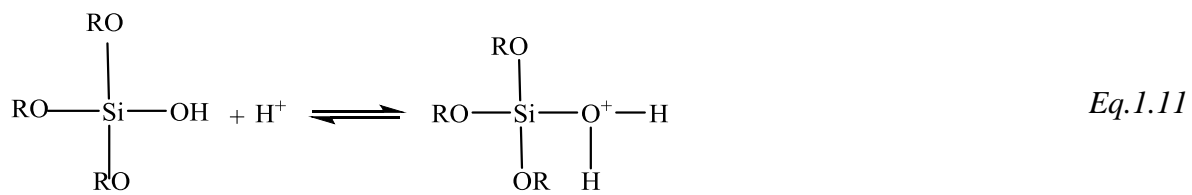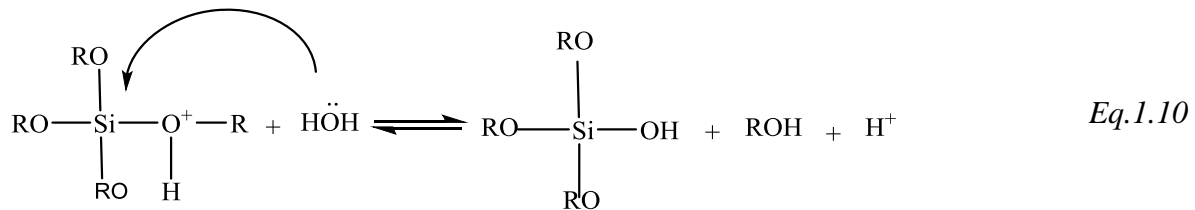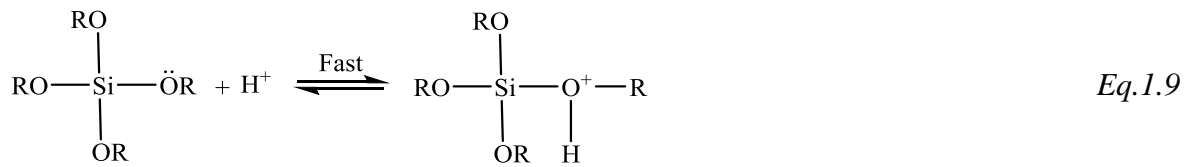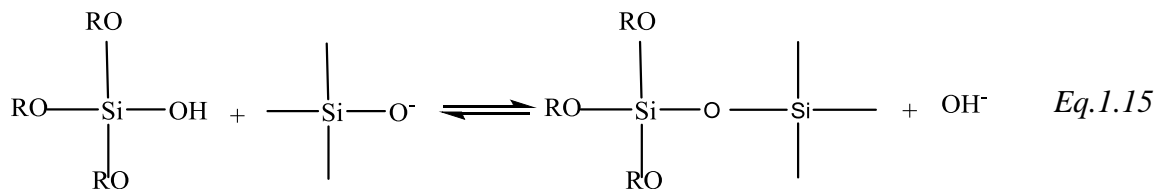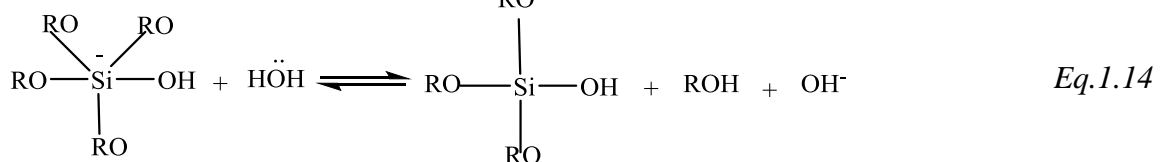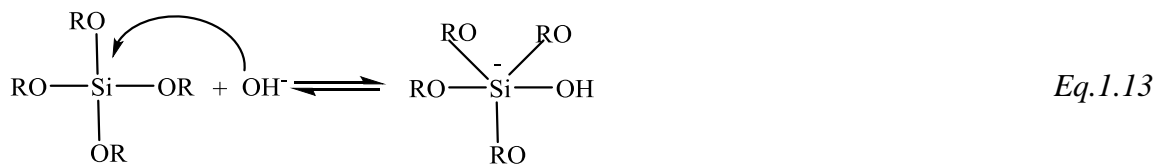
These reactions show that a gel is formed because of the condensation of partially hydrolyzed species into a three dimensional polymeric network and any factors affect either or both of these reactions are likely to impact on the properties.

The pH of the sol plays a very important role on the further formed gel. Under acidic conditions, the hydrolysis reaction occurs at a faster rate than the condensation reaction and

the thus resulting gel is weak due to the low linking between the formed long chains. However, by increasing the pH, the condensation reaction is accelerated relatively to the hydrolysis reaction.Thus, the formed gel under basic condition is highly branched (see Figure 1.13) [38].

Figure 1.13: A cartoon showing linear weakly cross-linked and highly branched clusters, A: acid catalyzed B: base catalyzed hydrolysis.

Various factors that can influence the film structure are presented in Figure 1.14 [18].
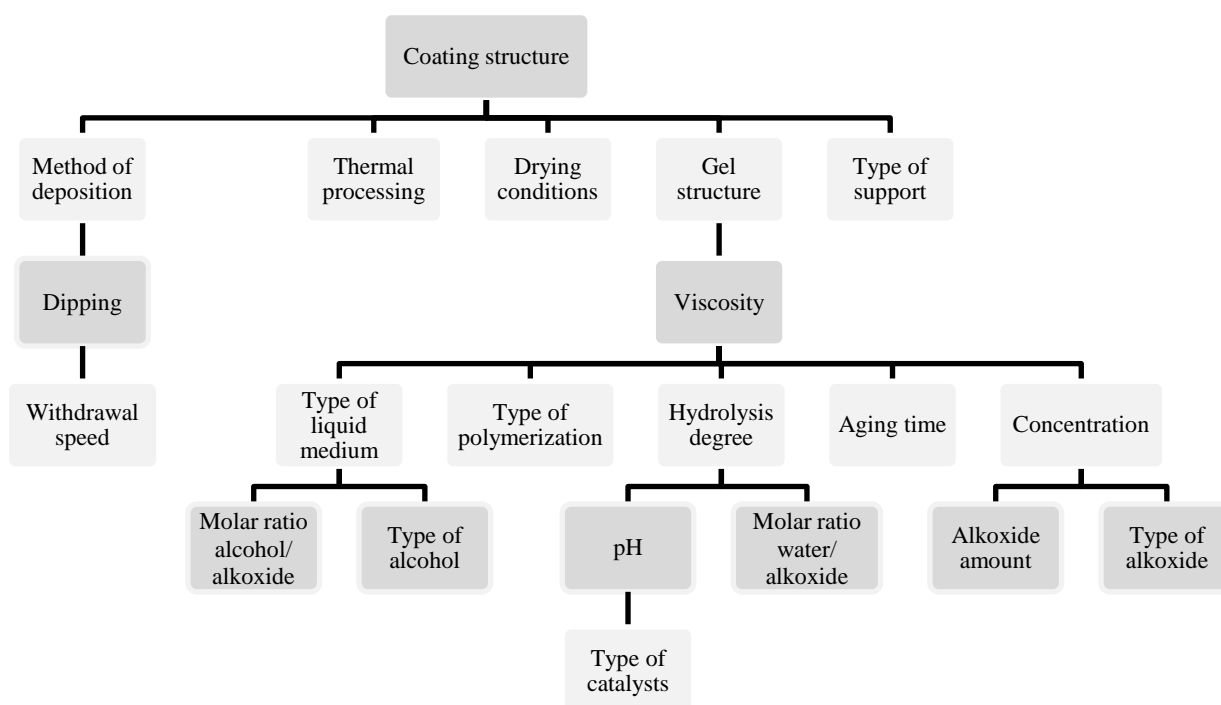
Figure 1.14: The factors that influence the film structure.

1.5.2   Coating Process

To deposit the materials prepared by the sol-gel technique on the required substrate (e.g., on a glass or polymer surface), spin, spray, or dip coating processes are used.

1.5.2.1   Spin coating

In general, the spin coating is divided into four stages: the deposition, spin up, spin off, and the evaporation (Figure 1.15). The deposition, spin up, and spin off stages occur sequentially while the evaporation stage occurs throughout the process.
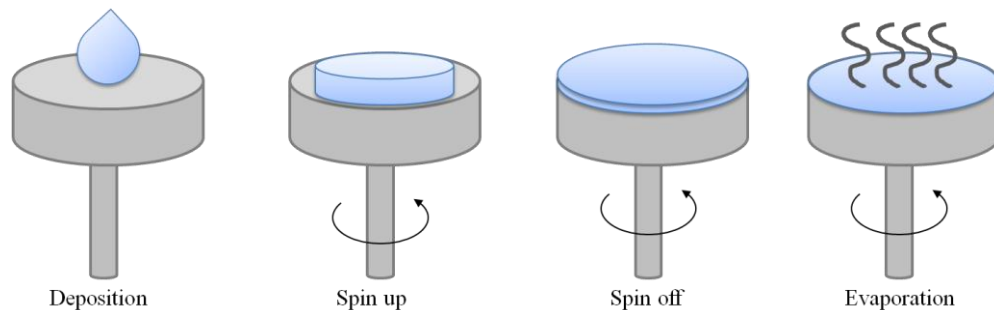
Figure 1.15: The steps of film deposition by a spin coating process.

The turntable is accelerated to distribute the applied solution by centrifugal force. The remaining layer is thinned as a result of the high spinning speeds. This stage is followed by the drying of the applied layer. By the rapid rotation, a uniform evaporation of the solvent used is made possible. By the evaporation stage or simply by "drying", the solvents are removed from the surface and the low volatile components of the solution remain on the surface of the substrate. The speed of rotation and the viscosity of the coating solution affect the thickness of the layer [47].

Spin coating is a process used, e.g., for microelectronic applications. The spin coating sol-gel synthesis is furthermore used for coating surfaces of a rotational symmetry (e.g., for lenses and eyeglass lenses).

The disadvantages of spin coating are few, but they are becoming more important as the substrate size increases. Large substrates cannot be spun at a sufficiently high rate in order to

allow the film to thin. The biggest disadvantage of spin coating is its lack of material efficiency. Typical spin coating processes utilize only 2–5% of the material dispensed onto the substrate, while the remaining 95–98% is flung off into the coating bowl and disposed [49].

1.5.2.2   Spray coating

Spray coating techniques are widely used in industry fields for coating of complex shapes on various (curved and flat) substrates (silicon wafers, glass slides, and plastics). In this process, very fine droplets are formed from the solution using atomizers or nebulizers. These fine droplets are then carried into the coating chamber with a carrier gas and deposited on the substrate by gravity or with an electrostatic field. The quality of the coating is determined by the size of the droplet, which can be reduced by decreasing the viscosity of the solution, increasing the atomizing pressure or using a venturi nozzle (cf. Figure 1.16). Although the spray coating is a fast coating process with less waste of coating sols, the spray-coating method offers limited control of the uniformity of thickness [50].
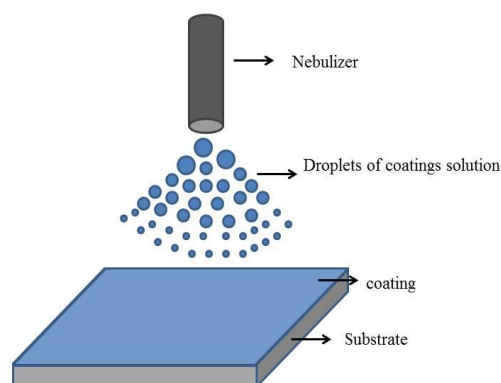
Figure 1.16 : The film deposition by a spray coating process.

1.5.2.3   Dip coating

In the dip coating process, the substrate is coated by it immersion in a liquid, i.e., the sol, followed by its withdrawal at a well-defined withdrawal speed under controlled atmospheric

conditions such as temperature and humidity due to their affecting the application or drying of the coating. During this process the sol is converted to a film via aggregation, gelation, and drying (Figure 1.17). The thickness of the layer increases by increasing the pull rate and by the use of a sol with a higher viscosity or lower surface tension [47]. One of the advantages of this coating technique is its ability to be applied on flat panels, cylinders or complex geometry with quite a large surface.
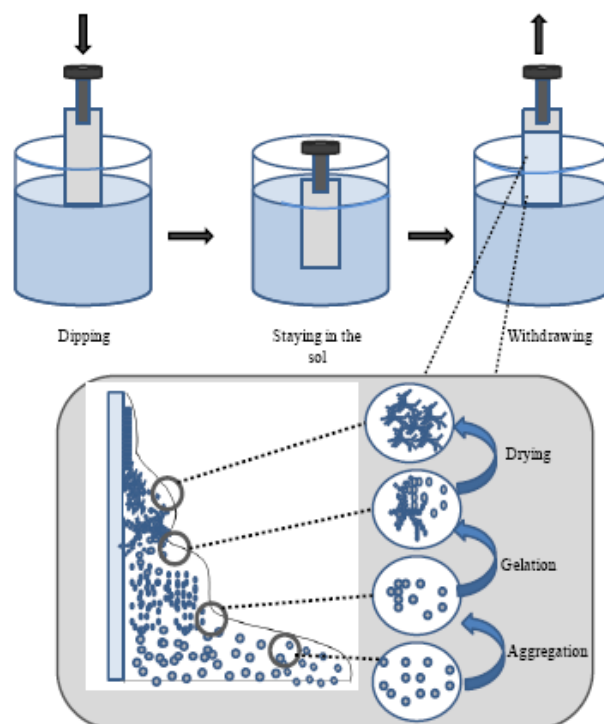
Figure 1.17: Steps of film deposition by the dip coating process.

1.6 Photochemistry and Photodegradation of Polycarbonate

When engineering plastics, such as polycarbonate (PC), are used in outdoor applications, the polymer starts to suffer changes in its mechanical properties and in its aesthetical properties. In fact, the polymer may degrade due to sunlight, humidity and oxygen. The chemistry of degradation processes in polycarbonates has been studied extensively over the past few decades [5]; however, what is happening under outdoor exposures is still under debate, since most of these studies were done under different exposure conditions. In Polycarbonate, the chemistry underlying the photodegradation has been ascribed to two

different mechanisms: photo-Fries rearrangement and photo-oxidation (side chain and ring oxidations) [51]. The importance of these mechanisms depends on the applied irradiation wavelengths.
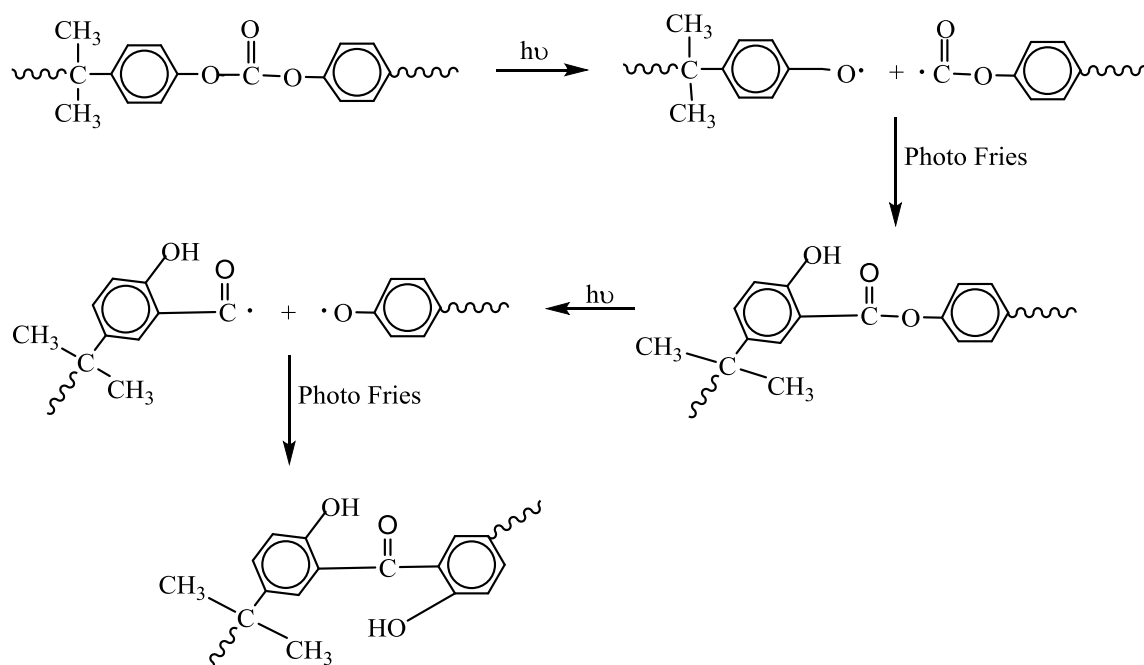
Figure 1.18:Photo-Fries rearrangement.

The photo-Fries rearrangement reaction is more likely to occur when light with wavelengths shorter than 300 nm is used, whereas photo-oxidation reactions are more important when light with longer wavelengths (>340 nm) is employed. The major part of the natural sunlight spectrum contains wavelengths longer than 300 nm, although, sunlight can contain wavelengths down to 295 nm. This means that there is a possibility that both photo-oxidation and photo-Fries rearrangement reactions take place under outdoor exposures [52].

Photo-Fries rearrangement is presented in Figure 1.18, which shows that irradiation of polycarbonate with short wavelengths drives the aromatic carbonate unit to rearrange itself into phenylsalicylate and dihydroxybenzophenone derivatives (see Figure 1.18).

The photo-oxidation reaction of polycarbonate is shown in Figure 1.19. In this reaction an initiating radical, which generally introduced from impurities, is required to start this autocatalytic oxidation process.
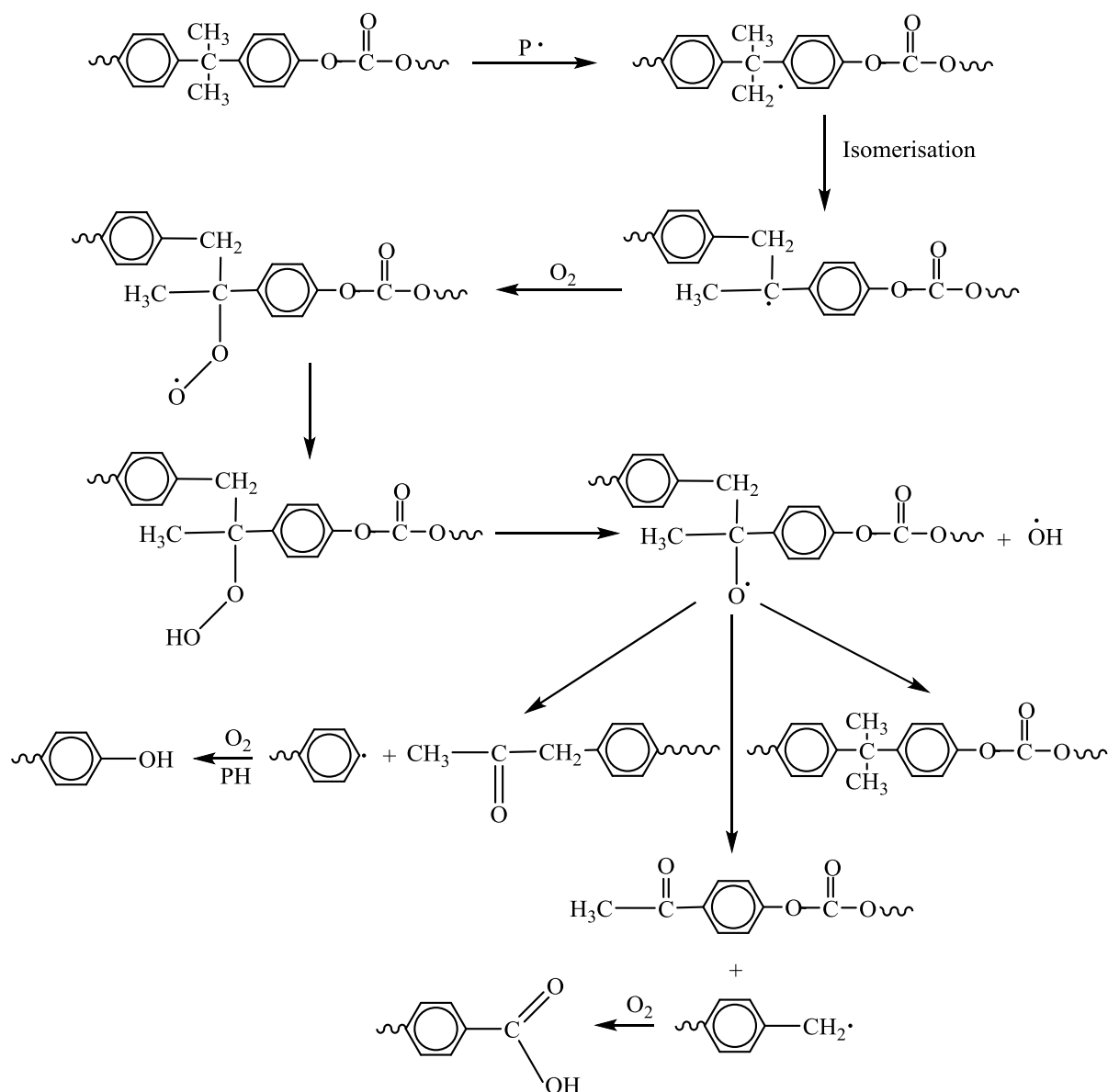
Figure 1.19: Photo-oxidation of bisphenol A polycarbonate.

1.7 Recent Work

Recently, thin transparent layers containing TiO_2 have been intensively studied based upon their interesting application potential including the formation of photocatalytically active and/or self-cleaning surfaces [1, 53-56].

TiO_2 and TiO_2-SiO_2 coatings on PC are well known but only a limited number of publications have been focusing on photocatalytically active self-cleaning TiO_2 and TiO_2-SiO_2 coatings on PC prepared by sol-gel methods [45, 57-63]. Langlet et al. [57, 58] have

prepared TiO_2 films on PC (and other substrates) by depositing acidic TiO_2 sols, drying them at room temperature followed by a heat-treatment (90–140°C) in an ethanol-water atmosphere. The optical transmission of the films in the visible range of the spectrum was found to be lower than that of bare polycarbonate. The films were photocatalytically active; the activity increased with increasing film thickness. Langlet and co-workers [45] also deposited a TiO_2 sol peptized under alkaline conditions. The prepared films on PC were characterized directly after deposition and after a subsequent heat treatment in air at temperatures up to 140°C.

Again, the transmission in the visible range of the spectrum was found to be lower than that of uncoated PC. The transmission was decreasing with increasing film thickness (about 70–370 nm) whereas the photocatalytic activity increased. The post-deposition heat treatment did not influence the photocatalytic activity for temperatures up to 110°C. Kwon et al. [59] have used different alkoxide precursors to prepare TiO_2 nano-crystalline thin films on polycarbonate, polymethyl methacrylate, glass, and aluminum via a sol–gel process. They observed that the films on PC exhibited poor adhesion and peeled off after a certain period of time. All films were found to photocatalytically decolourize an aqueous methylene blue solution under UV(A) irradiation. Lam et al. [60] studied the effect of NaOH-etching and UV(C) irradiation on the mechanical stability of TiO_2 coatings on PC slides. TiO_2 nanoparticles were found to adhere more strongly on UV(C)-treated PC than on NaOH-etched PC whereas the TiO_2 films on NaOH-etched PC exhibited a higher photocatalytic activity than the films on UV(C)-treated PC in a methylene blue degradation test. Yaghoubi et al. [61] prepared TiO_2 films on a PC surface chemically pretreated to create hydrophilic groups on the surface. The films were prepared by dip-coating using an anatase sol with TiO_2 nanoparticles of 30 nm size. A pre-coat by peroxotitanium complexes was employed to improve adhesion and to inhibit the substrate degradation. The TiO_2 coating reduced the transparency by 10–15%. The photocatalytic activity determined through decolourization of a methylene blue

solution was found to be linearly dependent on the film thickness. The TiO_2 coatings prepared in this study improved the hardness, scratch resistance, and the mechanical properties as was demonstrated by nano-indentation and nano-scratch tests. Matsuda et al. [62] have prepared transparent TiO_2/SiO_2 films with a 1:5 molar ratio on various types of substrates, including PC, by dip-coating and post-treatment at temperatures <100°C under ambient pressure. They observed that TiO_2 nanocrystals were precipitated mainly at the surface of the TiO_2-SiO_2 films during post-treatment in hot water, whereas the addition of poly(ethylene glycol) in the films led to the dispersion of TiO_2 nanocrystals in the whole of the films after the treatment. The films were found to be photocatalytic active in the methylene blue degradation test as well as in other test systems. The authors assumed that in the case of films where the TiO_2 are mainly precipitated at the surface the residual SiO_2 under-layer is acting as a protective layer for an organic polymer substrate against photocatalytic degradation. Horiuchi et al. [63] have prepared Ti-containing mesoporous SiO_2 thin films on PC by spin-coating a sol containing the metal ethoxides as the TiO_2 and SiO_2 source, and polyethylene stearyl ether as a structure-directing agent. After drying the organic structure-directing agent was photocatalytically removed resulting in superhydrophilc films after UV(A) irradiation for 4 to 5 days. The superhydrophilic state was maintained for several days under dark conditions.

1.8   Aim of this Work

Preparation of good self-cleaning coatings which exhibit a high photocatalytic activity, an excellent wettability by water, a strong adhesion to the surface of the substrate and sufficient stability against exfoliation and abrasion, as well as optical properties appropriate for the intended application is still a challenging topic especially on polymeric substrates, which can be photocorroded. The references given above have shown that photocatalytic coatings can indeed provide polycarbonate sheets with sufficient self-cleaning properties. However, an improvement of the adhesion strength, the mechanical stability, the wettability, and the

photocatalytic activity of such coatings on polycarbonate surfaces is still needed. Furthermore, the most common challenges which can be faced during the preparing of good self-cleaning coatings on polycarbonate and the suggested solution`s strategies are summarized in the Table1.4.

Table1.4: Challenges that can be faced during coating of polycarbonate and suggested solutions.

Challenge	suggested Solution
Low adhesion of layers on polycarbonate surface	Modification of the polycarbonate surface
Possibility of photocorrosion of polycarbonate	Deposition of intermediate photocatalytically inactive layers
Low thermal resistant of polycarbonate	Preparation of photocatalytically active layers at low temperature

Hence, the main aims of the present work are:

1. Improving the binding between the polymer (PC) and the photocatalytically active layer by modifying the PC surface by light as well as by photocatalytically inactive interlayers.

2. Providing the polycarbonate surface with stable photocatalytic and superhydrophilic thin films employing dip coating sol-gel methods. And examining the respective adhesion strength, the mechanical stability, and the self-cleaning properties.

3. Systematic study of the relationship between the structure of the prepared films and their properties required for a good self-cleaning surface to remedy the lack of knowledge in this field.

- Effect of the porosity of the films prepared from a semiconductor (TiO_2).

- Influence of the coupling of two semiconductors (TiO_2 and ZnO) on the properties of the prepared films.

- Effect of the addition of an isolator to a semiconductor (SiO_2 to TiO_2) on the properties of the prepared films.

4. Develop suitable mechanisms to explain the relationship between the structure of the film and the photoinduced superhydrophilicity.

2   Experimental Part

2.1   Film Preparation

2.1.1   Modification of the Polycarbonate Surface

Polycarbonate sheets (Makrolon AL 2647 obtained from Hella KGaA, 5 cm × 18 cm) were washed with water, deionised water (obtained from SARTORIUS ARIUM 611 apparatus (resistivity = 18.2 MΩ cm)), and propan-2-ol (Roth 99.9%) respectively, followed by furnace drying in air at 80° C. The surface modification of polycarbonate was then performed via a photo Fries reaction initiated by irradiation with UVC-light (Philips PL-L 36 W) for 2 h [64, 65].

2.1.2   Preparation of SiO_2 Intermediate Layers on Polycarbonate

SiO_2 layers were prepared from tetraethyl orthosilicate (TEOS). TEOS (Roth ≥ 98%, 29.2 ml) dissolved in ethanol (Roth 99.8%, 5.8 ml) and deionized water (7.2 ml). This solution was mixed and stirred for 30 min. Subsequently hydrochloric acid (Fluka 37%, 0.03 ml) was added into the solution to catalyze the hydrolysis followed by further stirring for 60 min. Finally, 10 ml of the resulting solution were diluted with absolute ethanol to give 200 ml and then stirred at ambient temperature for 24 h.
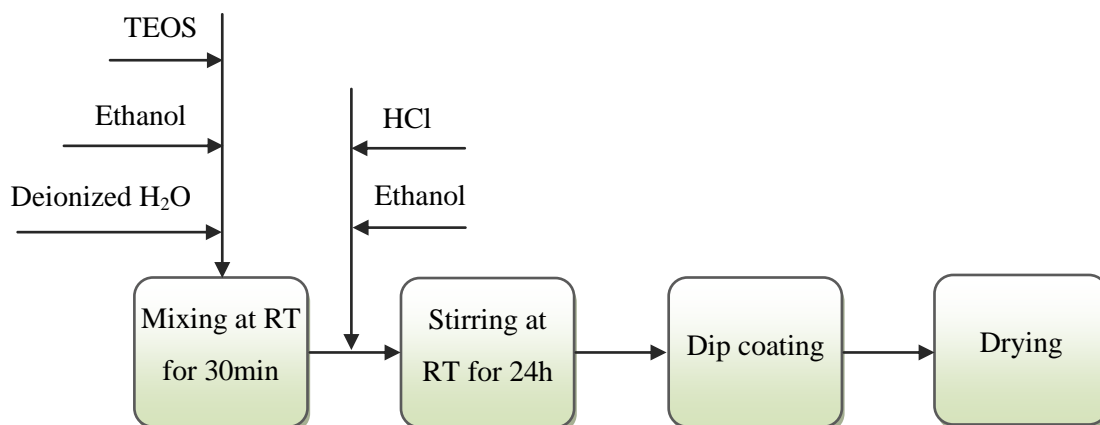
Figure 2.1: Flow-chart summarizing the preparation of a SiO_2 sol-gel and the PC coating procedure.

The SiO_2 sol was deposited on the polycarbonate surface by dip-coating. The PC slides were withdrawn into open air (temperature $T = (21\pm1)°C$, relative humidity $h_r = (44\pm3)\%$) with a pulling rate of 1 mm s^{-1}. The dip-coated films on the polycarbonate substrates were dried at 80°C for 24 h. Figure *2.1* summarises the preparation of a SiO_2 sol-gel and the PC coating procedure.

2.1.3 Preparation of the Photocatalytically Active Layers on Polycarbonate

The photocatalytically active layers were prepared starting from:

• Previously prepared materials (commercial material Hombikat UV100 and UV100-SiO_2) or (home made material (mesoporous TiO_2)).

• TiO_2 precursors prepared at low temperature for the preparation of bare TiO_2 and TiO_2-ZnO mixed oxides.

Figure 2.2 presents the methods of the preparation of the layers.
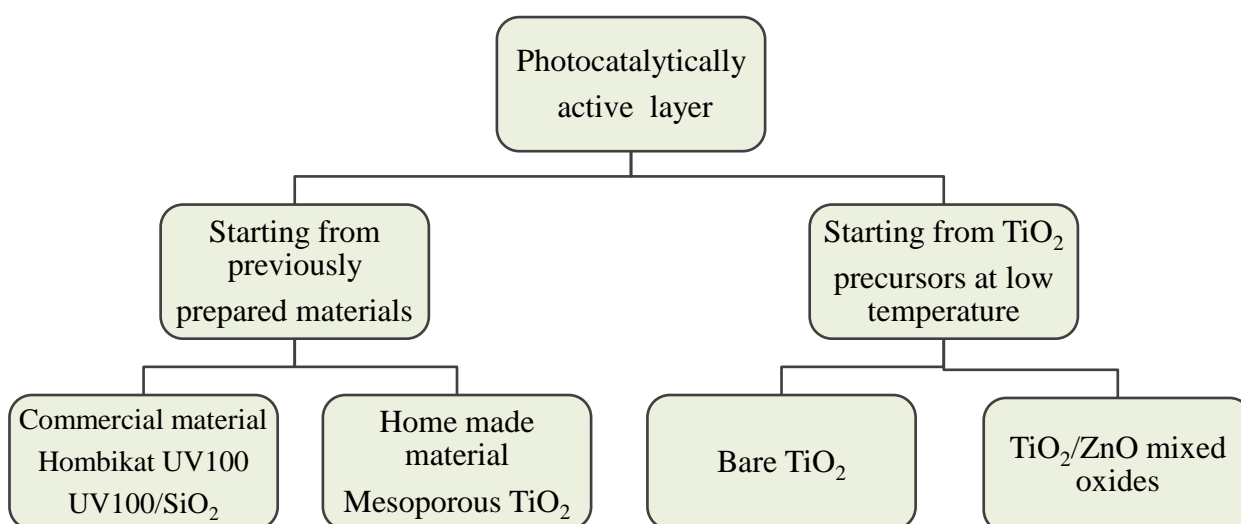
Figure 2.2: Scheme of the methods for the preparation of the layers.

The prepared photocatalytically active films are differentiated into in three sections:

• MesoporousTiO_2,

• TiO_2,SiO_2, and TiO_2-SiO_2,

• TiO_2, ZnO, and TiO_2-ZnO.

2.1.3.1   Preparation of Mesoporous Titania Thin Films

Mesoporous titania powder was prepared according to a procedure given in ref. [66] which yields photocatalyst materials with a hexagonal mesostructure. Typically, F127 ($EO_{106}PO_{70}EO_{106}$, MW 12 600 g mol^{-1}, Sigma-Aldrich, 1.6 g), CH_3COOH (Sigma-Aldrich, 2.3 ml) and HCl (Fluka 37%, 0.74 ml) were dissolved in 30 ml of ethanol and then added to tetrabutyl orthotitanate TBOT (Sigma-Aldrich, 3.5 ml). The mixture was subsequently stirred vigorously for 60 min. Ethanol was then evaporated at 40°C and a relative humidity of 40% for 12 h followed by the transfer of the sample into an oven and aging at 65 °C for an additional 24 h. The as-made mesostructured hybrids were calcined at 450 °C in air for 4 h to obtain hexagonal P*6m* mesoporous TiO_2. Figure 2.3 summarises the preparation procedure of mesoporous TiO_2.
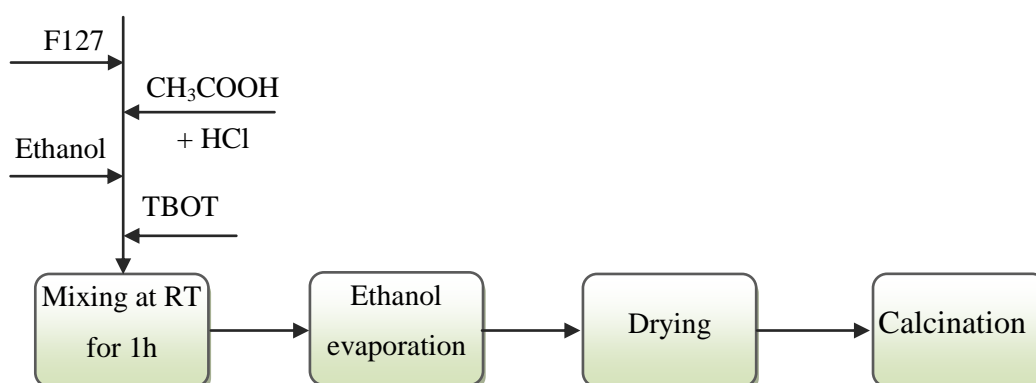
Figure 2.3: Flow-chart summarising the mesoporous TiO$_2$ preparation procedure.

The obtained mesoporous TiO_2 was suspended in a mixture of hydrochloric acid (0.1 N) and absolute ethanol by stirring at ambient temperature. PC slides pre-coated with SiO_2 (see section 2.1.2) were dipped in the suspension of mesoporous TiO_2 and subsequently withdrawn three times into the open air (T = (21±1)°C, h_r = (44±3)%) at a pulling rate of 6 cm s^{-1}. Then the films were aged at 80 °C in air for 24h to evaporate the organic solvent and HCl.

Figure 2.4 summarizes the preparation of TiO_2 thin films on SiO_2-coated PC.
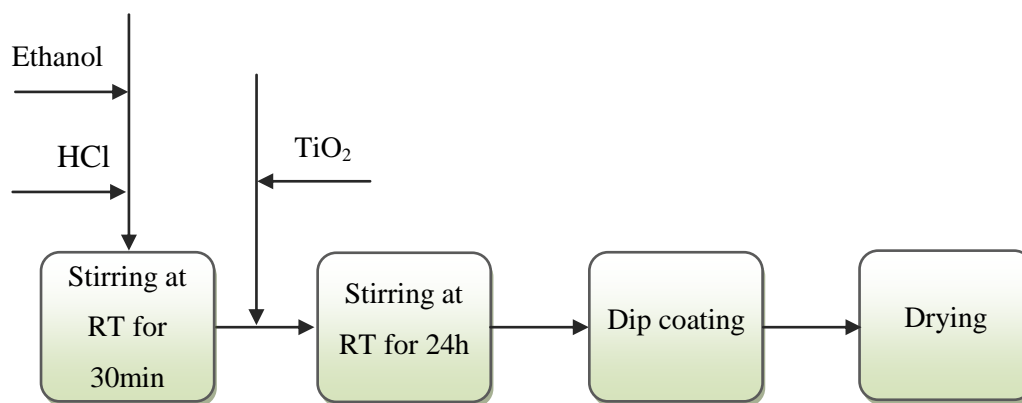
Figure 2.4: Flow-chart of the preparation of TiO$_2$ thin films on SiO$_2$-coated PC.

2.1.3.2   Preparation of the TiO$_2$-ZnO Films

Titanium tetraisopropoxide (TIPT) (Aldrich, 97 wt%) and zinc acetate (Zn(ac)$_2$), (Fluka, 99.99 wt%) were used as metal sources for the synthesis of TiO$_2$, ZnO, and TiO$_2$-ZnO films. The non-ionic amphiphilic triblock copolymer (PEO)$_{20}$(PPO)$_{70}$(PEO)$_{20}$ (Pluronic P123, Sigma-Aldrich) was employed as a templating agent.

Initially pluronic and ethanol were stirred at room temperature (RT) for 30 minutes. Then HCl and TIPT were added to prepare a TiO$_2$ sol. TIPT: P123: HCl: C$_2$H$_5$OH molar ratios in the reacting solution were 1: 0.01: 0.5: 41. Varying amounts of Zn(ac)$_2$ were added directly to the sol to obtain molar ratios of TIPT:Zn(ac)$_2$ 1 : 0, 1 : 0.025 , 1 : 0.05 , 1 : 0.1 , 1 : 0.2, 0 : 0.1). The resulting suspension was stirred until the Zn(ac)$_2$ was totally dissolved. The mixture was diluted with ethanol and stirred at RT for 24 h. Subsequently, the films on the SiO$_2$ coated polycarbonate were prepared by dip-coating (T = (21±1)°C, h$_r$ = (44±3)%). These dip-coated films were aged in an oven for 24 h at 80°C and then for 2h at 120C° followed by irradiation with UV(A) light (10 W m^{-2} , 20 W UV tube, Eurolite) in order to remove any residue. Figure 2.5 summarises the sol-gel preparation of TiO$_2$-ZnO and the PC coating procedure.
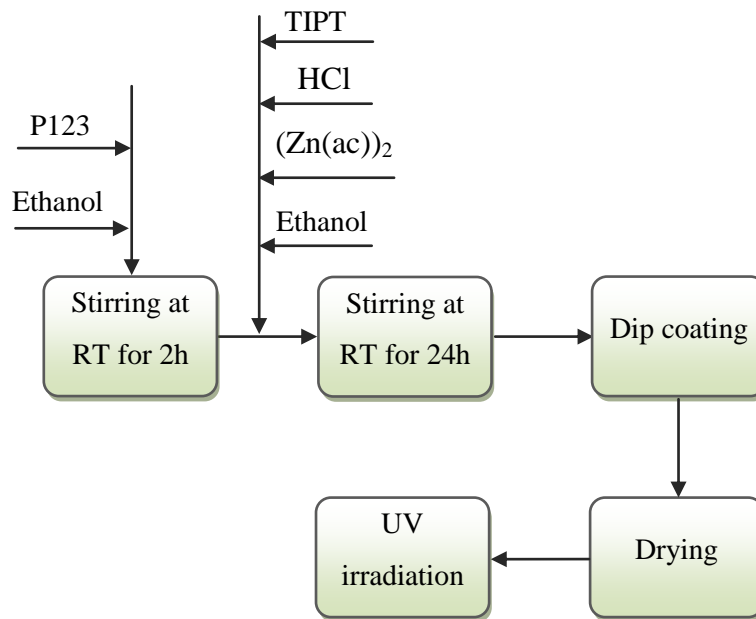
Figure 2.5: Flow-chart summarising the preparation of a TiO₂-ZnO sol-gel and the PC coating procedure.

2.1.3.3   Preparation of Hombikat UV100, and Hombikat UV100-SiO$_2$ Films

A mixture of TiO$_2$ powder (Sachtleben Hombikat UV100) and TEOS (Roth $\geq$ 98%) was used for the preparation of the thin films.

The TiO$_2$-SiO$_2$ sol-gel was prepared by adding TEOS (22.2 ml) to a mixture of ethanol (29.2 ml), water (7.2 ml) and hydrochloric acid (3.6%, 0.4 ml) followed by stirring at ambient temperature in air for one hour. TiO$_2$ (0.2 g) was added to the mixture (0.29 − 1.47 ml) which subsequently was diluted with absolute ethanol yielding the final volume of 50 ml. The resulting sol was dip coated onto the PC surface into open air (T = (21±1)°C, h$_r$ = (44±3)%) with a pulling rate of 6 cm.min^{-1} and then furnace dried in air at 80°C for 24 h. Figure 2.6 summarizes the preparation of TiO$_2$-SiO$_2$ thin films on SiO$_2$-coated PC.

TEOS

HCl

Ethanol

| Mixing at RT for 30min | → | Stirring at RT for 24h | → | Dip coating |

TiO$_2$

Drying
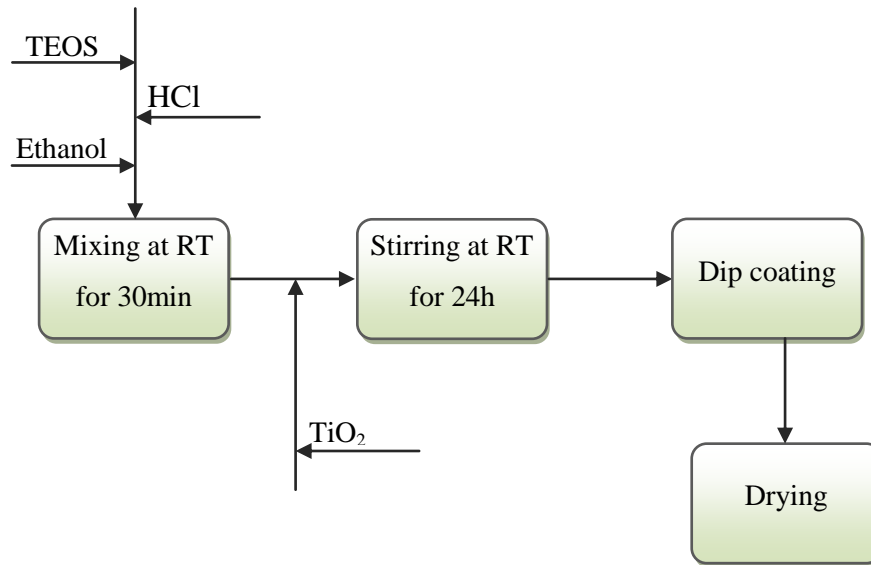
Figure 2.6: Flowchart of the preparation of TiO$_2$-SiO$_2$ thin films on SiO$_2$ coated PC.

2.2   Characterization

2.2.1   Optical Properties of the Films

To characterize the optical properties of the prepared films, the absorption spectra of the films in the range 400-800 nm were recorded using the UV/Vis spectrophotometer Cary 100Bio (Varian, Australia).

2.2.2   Films Thickness

The thickness of the films was determined by means of ellipsometry using an ellipsometer (ELX-02C, Dre Germany).

2.2.3   Hydrophilic Properties of the Film

The hydrophilic properties of the prepared films were determined by measuring the contact angle of water using a CAM 100 optical contact angle meter (KSV Instruments LTD, Helsinki).

2.2.4   High- Resolution Transmission Electron Microscopy

Transmission electron microscopy (TEM) was conducted at 200 kV with a JEOL JEM-2100F-UHR field emission instrument equipped with a Gatan GIF 2001 energy filter and a 1k-CCD camera in order to obtain EEL spectra.

2.2.5   X-Ray Diffraction

Wide-angle X-ray diffraction (WXRD) data were acquired on a Bruker AXS D4 Endeavor X-diffractometer using Cu KR1/2, λR1 = 154.060 pm, λR2 = 154.439 pm radiation, whereas, the small-angle X-ray diffraction (SXRD) patterns were recorded on a Bruker D8 Advance instrument.

 Also, the X-ray powder diffractometer STADI P from STOE (Cu-K α_1 radiation) equipped with a PSD detector was used. Each sample was measured for 90 s in the range between 5° and 75°(2θ).   A JEOL JSM-6610 LV Scanning Electron Microscope with a Bruker X-Flash Detektor 410-M was used to measure the EDX.

2.2.6   Specific Surface Area Measurements

The nitrogen adsorption and desorption isotherms at 77° K were measured using a Quantachrome Autosorb 3B after the samples were vacuum-dried at 200 °C overnight. The sorption data were analyzed using the Barrett-Joyner-Halenda (BJH) model with the Halsey equation.

2.2.7   Atomic Force Microscopy

The surface relief of the films was revealed by atomic force microscopy (AFM) using a digital instruments NanoScope apparatus.

2.2.8   Thermogravimetric Analysis

Thermogravimetric measurements were carried out on a Setaram Setsys evolution 1750 thermoanalyzer up to 600°C applying heating rates of 10 °C/min under oxygen.

2.2.9   Fourier Transform Infrared Spectroscopy

FT-IR spectra of the powders scratched from the prepared films were recorded with a BRUKER FRA 106 spectrometer using the standard KBr pellet method.

2.3   Photocatalytic Testing

2.3.1   Photocatalytic Degradation of Methylene Blue

The photocatalytic tests were performed in an aqueous solution using methylene blue (Aldrich, λ_{max} = 661 nm) as the probe molecule according to the procedure described in the DIN 52980 standard method [67].The samples were irradiated with 10 W m^{-2} UV(A) light (20 W UV tube, Eurolite). Figure 2.7 shows the setup used for the methylene blue photocatalytic test. The photodegradation of the dye was followed by measuring the absorption spectra using a UV/VIS spectrophotometer (Cary 100Bio, Varian, Australia). The photonic efficiency ζ was calculated for all tested films from these results.
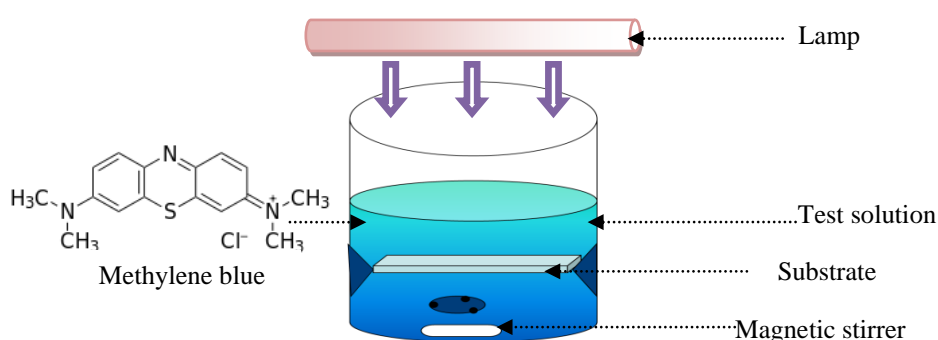
Figure 2.7: Setup for the photocatalytic methylene blue degradation test.

The photonic efficiency ξ is calculated from the following equation

$$\xi(\%) = \frac{k\,C_o\,V}{J_o\,A}\,100 \qquad\qquad Eq.\ 2.1$$

where,

k is the initial rate of the photoreaction in s^{-1} (slope of ln (C_o/C_i) *vs.* time);

C_o is the intial concentration of organic pollutant in $mol.L^{-1}$; V is the volume of solution in L;

A is the illuminated area in m^2; and J_o is the photonic flux in $mol.m^{-2}.s^{-1}$.

2.3.2   Photocatalytic Degradation of Methyl Stearate

For the solid phase tests, a thin film of methyl stearate (Aldrich) was coated onto a well-defined surface area of the coating being (5 cm × 7.5 cm) by evenly spreading a solution of methyl stearate in n-hexane (0.5 ml of a 5 mM solution). After UV(A) illumination for 24 h $(10Wm^{-2})$, the remaining methyl stearate film was washed from the surface employing 5 ml n-hexane. The concentration of methyl stearate was measured by gas chromatography (GC–2010, Shimadzu, Japan; column Rtx-5, carrier gas Helium, initial temperature 20 °C, end temperature 310 °C, heating rate 60 °C/min). Figure 2.8 presents the setup for the photocatalytic methyl stearate degradation.
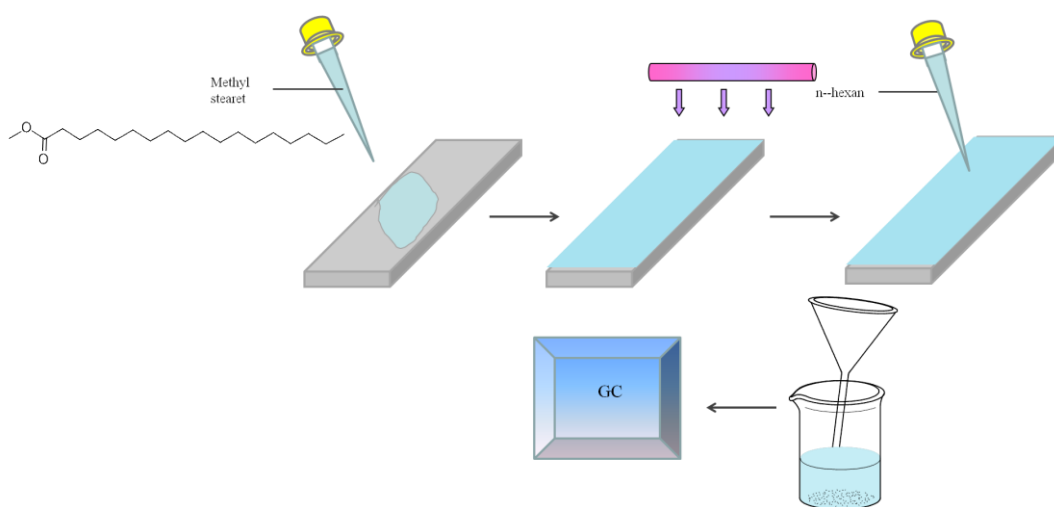
Figure 2.8: Setup of the methyl stearate photocatalytic degradation test.

2.3.3   Photocatalytic Degradation of Acetaldehyde

The photocatalytic degradation of acetaldehyde to ISO 22197-2:2011 [68] was carried out in an experimental setup consisting of the respective gas supplies, the photoreactor, and a gas chromatograph for acetaldehyde analysis (GC 955 Syntech Spectras) according (Figure 2.9).
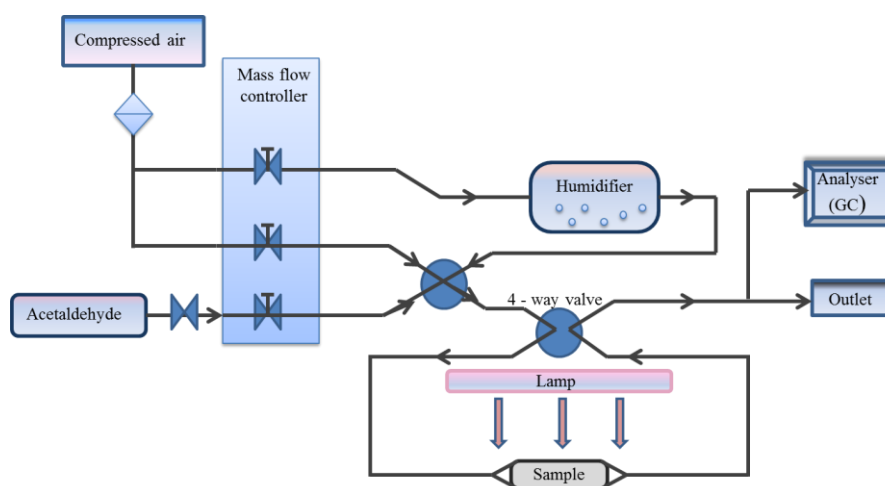
Figure 2.9: Setup for the photocatalytic acetaldehyde degradation test.

The films were placed in an acrylic glass reactor which was then subjected to a moist air flow of 1L.min^{-1} with an acetaldehyde concentration of 5 ppm. The acetaldehyde concentration in the outlet gas flow was monitored by using a Synspec Spectras GC955 gas chromatograph. Each sample was measured in the dark until an equilibrium concentration was reached and afterwards under illumination until an equilibrium concentration was attained. For irradiation, a CLEO Compact (Philips) ultraviolet light source was used.

2.4   Testing the Self Cleaning Performance of the Prepared Films

The combined effect of photooxidation and photo-induced wetability was determined according to the procedure described in the ISO 27448 standard method [69]. The procedure can be described as follows: a 0.5% (by volume) solution of oleic acid (Merck, extra pure) was prepared by dilution in n-heptane (Sigma-Aldrich, anhydrous 99%). The prepared solution was used to dip the polycarbonate test pieces (3.5cm × 2.5cm) at a speed 60 cm min^{-1}.

The test pieces were dried at 70° C for 15min. Then the polycarbonate test pieces were irradiated with UV(A) light at (10 ± 1) W m^{-2}. The contact angle of water was measured at regular intervals during the irradiation time at five different places on each test piece. The experiment was carried out at a temperature of $(21 \pm 1)°$C and a relative humidity of $(44\pm 3)\%$.

The initial contact angle θ_1 shall be greater than or equal to 20°. The final contact angle is calculated by

$$\bar{x} = \frac{\theta_{n1} + \theta_{n2} + \theta_{n3}}{3} \qquad\qquad Eq. \ 2.2$$

$$\frac{s}{\bar{x}} \leq 10\% \qquad\qquad Eq. \ 2.3$$

$$\theta_f = \bar{x} \qquad\qquad Eq. \ 2.4$$

where; θ_{n1} is the contact angle after n1 h, in degrees; θ_{n2} is the contact angle after n2 h, in degrees; θ_{n3} is the contact angle after n3 h, in degrees; $\bar{x}$ is the average of the three consecutive points , in degrees; s is the standard deviation of the three consecutive points , in degrees; and θ_f is the final contact angle, in degrees.

2.5   Evaluation of the Photoinduced Hydrophilicity of the Prepared Films
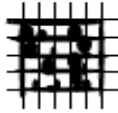
The photoinduced hydrophilicity of the prepared films was evaluated by water contact angle measurements. First of all the prepared films were irradiated by UV(A) light. Then they were stored in the dark under ambient conditions or in the presence of either acetone or propan-2-ol until their contact angles increased. The water contact angles were measured during the storage time. Following the increase of the contact angle of the prepared films during their storage in the dark, the films were irradiated by UV(A) until a superhydrophilic

surface was once again attained. Their contact angles were also measured during the irradiation time.

2.6 Quantitative Estimate of the Adhesion of the Prepared Films after UV Irradiation

A cross-cut test according to the DIN EN ISO 2409 standard [70] was applied to obtain a qualitative impression of the adhesion of the deposited layers on the polycarbonate surface after exposure to UV(A) light (10 W m^{-2}; 20 W UV tube, Eurolite) for a total time of three months.

Table 2.1: Illustration of the ISO 2409 standard.

Crumbling	Example	Ranking
No		0 = excellent
< 5%.		1 = very good
5%-15%.		2 = good
15%-35%.		3 = moderate
35%-65%.		4 = poor
>65%.	-	5 = very poor

The cross-cut test was applied manually. The coated polycarbonate sheets were crisscrossed with a razor blade to form small squares (0.5 cm × 0.5 cm). An adhesive tape was stuck on the network surface and hauled almost with constant force. A part of the squared

surface crumbled from the edge of the squares. The crumbling is a measure of the adhesion quality. A microscope (Olympus IXSO) with zoom lenses (×40) was used to clearly identify the possible cracks. According to DIN EN ISO 2409, the quality of adhesion is ranked by different numbers ranging from 0 to 5 as is shown in Table 2.1.

2.7   Abraison Resistance of the Thin Film

The abrasion resistance of the thin films was examined by felt - abrasion tests (felt 2.5 cm × 3.5 cm, 70 g cm^{-2}, 74 min^{-1}).

The abrasion of the felt can remove parts of the film while it moves forth and back across the film surface. The amount of the removed parts is depending on the mechanical stability of the films. The decrease of the photcatalytic activities for methylene blue degradation, and the change of water contact angles of the prepared films were measured after the abrasion test. Figure 2.10 presents the felt abrasion test device.
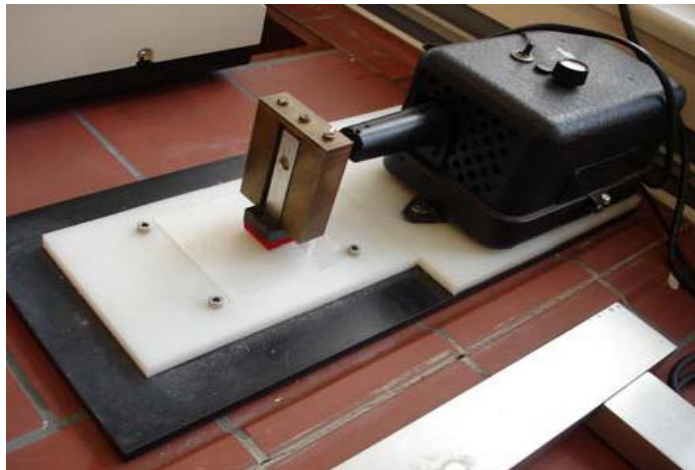
Figure 2.10: Felt - abrasion test device.

3   Results

3.1   Modification of Polycarbonate Surface

In order to form reactive groups, i.e. hydroxylated and/or carboxylated groups, suitable for the formation of chemical bonds with the metal oxides, the surface of the polycarbonate sheets was modified by irradiation with UV(C) at 254 nm.

First of all, the polycarbonate substrates were washed with water, deionized water, and propan-2-ol and dried. After that, the polycarbonate sheets were irradiated by UV(C) light to form hydroxylated and/or carboxylated surfaces.
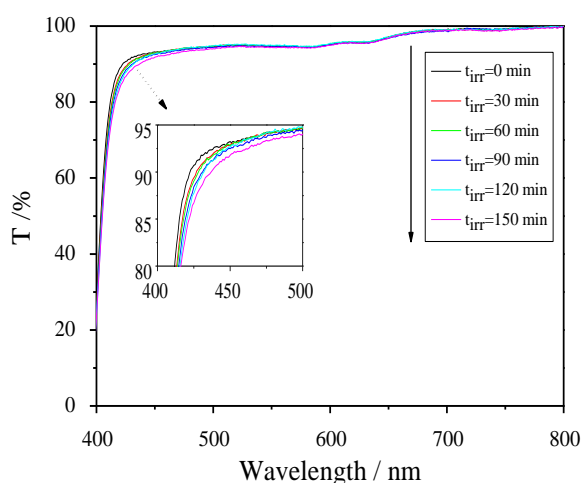
Figure 3.1: UV/Vis transmission spectra of irradiated PC at different times

As can be seen in the Figure 3.1, there is a shifting in the transmission spectra after the UV(C) irradiation of polycarbonate indicating a change of the optical properties. Thus, the irradiated polycarbonate sheets progressively turned to yellow during their exposure to UV(C) light.

The achieved modification of the polycarbonate surface after the irradiation was analysed by FT-IR measurements. As shown in Figure 3.2 an increase in the absorbance intensity at $3550-3700$ cm^{-1} was detected. The bands at 3470 and 3660 cm^{-1} are attributed to free O–H

groups and the aromatic O-H stretching of the rearrangement products, respectively. Moreover, the increase of the absorption at 1629 cm^{-1} and 1689 cm^{-1} suggests that photo-Fries products might be present in the irradiated films [51].
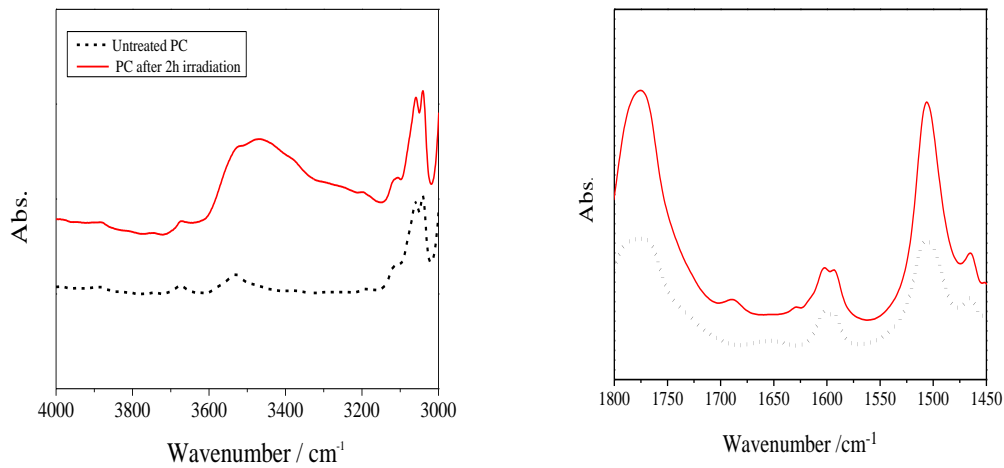
Figure 3.2: FT-IR transmission spectra of PC and of PC irradiated with UV(C) light for 2h.

The formation of hydroxyl groups upon UV(C) treatment was confirmed by water contact angle measurements. Table 3.1 presents the mean water contact angle of irradiated PC after different irradiation times. It is clearly seen that the mean contact angle of irradiated PC decreases gradually from 81° to 68° during 2h UV(C) irradiation.

Table 3.1: Water contact angle of irradiated PC in different UV(C) times

Irradiation time/min	CA/1°
0	81 ± 4
30	74 ± 4
60	71 ± 3
90	69 ± 5
120	68 ± 4
150	64 ± 2

3.2 SiO$_2$ intermediate Layer

After the modification of the polycarbonate sheet with UV(C) light, SiO$_2$ intermediate layers were coated on the irradiated polycarbonate surface. After preparing the SiO$_2$ sol by hydrolyzing tetraethylorthosilicate in the presence of hydrochloric acid (c.f. section 2.1.2), the SiO$_2$ sol was coated on the PC sheets surface forming a transparent SiO$_2$ layer. Some physical and physicochemical properties of the SiO$_2$ layers are presented in Table 3.2.

Table 3.2: Thickness, water contact angle, and transparency of a SiO$_2$ intermediate layers.

Property	Value
Thickness / nm	33 ± 9
Water contact angle / 1°	57 ± 5
Transparancy at 500nm /%	97.91

The prepared SiO$_2$ intermediate layer is transparent for visible light as can be seen in the UV/Vis spectrum presented in Figure 3.3. Moreover, the SiO$_2$ prepared by this method is amorphous with no crystallized phases, according to the XRD spectrum of SiO$_2$ particles obtained after scratching the SiO$_2$ layer from the surface of SiO$_2$ coated PC which is shown in Figure 3.4.
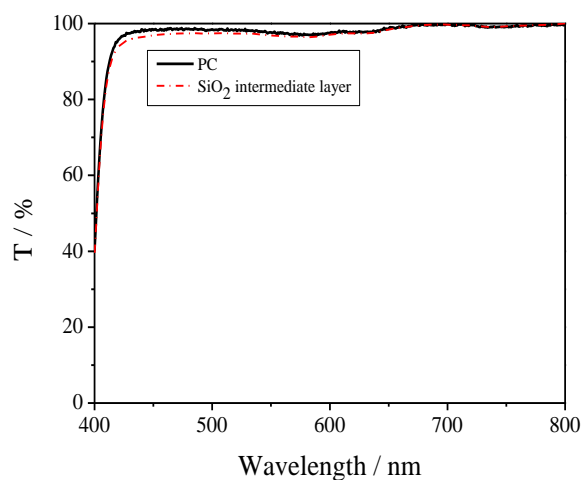
Figure 3.3: UV/Vis transmission spectra of uncoated PC and PC coated with a SiO$_2$ intermediate layer.
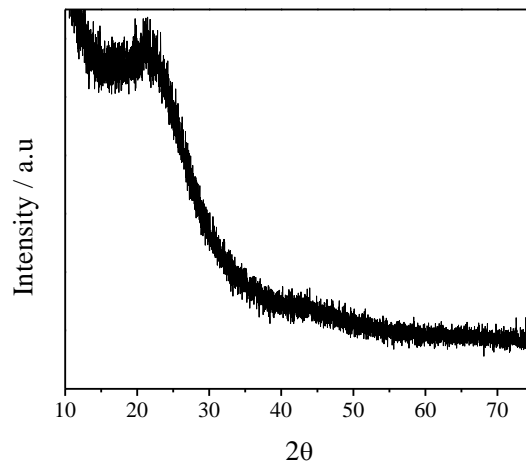
Figure 3.4: The XRD pattern of SiO₂ scratched from the surface of SiO₂ coated PC.
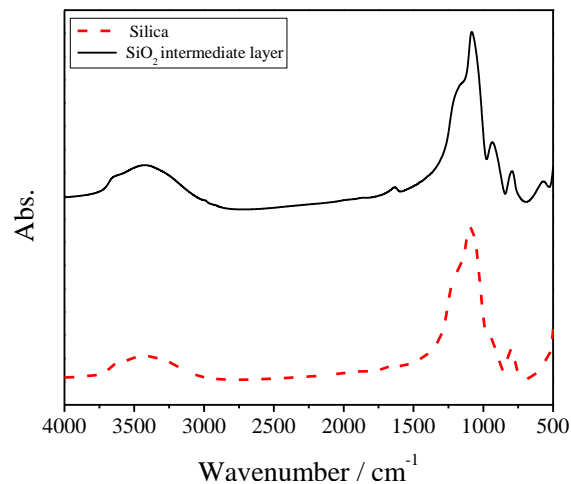
Figure 3.5: FT-IR transmission spectra of a SiO₂ intermediate layer.

Figure 3.5 shows the comparison between the FT-IR transmission spectra of a thus prepared SiO_2 intermediate layer and that of commercial silica. A peak around 1082 cm^{-1} is attributed to Si-O-Si bonds, and a broad signal around 3430 cm^{-1} is attributed to the stretching mode of adsorbed water and/or hydroxyl groups [71].

The AFM images of the UV(C) treated PC as well as of a SiO_2 intermediate layer are shown in Figure 3.6 and Figure 3.7, respectively. These images illustrate that coating of the polycarbonate with a SiO_2 intermediate layer decreases the roughness of its surface from 9.1 nm to 1.2 nm.
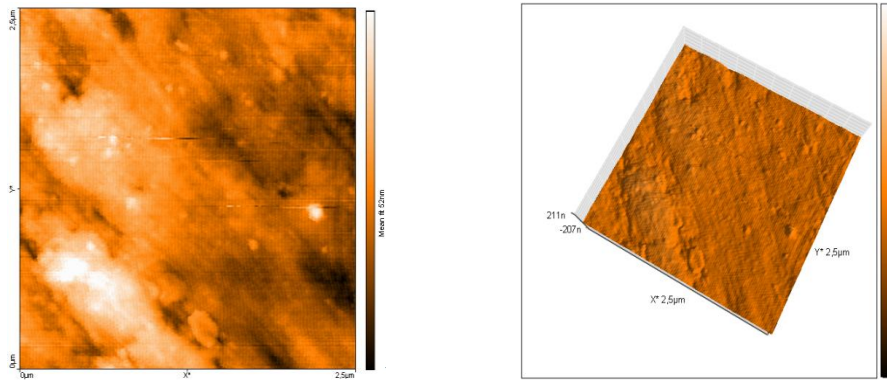
Figure 3.6: Two-dimensional and three-dimensional AFM image of the polycarbonate substrate after UV(C) irradiation.
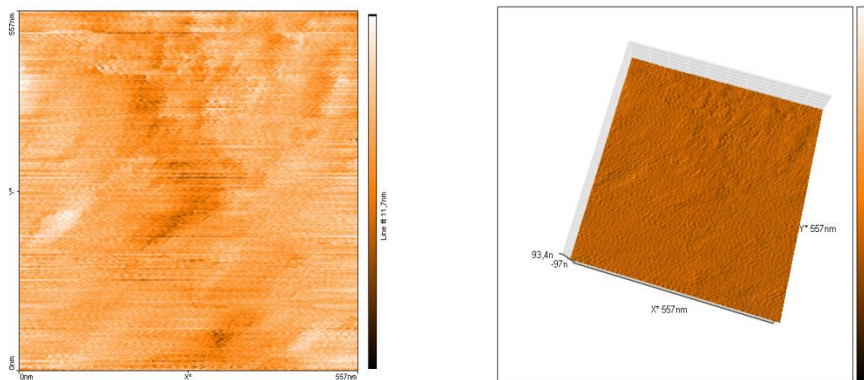
Figure 3.7: Two-dimensional and three-dimensional AFM image of the SiO$_2$ intermediate layer deposited onto a PC surface pre-treated with UV(C) irradiation.

3.3 Pilkington Activ^{TM} glass as a References

The photocatalytic activities of all prepared coatings were compared with that of the commercial Pilkington Activ^{TM} sheet glass. To ease the comparison between Pilkington Activ^{TM} and the prepared films, all obtained results of Pilkington Activ^{TM} are summarized here.

Figure 3.8 shows the changes of the UV/Vis absorption spectra of methylene blue during its photocatalytic decomposition on the Pilkington Activ^{TM} surface. The degradation rate was determined from the decrease of the concentration of methylene blue during the time of its photocatalytic degradation on Pilkington Activ^{TM} as shown in Figure 3.9. This rate was

employed to determine the photonic efficiency for the methylene blue degradation on Pilkington Activ^{TM} according to Eq. 2.1.
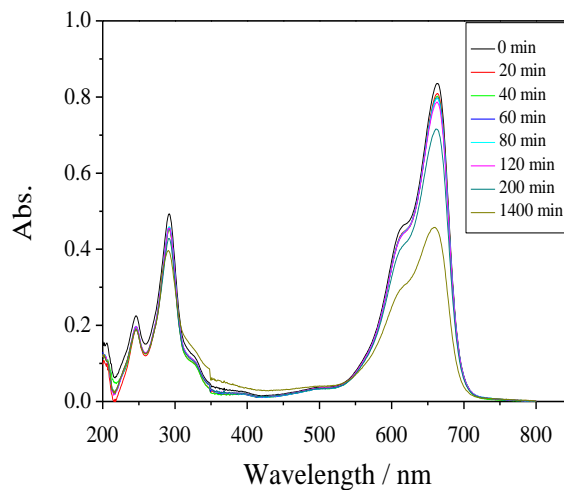
Figure 3.8: Absorbance vs wavelength as a function of illumination time for the photocatalytic degradation of methylene blue on Pilkington Activ^{TM} (I = 10W.cm^{-2},MB concentration [10 μmol.l^{-1}], volume of MB (test solution) = 100 ml, illuminated area =3.5 cm - 2.5 cm).
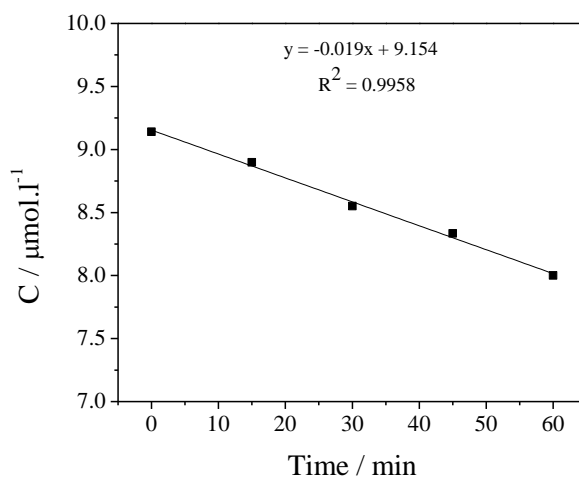
Figure 3.9: Decrease of the concentration of methylene blue during the time of its photocatalytic degaradation on Pilkington Activ^{TM}.

Similarly, the photonic efficiencies of Pilkington Activ^{TM} for methyl stearate and acetaldehyde photocatalytic degradation were calculated employing Eq. 2.1.

Figure 3.10 summarizes the obtained photonic efficiencies of Pilkington Activ^{TM} for the photocatalytic methylene blue, methyl stearate, and acetaldehyde degradation (PE% for MB, MS, and AA = 0.026%, 0.009%, and 0.020% respectively).
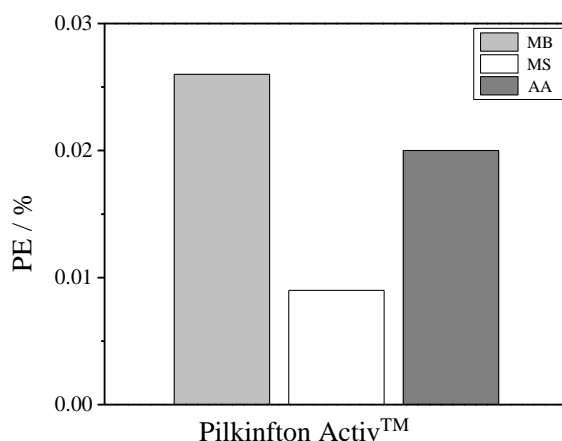
Figure 3.10: Photonic efficiencies ξ of the photocatalytic degradation of methylene blue (MB), methyl stearate (MS) and acetaldehyde (AA) on Pilkington Activ^{TM} glass.

Following the application of the felt abrasion test decrease of the photonic efficiency of Pilkington Activ^{TM} concerning the photocatalytic degradation of methylene blue is found to be 45%.

The contact angle of Pilkington Activ^{TM} was measured before and after UV(A) irradiation and was found to be 67 ± 2 and $\leq 5°$ respectively. Moreover, this commercial glass conserves its hydrophilic properties during its storage in the dark under an ambient atmosphere for 9 days. After a subsequent irradiation by UV light, the hydrophilic properties can be recovered again. Figure 3.11 shows the change of the water contact angle measured on Pilkington Activ^{TM} film after its storage in the dark and its irradiation by UV light.

The change of the water contact angle of Pilkington Activ^{TM} was studied during its storage in the dark, in the presence of Propan-2-ol as well as in the presence of acetone, and after subsequent irradiation by UV(A) light.
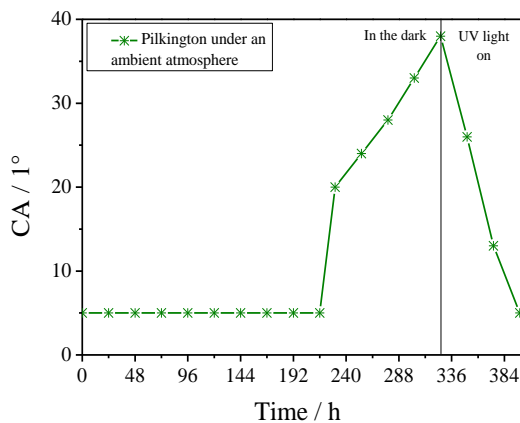
Figure 3.11: Change of the water contact angle on UV(A) pre-irradiated Pilkington Activ^{TM} glass during its storage in the dark and its subsequent irradiation by UV(A) light (10Wm^{-2}).
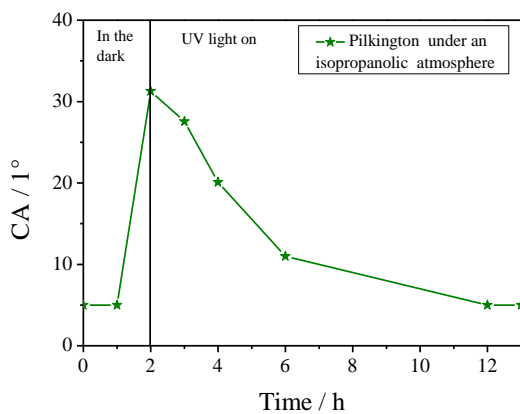
Figure 3.12: Change of the water contact angle on UV(A) pre-irradiated Pilkington Activ^{TM} glass during its storage in the dark in presence of Propan-2-ol and its subsequent irradiation by UV(A) light (10Wm^{-2}).
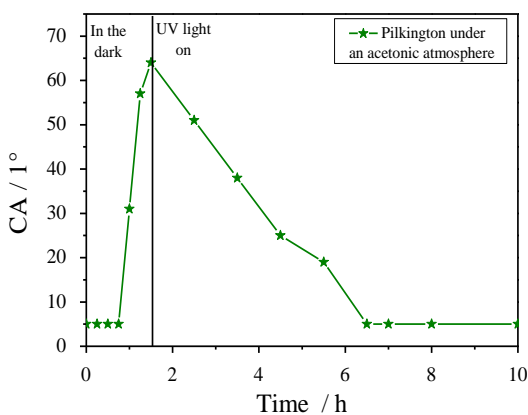
Figure 3.13: Change of the water contact angle on UV(A) pre-irradiated Pilkington Activ^{TM} glass during its storage in the dark in presence of acetone and its subsequent irradiation by UV(A) light (10Wm^{-2}).

Figure 3.12 and Figure 3.13 present the change of the water contact angle on Pilkington Activ^{TM} glass after its storage in the dark in the presence of the Propan-2-ol and acetone, respectively. It can be seen from these Figures that the water contact angle of Pilkington Activ^{TM} increased during 2h to decrease again to ≤5°after irradiation of Pilkington Activ^{TM} surface. However, in the presence of acetone, the surface lost its wettability just after 1h.
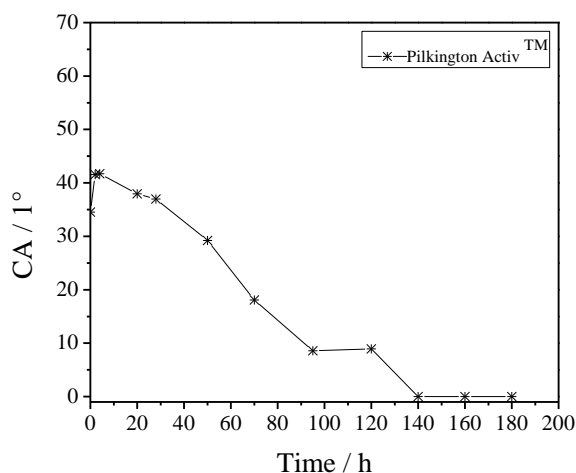
Figure 3.14: Change the contact angle of water during the photocatalytic degradation of oleic acid on Pilkington Activ^{TM} glass.

The self-cleaning properties of Pilkington Activ^{TM} were studied during the photocatalytic degradation of oleic acid which is monitored by the change of the water contact angle. As can be seen in Figure 3.14 Pilkington Activ^{TM} needs about 140h to degrade the entire amount of oleic acid on its surface and to recover its hydrophilicity.

3.4   The photocatalytically Active Films

3.4.1   Mesoporous TiO$_2$

3.4.1.1   Characterization

The polycarbonate (PC) substrates, which have been firstly pre-coated by a SiO$_2$ thin film, were subsequently dipped into ethanolic suspensions of the separately prepared mesoporous

TiO$_2$ to induce the formation of the photocatalytically active thin films on their surfaces. The films are found to be highly transparent, and the substrate has obviously not been damaged.

Figure 3.15 shows the optical transmission spectra of a PC substrate that has been pre-coated with SiO$_2$ and then coated with a mesoporous TiO$_2$ film. The inset in Figure 3.15 shows the digital photographs of the pre-coated PC substrate and of the mesoporous TiO$_2$ coating. It is obvious that the mesoporous films prepared here are transparent and homogenous.
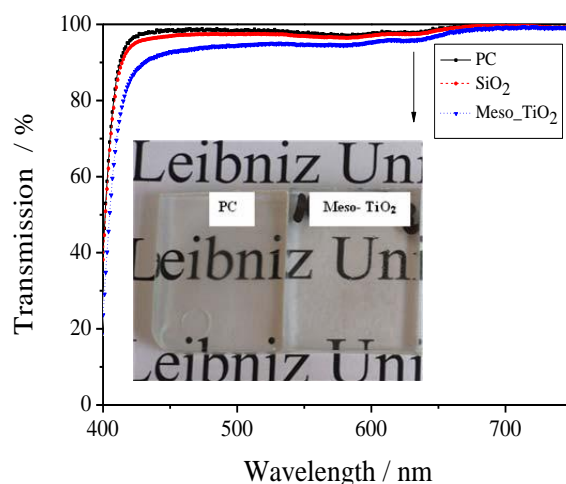
Figure 3.15: Optical transmission spectra of an uncoated polycarbonate (PC) substrate, a PC substrate precoated with SiO$_2$, and a PC subsequent coated with mesoporous TiO$_2$. Inset: digital photograph of a PC substrate (left) and a mesoporous TiO$_2$ coating on a PC substrate (right).

The thickness of the thus prepared TiO$_2$ layer is 203 ± 4 nm. Its initial water contact angle is 48° ± 5° and decreases to ≤ 5° after the UV irradiation of the prepared film for 700h.

The X-ray diffraction patterns of the prepared mesoporous TiO$_2$, and of Hombikat UV100 (as reference) are shown in Figure 3.16. XRD pattern for mesoporous TiO$_2$ and Hombikat UV100 show reflections with peaks characteristic for the (101), (004), (200), (211) and (213) lattice planes of the anatase phase. Moreover, it is found from the XRD measurements that the TiO$_2$ nanocrystal sizes are 10nm for both mesoporous TiO$_2$ or Hombikat UV100.
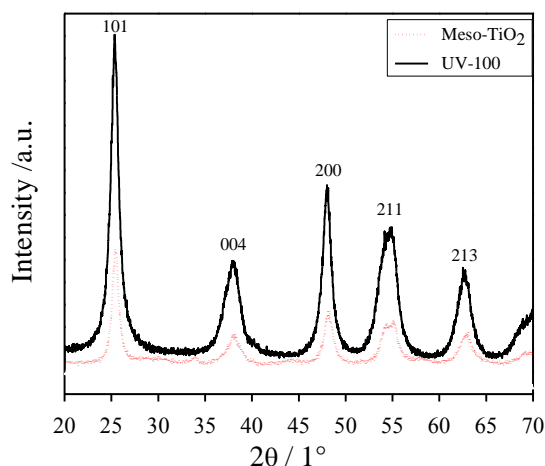
Figure 3.16: X-Ray diffraction pattern of the prepared mesoporous TiO₂ and of the commercial Hombikat UV100.

Nitrogen adsorption isotherms of mesoporous TiO_2 and of Hombikat UV100 are shown in Figure *3.17*.
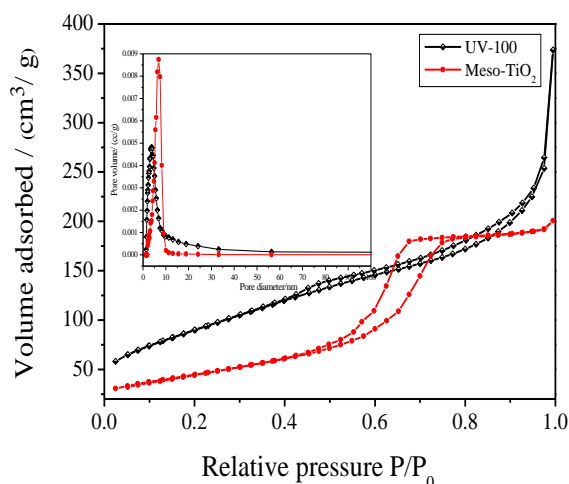
Figure 3.17: N₂ adsorption isotherms and pore size distributions (inset) of mesoporous TiO₂ and of commercial Hombikat UV100.

Typical reversible type IV adsorption isotherms are found for the mesoporous TiO_2, whereas, Hombikat UV100 also exhibits a certain porosity [72] which can be attributed to the formation inter-particle pores located between the agglomerates. The sharpness of the inflection resulting from capillary condensation at relative pressures P/P_0 between 0.45 and 0.7 is characteristic for mesopores ordered in two-dimensional hexagonal symmetry. The

BET surface areas of the mesoporous TiO_2 and of Hombikat UV100 are 174 and 234 m^2g^{-1}, respectively, and their pore volumes are 0.29 and 0.32 cm^3g^{-1}, respectively.
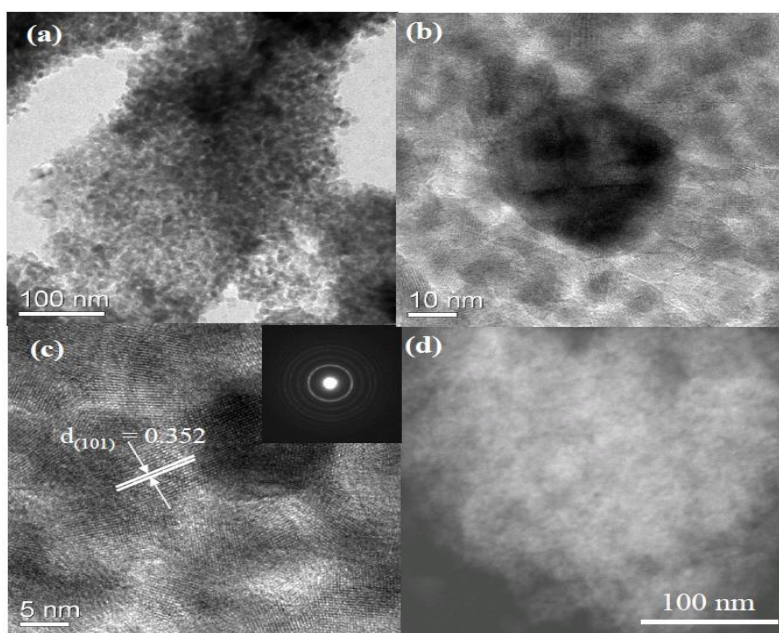
Figure 3.18: TEM images of mesoporous TiO_2 powder calcined at 450 °C (a). Overview image of mesoporous TiO_2 at low magnification (b). HRTEM image of the TiO_2 anatase phase showing the (101) face (c), the inset shows the SAED patterns for the anatase phase at 450°C (c). Dark-field TEM image of commercial Hombikat UV-100 (d).

TEM images of mesoporous TiO_2 and of Hombikat UV100 are presented in Figure 3.18. The particles are not agglomerated and quite uniform in size and shape (Figure 3.18 a). An overview image at low magnification illustrates that the self-prepared TiO_2 exhibits an ordered mesostructure (Figure 3.18 b). Both, the HRTEM image (Figure 3.18 c) and the selective area electron diffraction (SAED, inset Figure 3.18 c) show well resolved (101) lattice fringes (distance: 0.352 nm) and diffraction cycles indicative of a highly crystalline TiO_2 anatase framework. The particle size of these TiO_2 nanocrystals has been measured to be between 8 and 10 nm. The dark-field TEM image of commercial Hombikat UV-100 showed that TiO_2 is homogeneous with its particle size being around 10 nm (Figure 3.18 d).

Figure 3.19 shows the two and three dimensional AFM images of the meso-TiO_2 films, clearly evincing the distribution of TiO_2 on the PC substrate. It can be clearly seen from the height images that the nanoparticles present a relatively rough textured surface; with an rms

roughness of 1.32 nm (rms represents the standard division of the values Z, with Z being the

total height range analyzed).
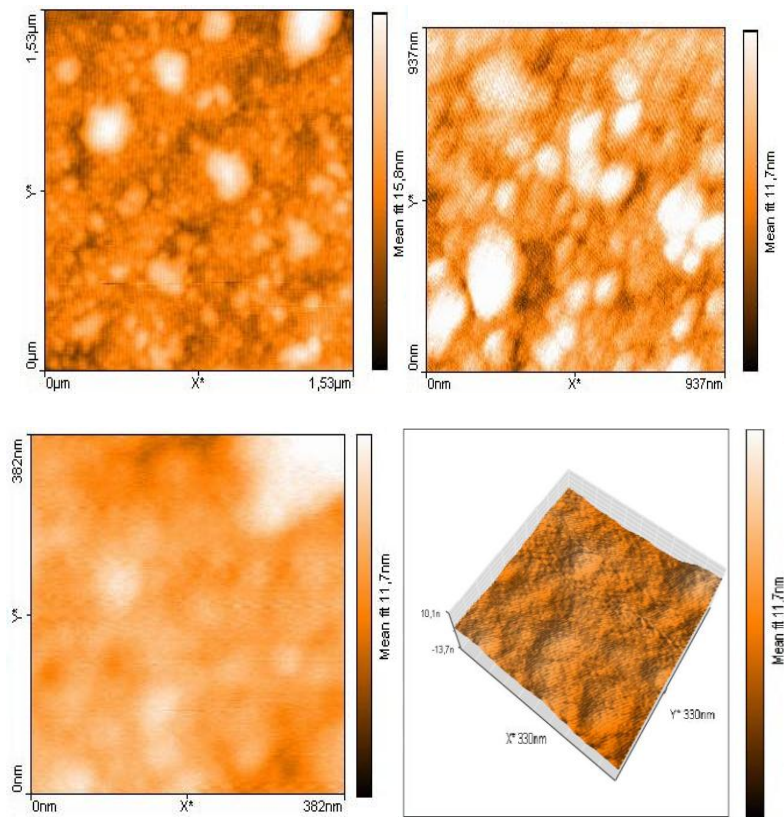
Figure 3.19: Two-dimensional and three-dimensional AFM images of a mesoporous TiO$_2$ film deposited onto the surface of a polycarbonate substrate.

3.4.1.2   Photocatalytic Testing

Photonic efficiencies ξ of the newly synthesized mesoporous TiO$_2$ films on PC were

assessed for the photocatalytic degradation of methylene blue (MB), of methyl stearate (MS)

and of acetaldehyde (AA) to be 0.078%, 0.016%, and 0.084%, respectively (see Figure 3.20).
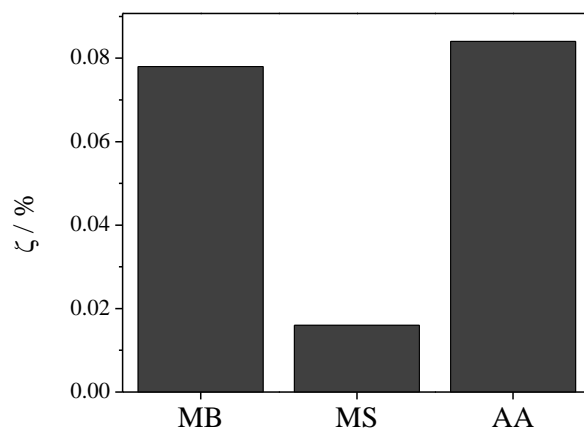
Figure 3.20: Photonic efficiencies ξ for the photocatalytic degradation of methylene blue (MB), methyl stearate (MS), and acetaldehyde (AA) on mesoporous TiO$_2$ thin films on polycarbonate.

The relationship between the thickness of the mesoporous TiO$_2$ thin films and their photocatalytic activity was assessed for the photodegradation of aqueous solutions of methylene blue. Three different films were prepared by dipping the polycarbonate into the ethanolic suspensions of mesoporous TiO$_2$ once, twice, and three times. The thickness of the film increased with the number of dipping cycles. Increasing the thickness from (148 ± 13) nm to (203 ± 4) nm resulted in an increase of the photonic efficiency from 0.038 to 0.078. The respective experimental results are shown in Table 3.3.

Table 3.3: Relationship between the thickness of mesoporous TiO$_2$ thin films and their photocatalytic activity.

Photocatalyst	Time of dipping	Thickness / nm	ζ / %
Meso-TiO$_2$	1	148 ± 13	0.038
Meso-TiO$_2$	2	184 ± 6	0.055
Meso-TiO$_2$	3	203 ± 4	0.078

It is noteworthy that the relationship between the film thicknesses and the photonic efficiencies presented in Table 3.3 is not linear. This may be attributed to the less absorbed

photons by the thinner film compared with that absorbed by the thick one while the photonic efficiencies were calculated for the total incident light.

3.4.1.3   Evaluation of the Photoinduced Hydrophilicity

To evaluate the photoinduced hydrophilicity conversion of the mesoporous TiO_2 films, the changes of the water contact angle during the UV irradiation, the storage in the dark, and during the subsequent re-irradiation period were elucidated.
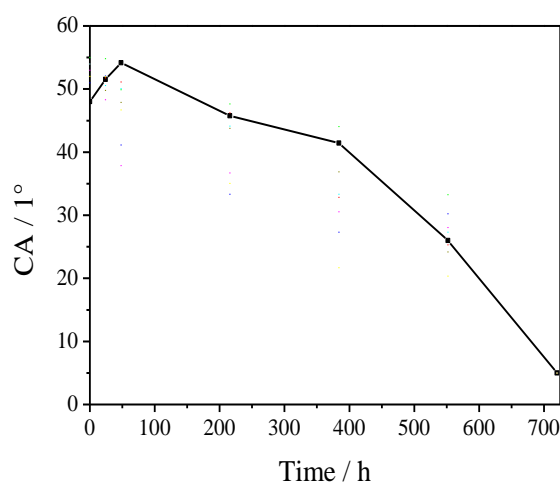
Figure 3.21: Change of the water contact angle of mesoporous TiO_2 thin films on polycarbonate during irradiation with UV(A) light (I=10Wm^{-2}).
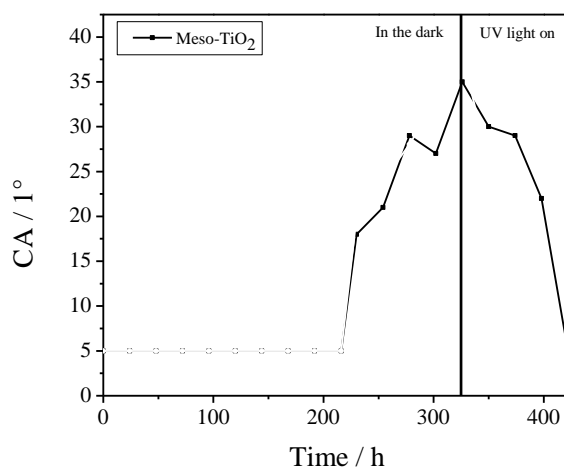
Figure 3.22: Change of the water contact angle on mesoporous TiO_2 thin films on polycarbonate after their storage in the dark and its subsequent irradiation by UV(A) light (10Wm^{-2}).

.

The change of the water contact angle of a mesoporous TiO_2 thin film on polycarbonate during the initial irradiation with UV(A) light is presented in Figure 3.21. When the thus prepared film was irradiated by UV(A) light, the water contact angle of the film decreased to around $\leq 5°$ after 700 h. After storage in the dark for 326 h, the water contact angle of this film increased to 35°. The film recovered its superhydrophilicity after the irradiation by UV(A) light for 96h (Figure 3.22).

3.4.1.4   Test of the Self Cleaning Performace

Figure 3.23 shows the change of water contact angle under UV(A) irradiation after dip - coating the prepared films with a thin layer of oleic acid. After applying oleic acid on a superhydrophilic surface, thus surface became hydrophobic. However, the surface becomes hydrophilic again after irradiation by UV(A) light as can be seen from Figure 3.23.
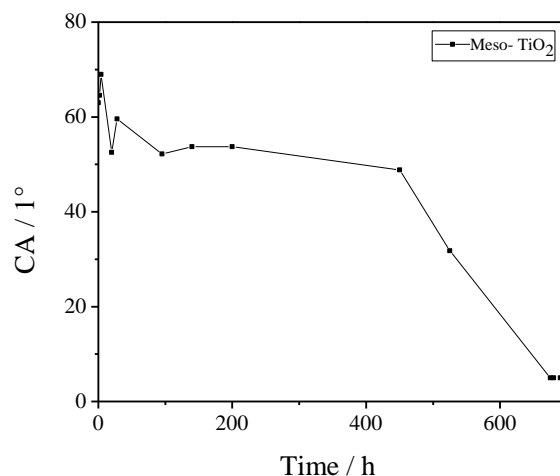
Figure 3.23: Change the contact angle of water during the photocatalytic degradation of oleic acid on a mesoporous TiO_2 film.

3.4.1.5   Quantitative Estimate of the Adhesion

To test the stability and the adhesion quality of the meso-TiO_2 film before and after irradiation, the adhesion quality was measured using optical microscopy (Figure 3.24). The samples were subjected to UV radiation for three months, and then a network of small squares was applied to the surface using a sharp instrument in order to facilitate the removal of the

TiO$_2$ and SiO$_2$ layers. A tape placed on the surface and subsequently removed at 60° degrees applying a certain constant force. The results revealed that the thus prepared films are stable against UV light and adhesive since no change is observed before and after long time irradiation.
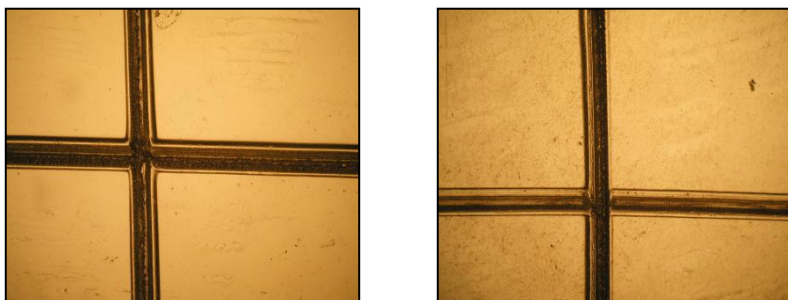
Figure 3.24: Images of a mesoporous TiO$_2$ film before and after applying a cross-cut test after three months of UV irradiation.

3.4.1.6   Abrasion resistance

A felt-abrasion test was performed to evaluate the mechanical strength of the mesoporous TiO$_2$ film against abrasion.
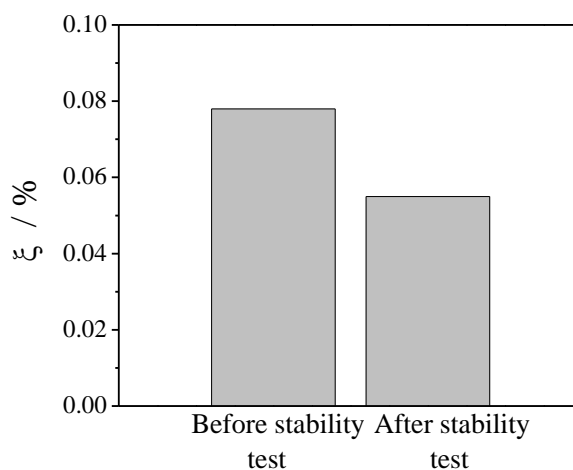
Figure 3.25: Photonic efficiencies of the photocatalytic degradation of methylene blue (MB) before and after the stability test of a mesoporous TiO$_2$ films on polycarbonate.

The decrease of the photonic efficiency for MB degradation on a mesoporous TiO$_2$ film after the abrasion test was quantitatively determined and was found to be around 30% as can be seen from Figure 3.25. In addition, the change of the water contact angle of meso-TiO$_2$ was

determined before as well as after the stability test and after its re-irradiation by UV (A) light. The water contact angle of the mesoporous TiO_2 film increased to $61° \pm 6°$ after the abrasion test and decreased again approaching superhydrophilicity after an UV irradiation for 24 h.

3.4.2 TiO_2-ZnO

3.4.2.1   Characterization

TiO_2-ZnO thin films on a SiO_2 interlayer have been successfully deposited on the polycarbonate surface by dip-coating to provide the polymeric sheets with a self-cleaning superhydrophilic and photocatalytically active surface layer.

Since organic compounds have been used during the preparation it became necessary to remove them. Therefore, the prepared films were irradiated by UV(A) light.
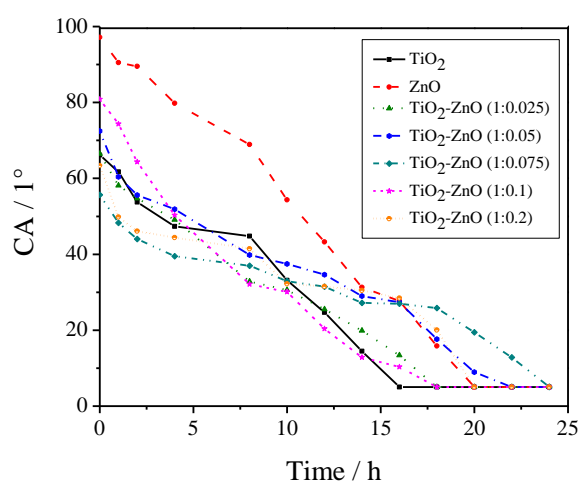
Figure 3.26: Change of the water contact angle of TiO_2, ZnO, and TiO_2-ZnO films on polycarbonate during their irradiation with UV (A) light.

The change of the water contact angle of the TiO_2-ZnO coatings during UV (A) irradiation to remove the organic compounds was studied. As can be seen from Figure 3.26, the water contact angle of the TiO_2-ZnO (1:0.05) coated surface decreases from 85º to <5º after 18 h

UV (A) irradiation while TiO$_2$-ZnO (1:0.2) needed an irradiation time of 24 h to reach a contact angle <5º.

To ensure that the structure-building agent Pluronic 123 was completely degraded thermogravametric experiments have been performed. Figure *3.27* shows the thermogravimetric curve of a TiO$_2$-ZnO film (1:0.05) (a) before and (b) after UV irradiation. The total weight loss is about 52% and 37% for TiO$_2$-ZnO (1:0.05) before and after irradiation by UV light, respectively. This significant drop is mainly attributed to the combustion of the template P123. Most of the template P123 completely decomposes at 309°C.
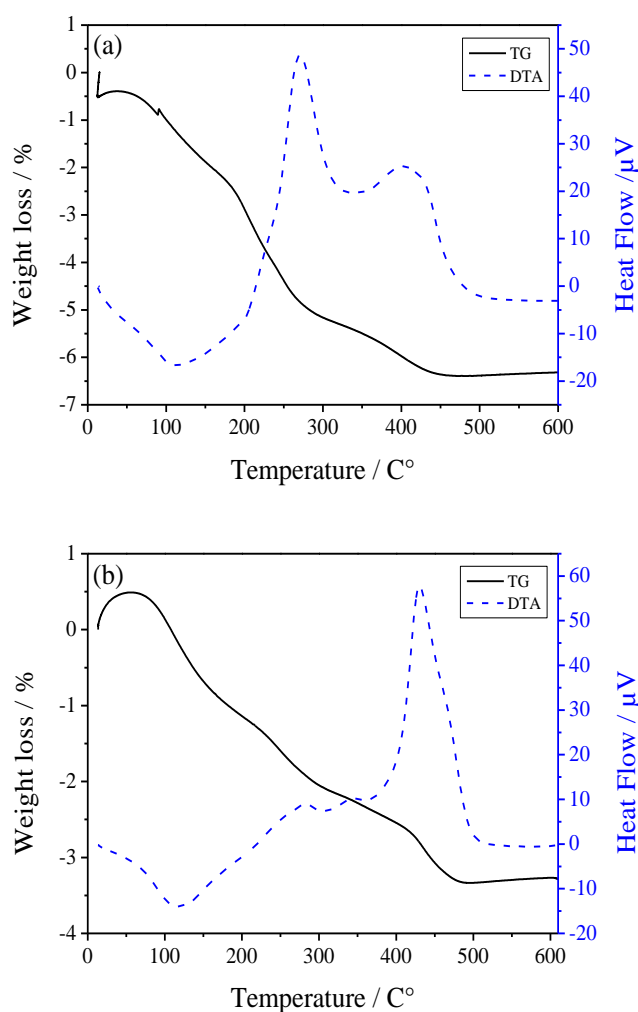
Figure 3.27: TG-DTA curves of TiO$_2$-ZnO (1:0.05) before (a) and after (b) UV irradiation.

The prepared films were characterized by elucidating their optical properties, their hydrophilicity, thickness, crystal structure, and pore size distribution.
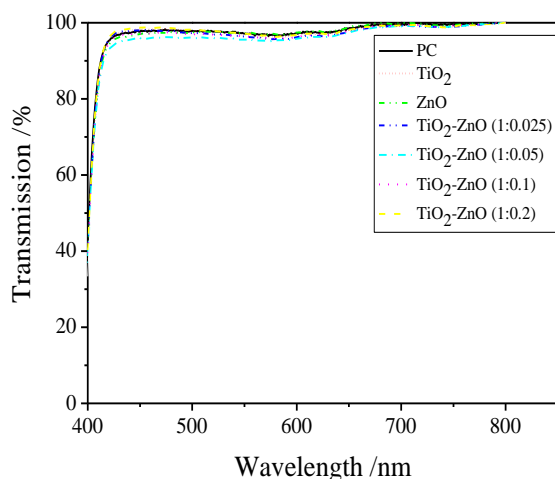
Figure 3.28: UV-Vis spectra of TiO$_2$, ZnO, and TiO$_2$-ZnO prepared films on SiO$_2$ pre-coated PC.

The optical properties of the prepared films were determined by recording the absorption spectra in the range 400-800 nm with the thus obtained spectra being shown in *Figure 3.28*. The transmission values of uncoated and coated polycarbonate plates at $\lambda = 500$ nm are summarized in Table *3.4* indicating that all resultant coatings are highly transparent.

Table 3.4: Mean contact angle, transmission, and thickness of TiO2-ZnO thin films on polycarbonate.

Thin Film	Thickness/ nm	Trancparency at 500nm/%	CA/ 1°	CA/ 1° after stability test (20 times)	CA/ 1°after stability test and UV(A) irradiation for 24 h
none	-	98	85 ± 1	-	-
TiO$_2$	132 ± 10	98	<5	<5	<5
ZnO	210 ± 23	97	<5	56 ± 2	<5
TiO$_2$-ZnO (1:0.025)	248 ± 4	98	<5	<5	<5
TiO$_2$-ZnO (1:0.05)	169 ± 15	96	<5	<5	<5
TiO$_2$-ZnO (1:0.1)	202 ± 4	97	<5	35 ± 1	<5
TiO$_2$-ZnO (1:0.2)	213 ± 10	98	<5	36 ± 1	<5

Table 3.4 shows also the values of the thickness of the TiO_2-ZnO thin films on polycarbonate, which was measured at different points on the surface of the coated plates by ellipsometery. The thicknesses of the prepared films were in the range from 120 to 250 nm. However, there is no clear relationship between the thickness of the films and the amount of added ZnO is observed.

To reveal information about the crystallinty, the XRD pattern of the TiO_2, ZnO, and TiO_2-ZnO (1:0.05) coating has been recorded. The results are presented in Figure 3.29, Figure 3.30, and Figure 3.31.
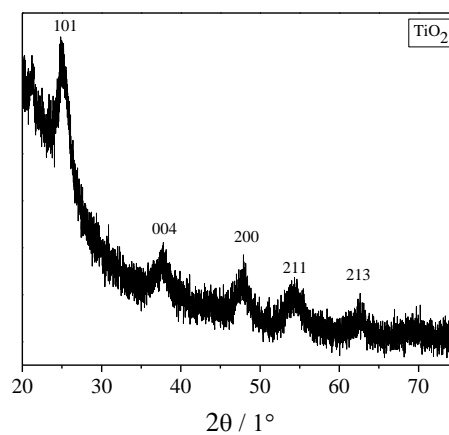
Figure 3.29: X-ray diffraction pattern of TiO_2.
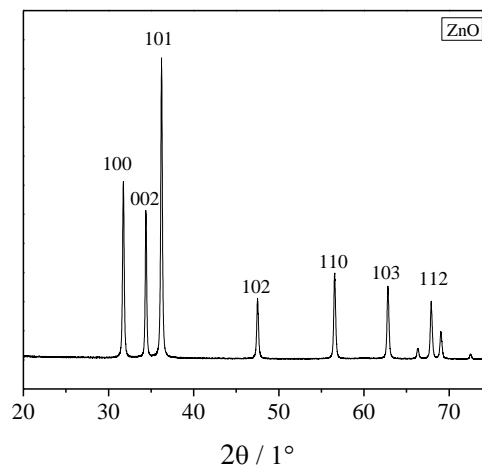
Figure 3.30: X- ray diffraction pattern of ZnO.
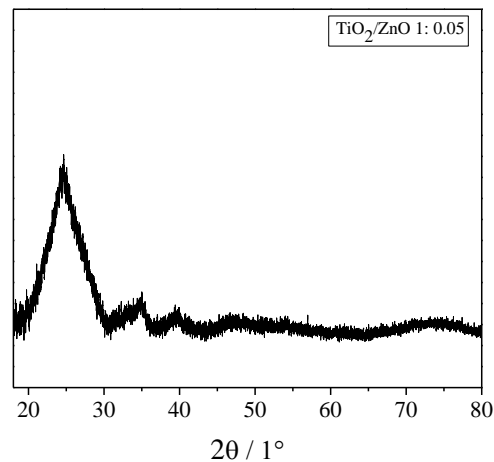
Figure 3.31: WAXS of a TiO$_2$-ZnO (1:0.05) film.

The results indicate the formation of anatase TiO$_2$ with a quite good crystallinity, and of ZnO as zincite with a high cristallinity, when both prepared separately. In the case of the in situ preparation of TiO$_2$-ZnO, the particle formation and the crystallinity of TiO$_2$ and ZnO affect each other negatively. These results are compatible with the results in ref.[73].

Adsorption experiments were carried out in order to investigate the pores of the prepared films and to study the influence of the ZnO addition on the porosity.
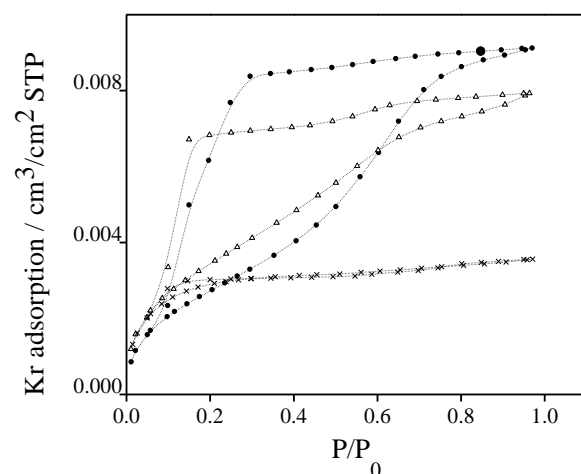
Figure 3.32: Adsorption isotherms of Kr at ca 77° K on TiO$_2$ (●), TiO$_2$-ZnO (1:0.05) (Δ) and TiO$_2$-ZnO (1:0.2) (×) films deposited on polycarbonate.

The TiO_2 and TiO_2-ZnO (1:0.05) films exhibit similar porosity characterized by ink bottle pores, i.e. cavities connected with each other and with the external space via very narrow pores. However, an increase in the percentage of ZnO to 0.2 leads to the transformation of the ink-bottle pores to micropores (comparable to the type of the hysteresis described in ref. [74]). The isotherm on the TiO_2-ZnO (1:0.2) films resembles a Langmuirian type isotherm, as the hysteresis loop has become rather narrow and has almost disappeared. Table 3.5 presents an overview of their textural properties. The pore size distributions for the TiO_2 and TiO_2-ZnO (1:0.05) films have been calculated from the adsorption isotherms of Kr at 77° K (Figure 3.32).

Table 3.5: Overview of the textural properties of selected films calculated from the adsorption isotherms of Kr at ca 77°K

Sample	S_{geom} / cm^2	Thickness / nm	S_{BET}^{a} / cm^2	V_{pore}^{a}/cm^3 x 10^6	S_{BET}^{b} / m^2/g	V_{pore}^{b} / cm^3/g	D^{c} / nm
TiO_2	44	132	1544	124	86.7	0.069	5.2
TiO_2-ZnO 1:0.05	44	169	2226	131	93.0	0.055	4.7
TiO_2-ZnO 1:0.2	29.5	213	2002	71	92.2	0.033	microporous

[a] total BET surface area and pore volume of the corresponding film

[b] BET surface area related to 1 g of titanium oxide was calculated using the pore volume per cm^3 and the density of TiO_2 of 3.9 g.cm^{-3}

[c] pore size corresponding to the maximum of the pore size distribution for TiO_2 and TiO_2-ZnO (1:0.05).

The SEM results clearly demonstrate an influence of the presence of hydrochloric acid, HCl, on the obtained morphology (Figure 3.33). While the presence of HCl leads to the formation of very small granular TiO_2, the use of HCl during the preparation of the ZnO films results in the formation of rod-like nanostructures with pointed tips [75, 76].
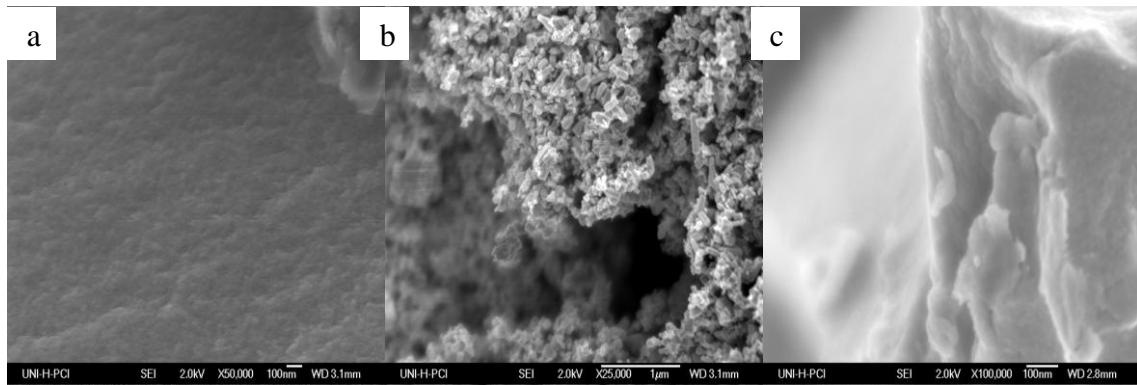
Figure 3.33: SEM images of TiO$_2$ (a), ZnO (b), and TiO$_2$-ZnO (1:0.05) (c).

TEM images of a mesoporous TiO$_2$-ZnO film with the molar ratio 1:0.05 are presented in Figure 3.34. It can be clearly seen from this Figure that the pores of the TiO$_2$-ZnO film on the polycarbonate surface are homogenously distributed.
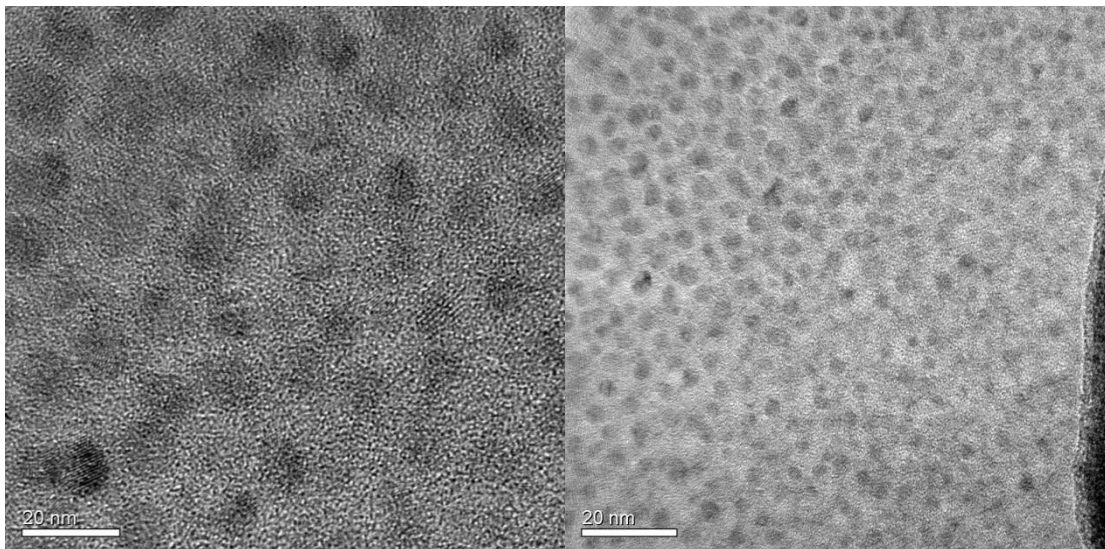
Figure 3.34: TEM images of a mesoporous TiO$_2$-ZnO (1:0.05)film.

Two-dimensional and three-dimensional AFM images of TiO$_2$-ZnO thin films deposited onto the surface of the polycarbonate substrates are presented in Figure 3.35. Figure 3.35 reveals that the addition of ZnO to TiO$_2$ results in a decrease of the roughness of the film's surface with increasing ZnO/ TiO$_2$ molar ratio.

TiO$_2$
RMS = 2.36 nm
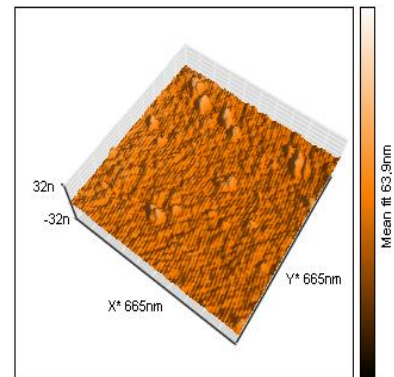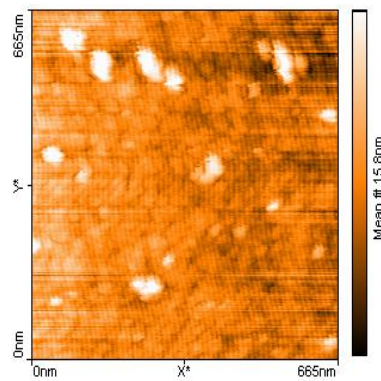
TiO$_2$-ZnO (1:0.025)
RMS = 1.6 nm
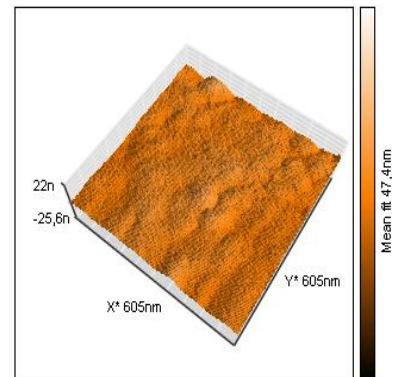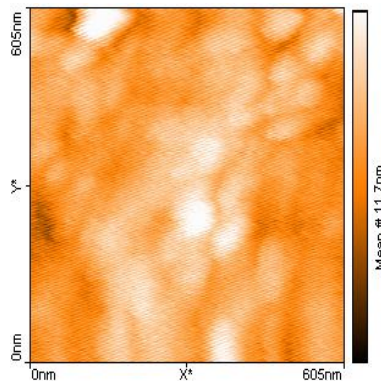
TiO$_2$-ZnO (1:0.05)
RMS = 1.32 nm

TiO$_2$-ZnO (1:0.075)
RMS = 1.38 nm
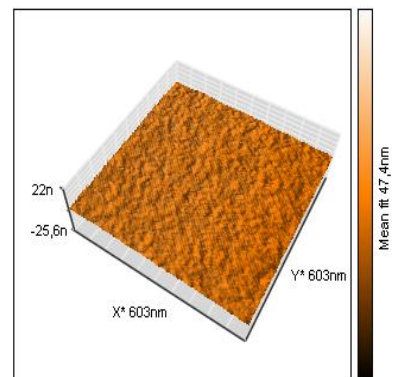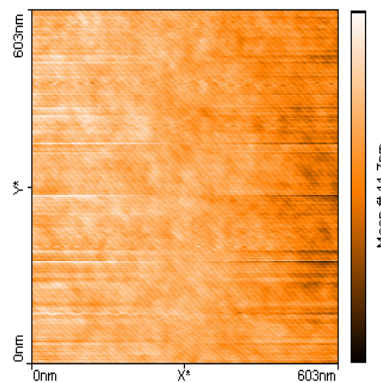
TiO$_2$-ZnO (1:0.1)
RMS = 1.06 nm

ZnO
RMS = 1,1 nm
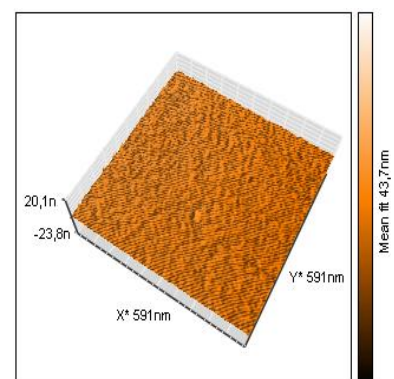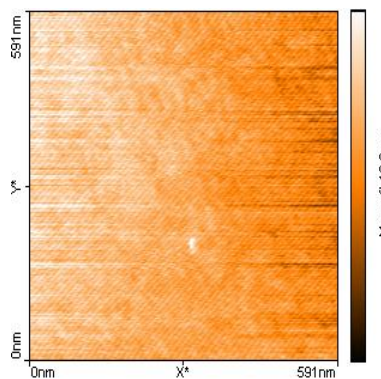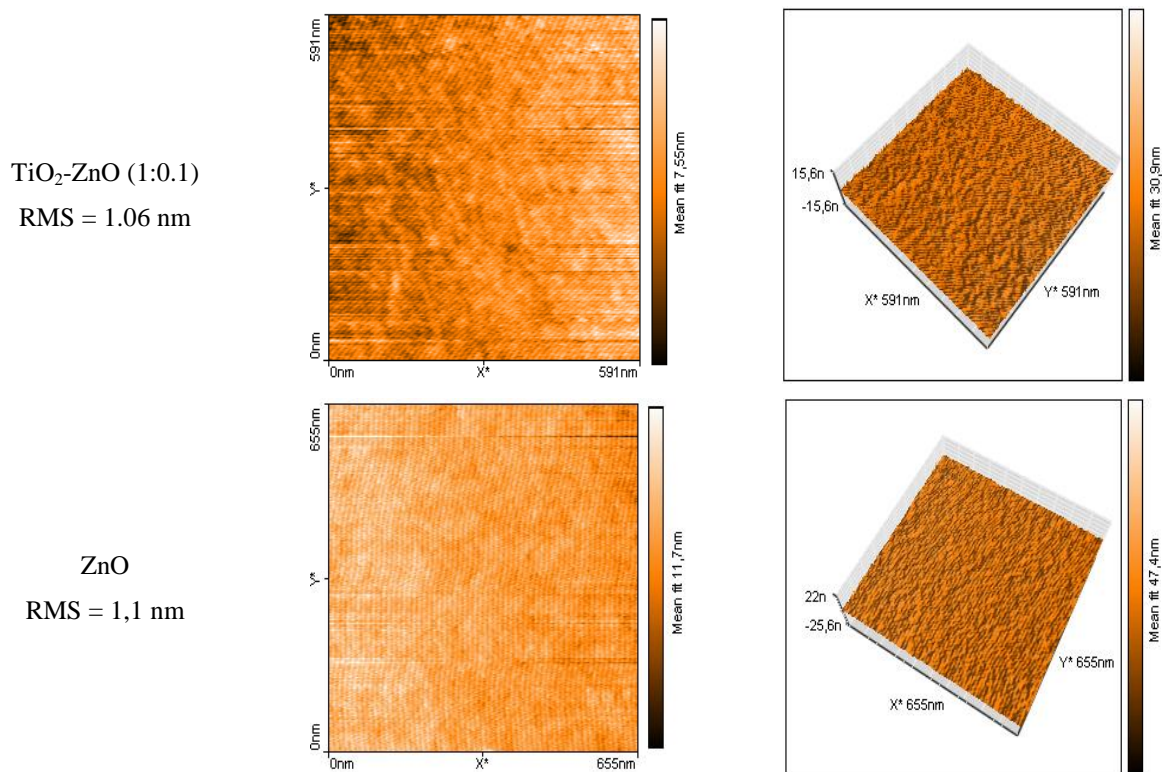
Figure 3.35: Two-dimensional and three-dimensional AFM images of TiO$_2$-ZnO thin films.

3.4.2.2   Photocatalytic Testing

Photonic efficiencies as a measure for the photocatalytic activity of the prepared TiO$_2$-ZnO thin films on polycarbonate were calculated, again, from the kinetics of the photocatalytic degradation of methylene blue (MB), methyl stearate (MS), and acetaldehyde (AA). The respective values are given as columns in Figure 3.36.

The results demonstrate that insertion of ZnO into the TiO$_2$ coating resulted in an increased photocatalytic activity of the prepared coatings employing both the degradation of methylene blue or of acetaldehyde. However, a decrease of the photocatalytic activity of the prepared coatings occurs in the case of methyl stearate being the probe molecule. TiO$_2$-ZnO with a molar ratio 1:0.05 was found to exhibit the highest photonic efficiency of the MB degradation which is comparable with that of Pilkington Activ™ .
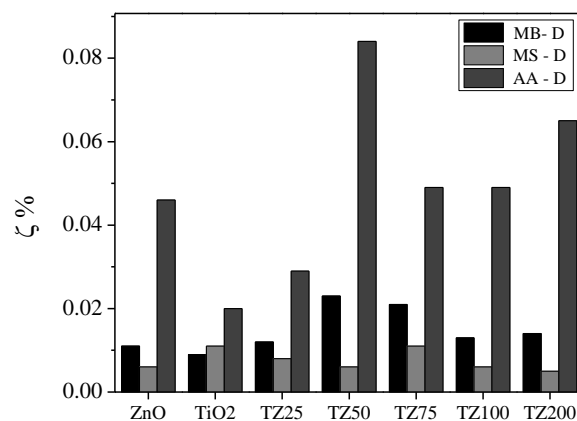
Figure 3.36: Photonic efficiencies of the photocatalytic degradation of methylene blue (MB), of methyl stearate (MS) , and of acetaldehyde (AA)on TiO_2, ZnO, TiO_2-ZnO 1:0.025 (TZ25), TiO_2-ZnO 1:0.05 (TZ50), TiO_2-ZnO 1:0.075 (TZ75), TiO_2-ZnO 1:0.1 (TZ100), and TiO_2-ZnO 1:0.2 (TZ200) thin films on polycarbonate under UV (A) ($10Wm^{-2}$) illumination.

3.4.2.3   Evaluation of the Photoinduced Hydrophilicity

Directly after the preparation of the superhydrophilic films, the photoinduced properties of the films prepared under different conditions were studied and compared with the photoinduced properties of Pilkington Activ [TM].
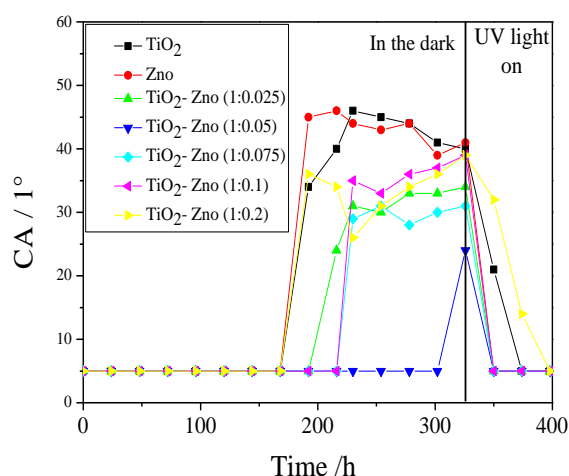
Figure 3.37: Change of water contact angle on TiO_2, ZnO, and TiO_2-ZnO thin films on polycarbonate during their storage in the dark followed by UV(A) irradiation ($10Wm^{-2}$).

The prepared films and Pilkington Activ ^{TM} glass were stored in the dark under atmospheric condition. Figure 3.37 shows the change of the water contact angle of TiO_2, ZnO and TiO_2-ZnO thin films on polycarbonate during their storage in the dark as well as during subsequent UV(A) irradiation. As can be seen from this Figure, the addition of ZnO to TiO_2 helps to improve the hydrophilicity of the prepared films.

The water contact angle of TiO_2 and ZnO films increased after 7 days (168h) of storage under ambient conditions in the dark while Pilkington Activ^{TM} maintained a contact angle $<5°$ for 9 days (216h) of storage in the dark. The contact angle of the prepared film TiO_2-ZnO with the molar ratio 1:0.05 increased after 13 days (312h) of the dark storage. In all cases investigated here the water contact angle decreased to a value $<5°$ within 24h of UV(A) irradiation with an intensity of 10 W m^{-2}.

Exposure of the superhydrophilic films to an atmosphere containing a high concentration of an organic solvent (acetone or propan-2-ol) resulted in an increase of the contact angle from values $<5°$ to values of $>30°$ within two hours of exposure (Figure 3.38 and Figure 3.39).
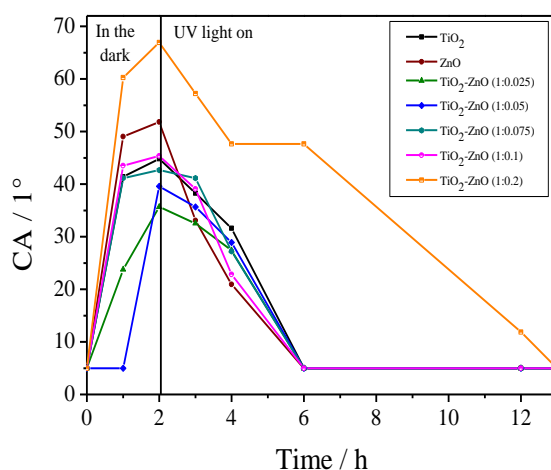
Figure 3.38: Change of water contact angle on TiO$_2$, ZnO, and TiO$_2$-ZnO thin films on polycarbonate during their storage in the dark in presence of propan-2-ol followed by irradiation by UV light (10Wm^{-2}).
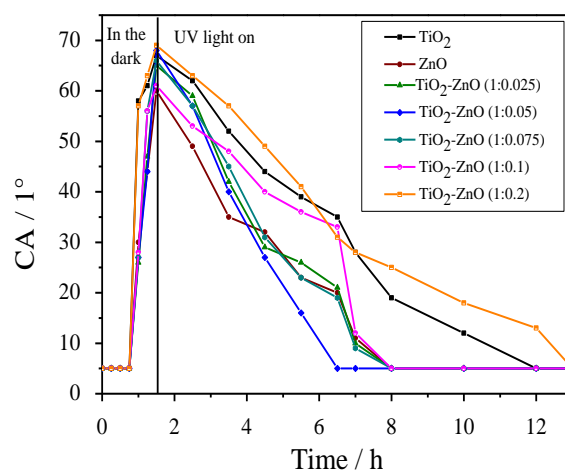
Figure 3.39: Change of water contact angle on TiO₂, ZnO, and TiO₂-ZnO thin films on polycarbonate during their storage in the dark in the presence of acetone followed by their irradiation by UV light (10Wm⁻²).

When the prepared films and Pilkington Activ[TM] were stored in the dark in an atmosphere containing propan-2-ol, the TiO_2 and ZnO films maintained their superhydrophilicity for 1h while the TiO_2-ZnO film with a molar ratio 1:0.05 and Pilkington Avtiv[TM] preserve their superhydrophilicity for 2h. After the increase of their water contact angles, all films were irradiated with UV light. As a consequence, the contact angles of the prepared films decreased to values < 5° after 6h whereas the contact angle of Pilkington Activ[TM] became <5° after 12h

The effect of the addition of ZnO to TiO_2 on the photoinduced properties was less pronounced in the case of acetone being the gas phase pollutant. Figure 3.39 presents the time dependence of the change in water contact angle for TiO_2 -ZnO films during their storage in the dark under an atmosphere of acetone and during subsequent UV(A) irradiation with10 W m⁻². The contact angle of the TiO_2-ZnO (1:0.05) film increased after 1h of storage in the dark in an acetone containing atmosphere. After UV irradiation for 5h, its contact angle decreases again from 65° to <5°. The compared Pilkington Activ[TM] glass has stable superhydrophilic properties for 0.75h. After this time its contact angle increases. Subsequently, its surface was

irradiated by UV(A) light. Consequently, its contact angle drops from 64° to <5° within 5h of UV irradiation.

3.4.2.4   Test of the Self Cleaning Performance

The changes of the water contact angle under UV irradiation after dip coating of oleic acid on the prepared films are shown in Figure 3.40.

After applying oleic acid, the surface of every film was converted to a hydrophobic surface. However, when the surface was irradiated by UV light, the film became again hydrophilic. The contact angle of TiO_2 film decreases with a quite good photoinduced hydrophilicity conversion rate of around 5° after 120h of the UV irradiation. The contact angle of ZnO film decreased gradually to be <5° after 180h of the irradiation using UV(A) light with an intensity of 10 Wm^{-2}.
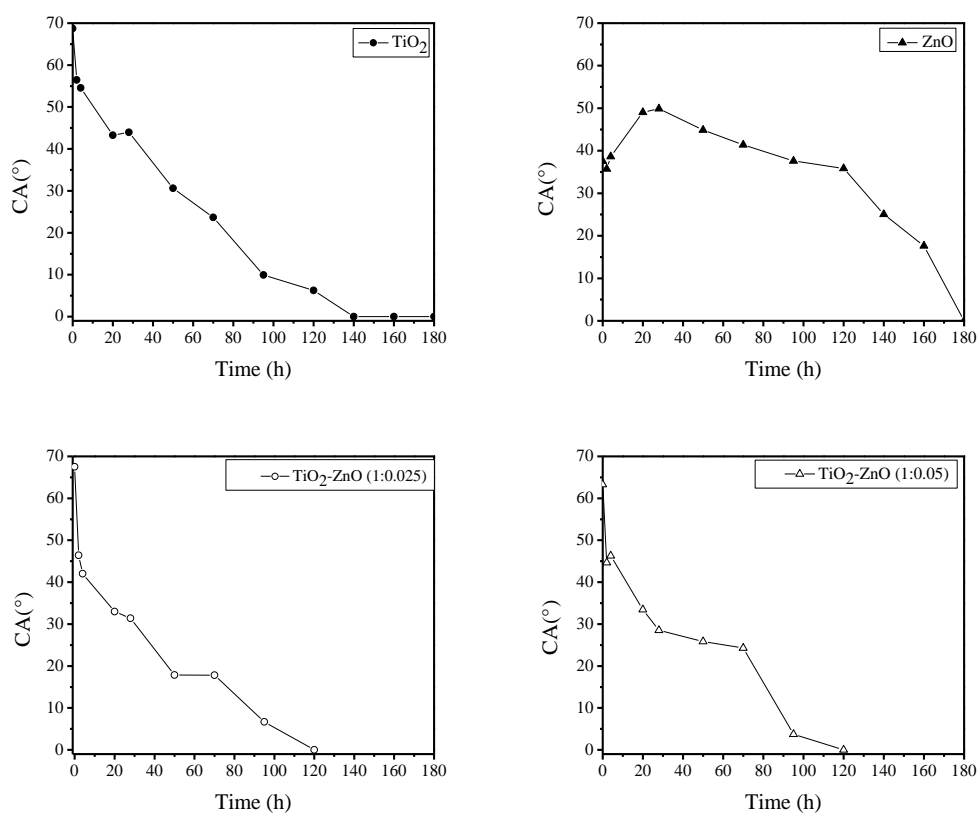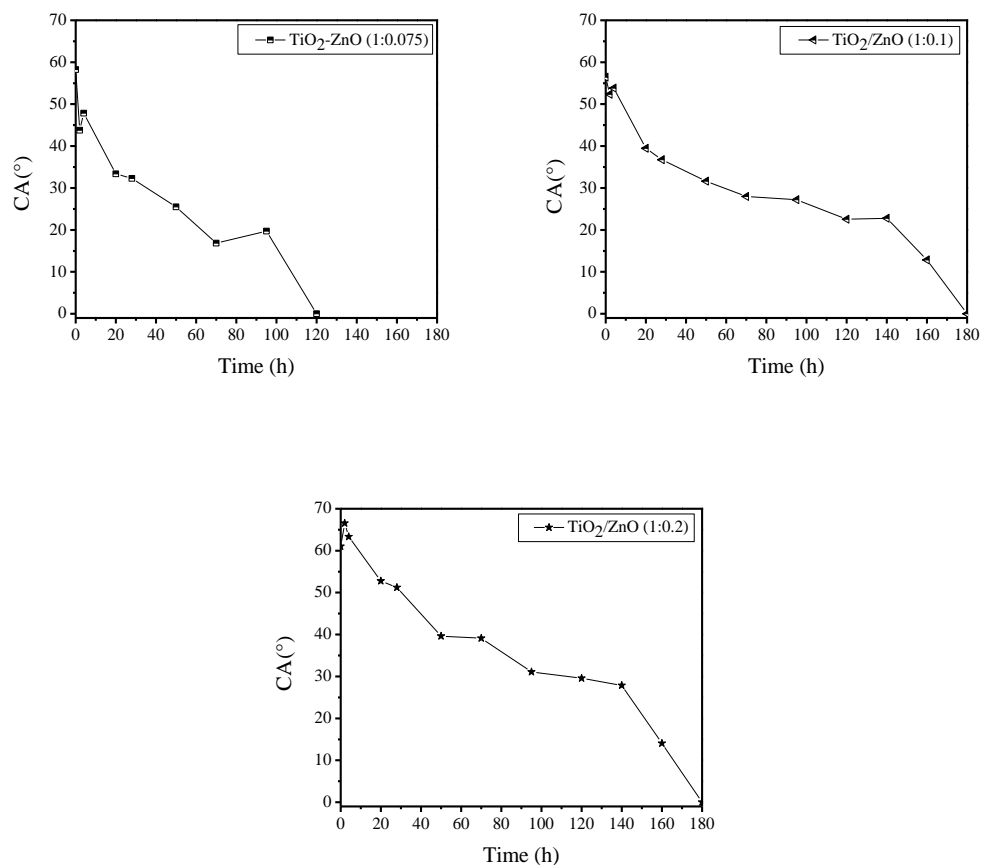
Figure 3.40: Change of water contact angle of water during the photocatalytic degradation of oleic acid on TiO$_2$, ZnO, and TiO$_2$-ZnO deposited films.

The photoinduced hydrophilicity conversion rate of the ZnO film was found to be much lower than that of the TiO$_2$ film. The addition of ZnO to the TiO$_2$ film with different molar ratios leads to an improvement of the photoinduced superhydrophilicity conversion. The TiO$_2$-ZnO film with molar ratio 1: 0.05 coated by oleic acid becomes superhydrophilic after 100h of the UV irradiation due to the photocatalytic degradation of oleic acid. Furthermore, it is observed that the addition of ZnO to the TiO$_2$ film with a different molar ratio leads to the appearance of a short threshold on the self-cleaning curve.

3.4.2.5   Quantitative Estimate of the adhesion after UV irradiation

Figure 3.41 shows microscopic photographs (40 ×magnifications) of the prepared films (SiO$_2$, TiO$_2$, ZnO, and TiO$_2$-ZnO mixtures with different molar ratios (0.025, 0.05, 0.075, 0.1,

and 0.2)) after the cross-cut tests. The adhesion of the prepared film after UV(A) irradiation for three months was estimated quantitatively.

According to this ISO 2409 method, the quality of the SiO_2 interlayer is ranked as 2 (good) (see Table 2.1). All TiO_2-ZnO films except for the TiO_2-ZnO film with molar ratio 1:0.2 also exhibit good adhesion qualities. TiO_2, ZnO, and TiO_2-ZnO films with molar ratios of 0.025, 0.05, 0.075, and 0.1 are ranked as 0 (excellent) while the TiO_2-ZnO film with a molar ratio of 1:0.2 is ranked as 4 (poor).

Film	TiO_2	TiO_2-ZnO 1:0.025	TiO_2-ZnO 1:0.05	TiO_2-ZnO 1:0.075
Before Irradiation				
After irradiation				

Film	TiO_2-ZnO 1:0.1	TiO_2-ZnO 1:0.2	ZnO	intermediate layer SiO_2
Before Irradiation				
After irradiation				
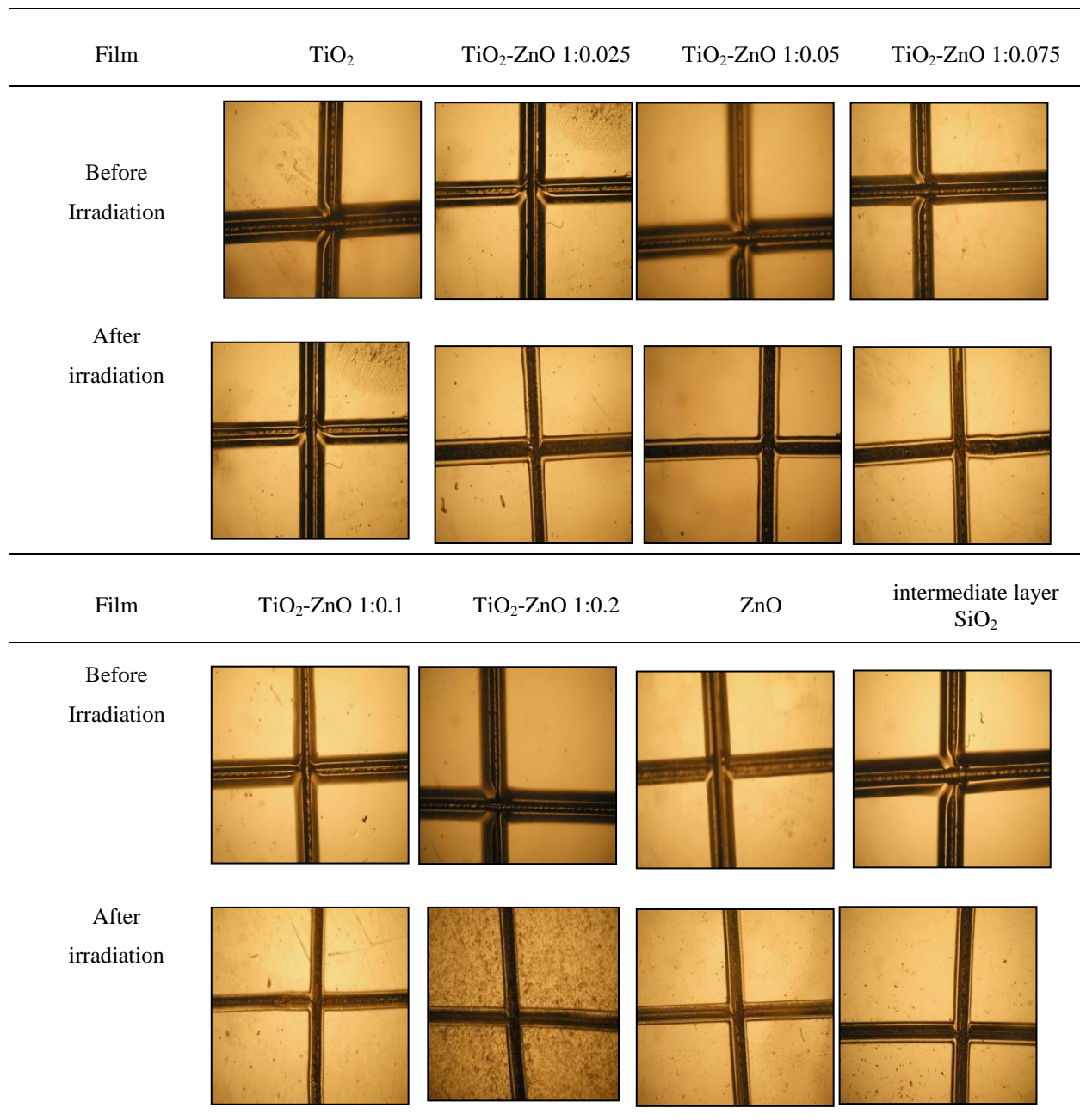
Figure 3.41: Photographs of TiO_2, ZnO, and TiO_2-ZnO films after applying the cross cut test.

3.4.2.6   Abrasion resistance

The abrasion resistance of the TiO_2-ZnO thin films was proved by a felt-abrasion test followed by the measurement of the water contact angle and by the determination of the photonic efficiencies for the photocatalytic degradation of MB.

The respective data is included in Table *3.4* and in Figure 3.42. It is obvious from Table *3.4* that the water contact angles of the samples usually increase by rubbing the surface with the felt but in all cases the superhydrophilic state with water contact angles <5° was reconstituted within 24h by UV(A) irradiation. However, the photonic efficiency of the photocatalytic degradation of MB was considerably affected by the felt-abrasion test (Figure 3.42). The decrease of the photonic efficiency was most pronounced for the pure ZnO coating (87%), while for pure TiO_2 and ZnO rich TiO_2 thin films the photonic efficiencies decreased by ca. 40%. On the contrary, the decrease of the photonic efficiencies of the TiO_2-ZnO thin films with a TiO_2-ZnO ratio ≤ 1 : 0.05 was less than 25%, indicating that the presence of a low ratio of ZnO in the TiO_2 layer enhances the stability of the prepared layer.
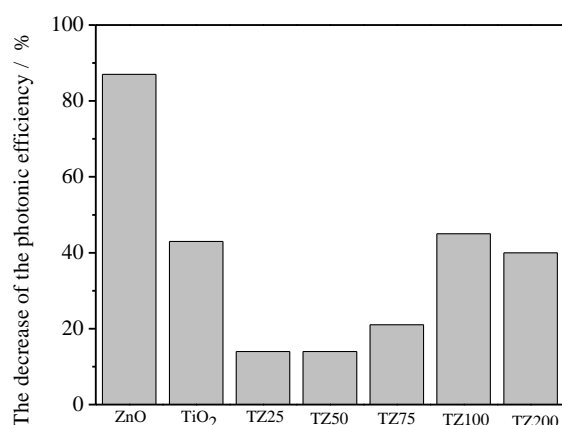
Figure 3.42: Decrease(in %) of the photonic efficiencies for the photocatalytic degradation of methylene blue (MB) after the stability tests on TiO_2, ZnO, TiO_2-ZnO 1:0.025 (TZ25), TiO_2-ZnO 1:0.05 (TZ50), TiO_2-ZnO 1:0.075 (TZ75), TiO_2-ZnO 1:0.1 (TZ100), and TiO_2-ZnO 1:0.2 (TZ200) thin films on polycarbonate (TiO_2-ZnO symbolized by TZ).

3.4.3   Hombikat UV100, UV100-SiO$_2$ Film

3.4.3.1   Characterization

After the deposition of the SiO$_2$ intermediate layer, mixtures of a commercial TiO$_2$ (Sachtleben Hombikat UV100) powder with varying amounts of tetraethoxysilane in acidic ethanol were prepared and applied to coat precoated PC sheets with TiO$_2$-SiO$_2$ thin films.

The optical properties of the prepared films were determined by recording the absorption spectra in the 400 – 800 nm range. Figure 3.43 exemplarily shows the transmission spectra of a bare TiO$_2$ film and of TiO$_2$-SiO$_2$ films with different molar ratios thin films on PC and a photographic image of a PC sheet coated with a TiO$_2$-SiO$_2$ (1:0.9) thin film. This figure and the transmission values of uncoated and coated polycarbonate plates at $\lambda = 500$ nm (cf. Table 3.6) witness that all coatings were highly transparent in the visible range of the spectrum with a transmission $> 94\%$ at 500 nm. All spectra show a drastic decrease of the transmission in the range from 420 to 380 nm corresponding to the absorption intrinsic to PC.
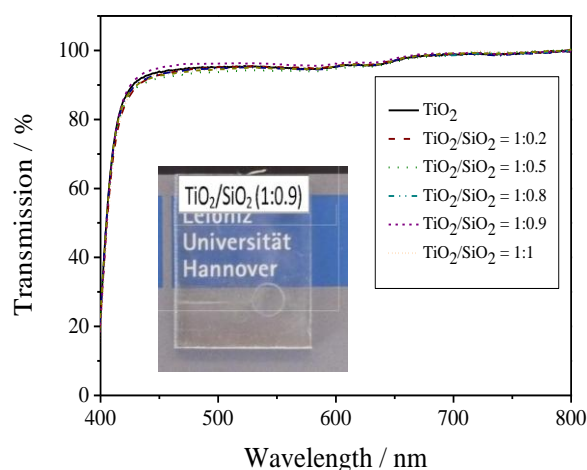
Figure 3.43: UV-Vis transmission spectra of TiO$_2$-SiO$_2$ thin film coated on PC.

Table 3.6: Thickness, transmission at 500nm, and BET surface area of TiO$_2$-SiO$_2$ thin films on PC.

Thin film	Thickness / nm	Transmission at 500 nm / %	BET surface Area m^2/g
none	-		-
TiO$_2$(UV100)	186 ± 19	95	270
TiO$_2$-SiO$_2$ (1:0.2)	222 ± 5	95	n.d
TiO$_2$-SiO$_2$ (1:0.5)	216 ± 11	94	n.d
TiO$_2$-SiO$_2$ (1:0.8)	170 ± 30	94	374
TiO$_2$-SiO$_2$ (1:0.9)	144 ± 13	96	428
TiO$_2$-SiO$_2$ (1:1)	148 ± 25	95	391
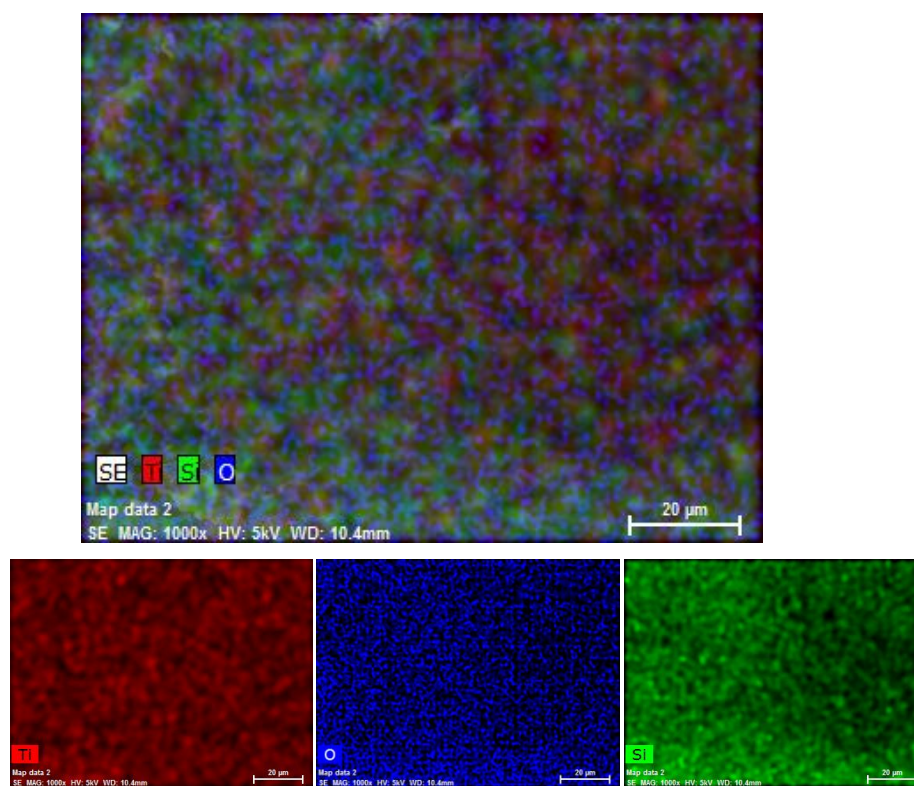
Figure 3.44: EDX mapping of a TiO$_2$-SiO$_2$ (1:0.9) thin film on PC.

Moreover, the thicknesses of the prepared films as determined by ellipsometry were found to range between 140 nm and 220 nm (cf. Table 3.6). The thickness of the prepared films decreases with an increase in the molar ratio of SiO_2 in the TiO_2-SiO_2 films.

The three elements Ti, Si, and O are uniformly distributed in the covering thin films as revealed by EDX mapping (Figure 3.44). The EDX measurement at a $TiO_2/SiO_2(1:0.9)$ thin film showed the molar ratio of Ti, Si, and O being 15.5, 14.5, and 70.0, respectively, corresponding to a calculated Ti-Si ratio of 1 : 0.935.
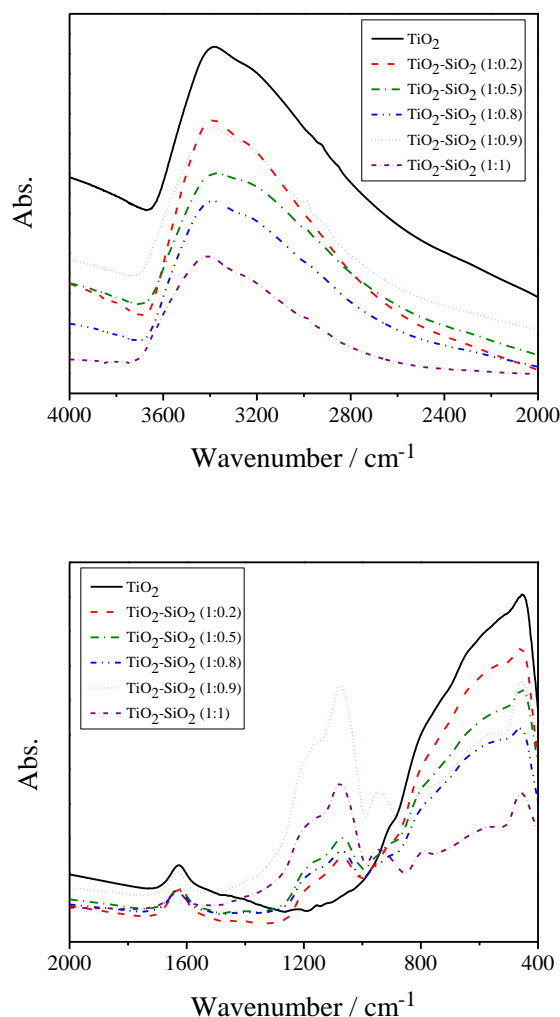
Figure 3.45: FTIR spectra of a TiO₂ and TiO₂-SiO₂ thin films on PC.

The FTIR spectra of TiO_2, SiO_2, and TiO_2-SiO_2 films in the wavenumber range $400 - 4000$ cm^{-1} are presented in Figure 3.45. The spectra show broad peaks within $500 - 1000$ cm^{-1}

attributed to the stretching vibration of Ti-O, a peak at 964 cm^{-1} corresponding to the

vibration of Si-O-Ti, a peak around 1082 cm^{-1} attributed to Si-O-Si, and a broad peak in the

range 2840 cm^{-1} - 3430 cm^{-1} which is attributed to the stretching mode of water and hydroxyl

groups [71].

The wettability of the prepared TiO$_2$-SiO$_2$ thin films on the polycarbonate substrate by

water was studied by measuring the water contact angle after UV(A) irradiation of the films

(Figure 3.46).
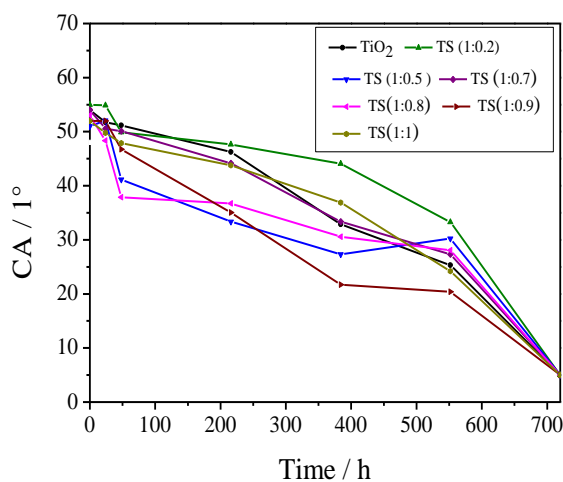
Figure 3.46: Change of the water contact angle of TiO$_2$-SiO$_2$ thin films on polycarbonate during irradiation with UV(A) light (TiO$_2$-SiO$_2$ symbolized by TS).

Directly after the preparation and before illumination all prepared films have almost the

same value of 53° for the water contact angle which decreases during UV(A) irradiation

reaching constant values <5º after 700 hours showing the photoinduced superhydrophilicity

properties of these films.

A felt abrasion test applied to the superhydrophilic samples resulted in a considerable

increase of the water contact angle. However, this effect was found to be reversible under

UV(A) irradiation (see Table 3.7).

Table 3.7 : Water contact angles of TiO$_2$- SiO$_2$ thin films on PC.

Photocatalytic	CA / 1°			
thin film	before irradiation	after irradiation for 700 h	after storage in the dark for 326 h	after felt abraison test
None (PC)	85 ± 1	n.d.	n.d.	85 ± 1
TiO$_2$	54 ± 3	<5	53 ± 2	65 ± 2
TiO$_2$-SiO$_2$ (1:0.2)	55 ± 2	<5	48 ± 5	54 ± 8
TiO$_2$-SiO$_2$ (1:0.5)	51 ± 4	<5	17 ± 6	51 ± 2
TiO$_2$-SiO$_2$ (1:0.8)	53 ± 6	<5	36 ± 3	53 ± 2
TiO$_2$-SiO$_2$ (1:0.9)	52 ± 2	<5	25 ± 4	56 ± 9
TiO$_2$-SiO$_2$ (1:1)	52 ± 1	<5	31 ± 5	55 ± 5

Figure 3.47 shows the two- and three-dimensional AFM images of bare TiO$_2$ and TiO$_2$-SiO$_2$ (1:0.9) films. It can clearly be seen from the height images that the nanoparticles cause a rough-textured surface. The roughness of the surface was found to be 1.6 nm and 7.4 nm for the bare TiO$_2$ and the TiO$_2$-SiO$_2$ (1:0.9) film, respectively, clearly indicating that the roughness of the surface is increasing with increasing amounts of SiO$_2$ in the functional thin films. This observation was confirmed by BET surface measurements of the prepared TiO$_2$-SiO$_2$ thin films on PC (cf. Table 3.7).

The addition of SiO$_2$ to TiO$_2$ resulted in an increase of the surface area from 270 m^2 g^{-1} up to a maximum value of 428 m^2 g^{-1} at a molar ratio of 1:0.9.
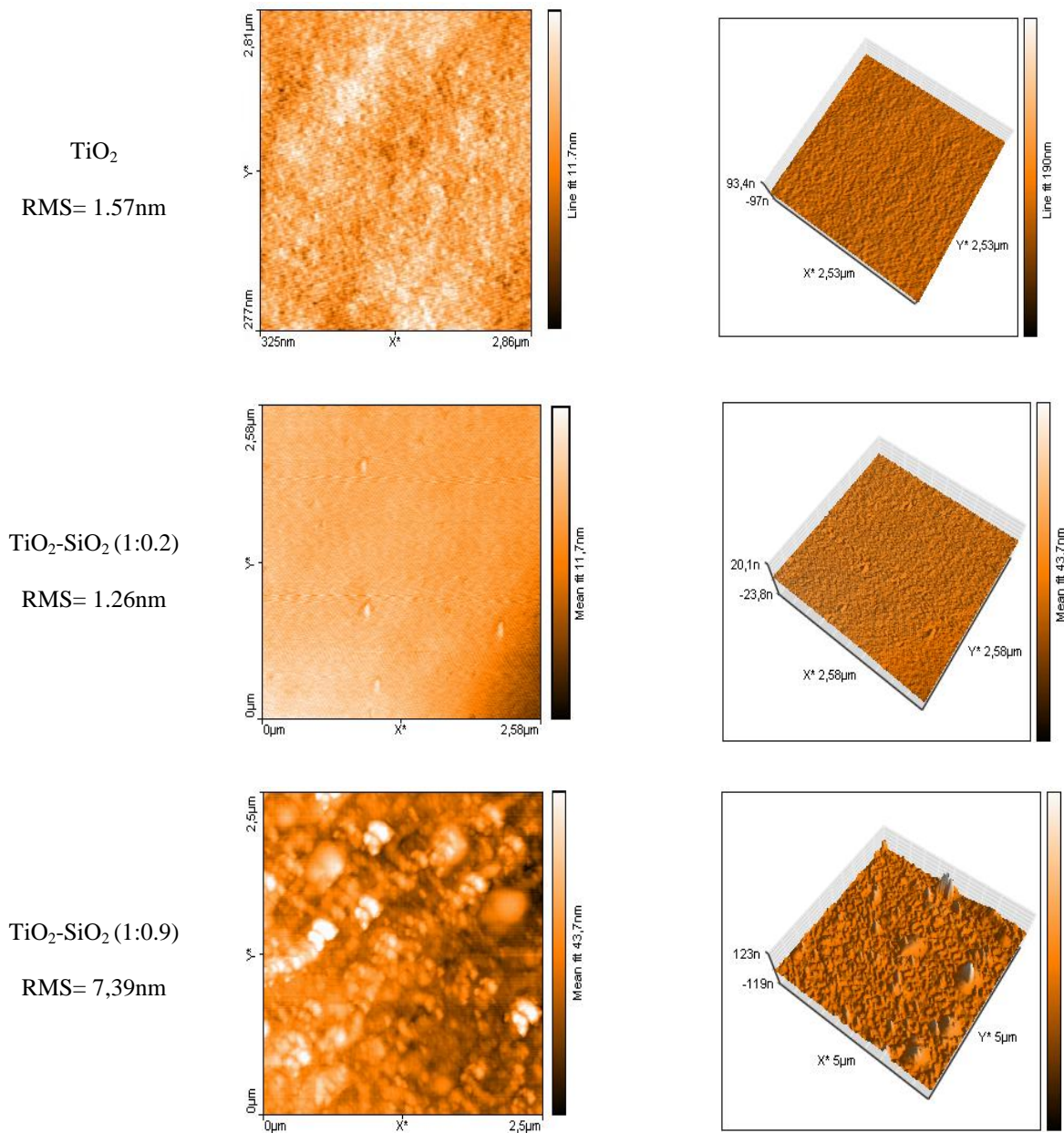
Figure 3.47: Two-dimensional and three-dimensional AFM images of TiO_2-SiO_2 films deposited onto the surface of polycarbonate substrate.

3.4.3.2   Photocatalytic Testing

The photocatalytic efficiency of the TiO_2-SiO_2 films was assessed for the photodegradation of the examined three phases pollutant, i.e., MB, MS, and AA. Figure 3.48 shows that all TiO_2 containing films prepared in this work are photocatalytically active and exhibit a higher photonic efficiency than Pilkington Activ^{TM}. The addition of SiO_2 up to 90% results in an increase of the photocatalytic activity of the prepared films to reach a photonic

efficiency equal to 0.064% for the photocatalytic MB being more than twice as high as the photonic efficiency of Pilkington Activ^{TM}.

On the other hand, the photodegradation of a solid phase pollutant (methyl stearate) on the prepared films is improved by the addition of SiO_2 with molar ratio 1:0.2. However, the addition of SiO_2 with molar ratios above 1:0.5 negatively affects the photoactivity of the prepared films (Figure 3.48).

In the case of the photodegradation of gas phase pollutant (acetaldehyde) on the prepared films, the addition of SiO_2 improves the photocatalytic efficiency of the TiO_2-SiO_2 films. The film TiO_2-SiO_2 with the molar ratio 1:0.9 has the highest photonic efficiency value (Figure 3.48).
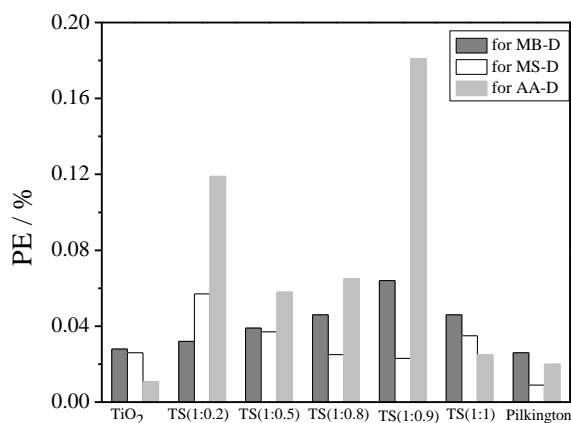
Figure 3.48: Photonic efficiencies of the photocatalytic degradation of methylene blue (MB), methyl stearate (MS), and acetaldehyde (AA) on TiO_2-SiO_2 thin films on polycarbonate (TiO_2-SiO_2 symbolized by TS).

3.4.3.3   Evaluation of the Photoinduced Hydrophilicity of TiO_2-SiO_2 Films

The photoinduced hydrophilicity conversion of the TiO_2-SiO_2 films was estimated by changes of the water contact angle measured during the initial UV(A) irradiation and the UV(A) irradiation after the storage of the prepared films in the dark. During adjacent storage in the dark the superhydrophilic state with a CA < 5° persisted for more than 150 hours.

Subsequently, the CA values slowly increased to reach the values presented in Table 3.7 after 326 hours in the dark.
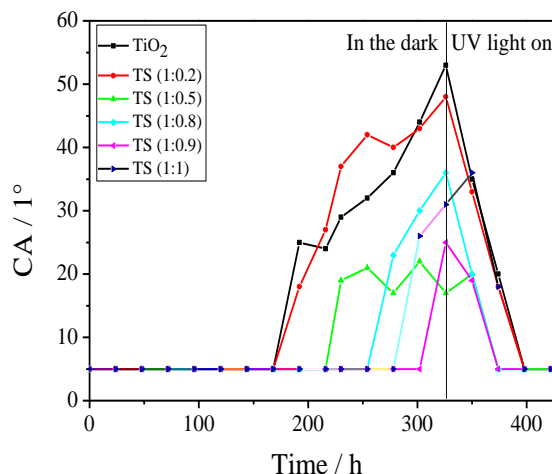
Figure 3.49: Change of contact angle on TiO$_2$-SiO$_2$ thin films on polycarbonate after their storage in the dark (TiO$_2$-SiO$_2$ symbolized by TS) followed by irradiation under UV(A)light (10Wm^{-2}).

After the increase of the water contact angles of the prepared films, the films were irradiated by UV light to become again superhydrophilic. Figure 3.49 shows the change of contact angle on TiO$_2$-SiO$_2$ thin films on PC after their storage in the dark and during their subsequent irradiation.

3.4.3.4   Test of the Self-Cleaning Performance

In order to elucidate the self-cleaning properties of the prepared films, the ISO 27448 test was applied.

After applying oleic acid, the surface of every film converted to a hydrophobic surface. When the surface was irradiated by UV(A) light it became hydrophilic again, and the water contact angles of all films eventually decreased to <5° . Figure 3.50 shows the change of the water contact angle under UV(A) irradiation after dip coating the prepared films with a thin layer of oleic acid. The water contact angles of a pure TiO$_2$ film decrease slowly reaching

value <5° after 675h UV(A) illumination. Although, all prepared films became superhydrophilic after 675h.
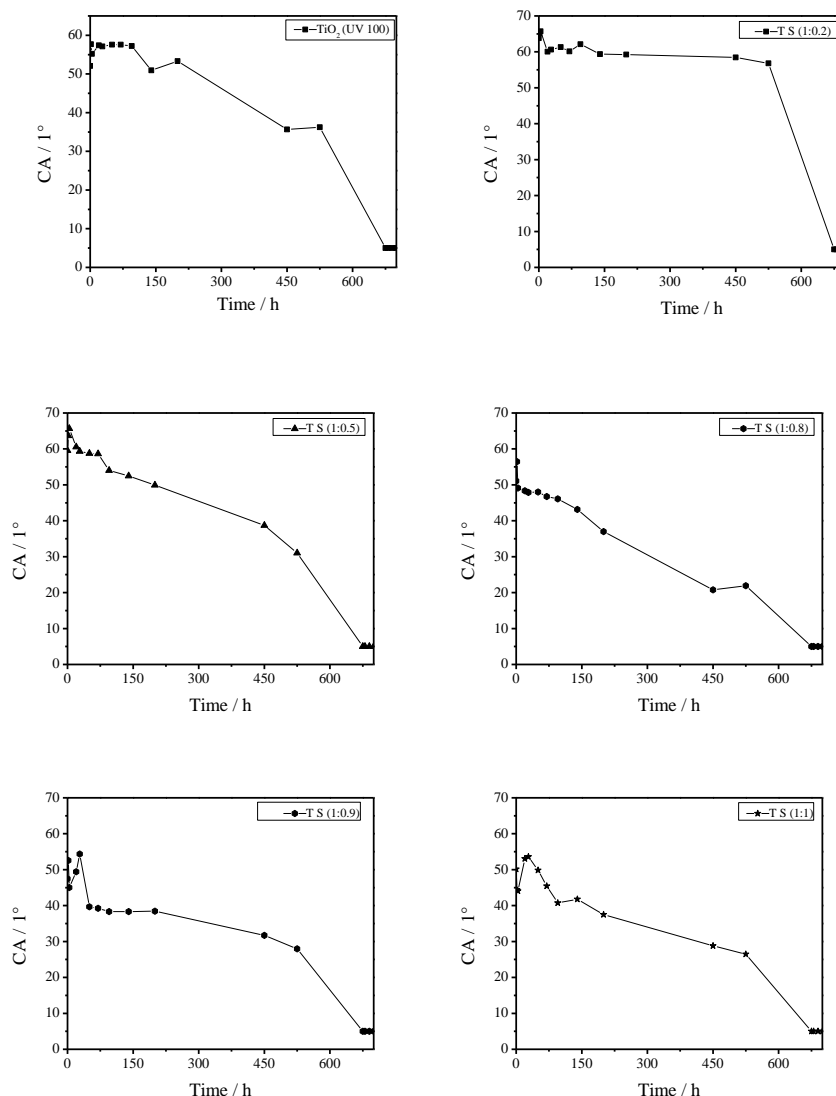
Figure 3.50: Changes of the water contact angle of water during the photocatalytic degradation of oleic acid on TiO₂-SiO₂ deposited films (TiO₂-SiO₂ symbolized by TS).

3.4.3.5   Quantitative Estimate of the Adhesion after UV Irradiation

To test the stability and the adhesion quality of the thin films before and after irradiation, the adhesion quality was measured using optical microscopy to examine possible cracks clearly (Figure 3.51). Crumbling of less than 5% of the prepared films was observed revealing the prepared films to be quite stable and adhesive even after prolonged UV(A) irradiation. Figure 3.51 together with Table 2.1 allows a ranking of the quality of the prepared TiO_2-SiO2

thin films on PC as 1 (with 0 being the most stable and 5 the least stable films according to ISO 2409).

Film	TiO$_2$	TiO$_2$-SiO$_2$ 1:0.2	TiO$_2$-SiO$_2$ 1:0.5
Before Irradiation			
After irradiation			

Film	TiO$_2$-SiO$_2$ 1:0.8	TiO$_2$-SiO$_2$ 1:0.9	TiO$_2$-SiO$_2$ 1:1
Before Irradiation			
After irradiation			
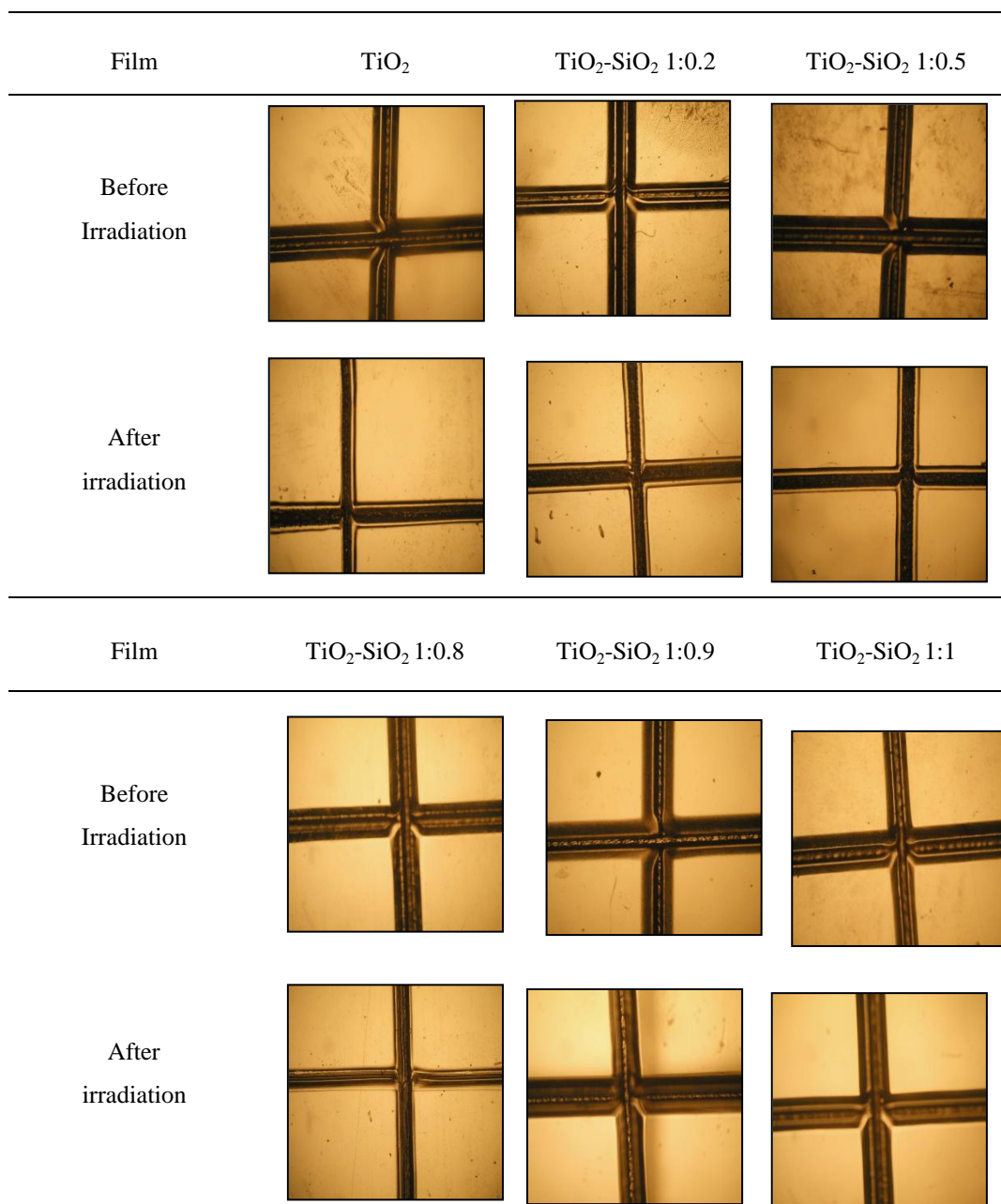
Figure 3.51: Images of prepared films before and after applying a cross-cut test after three months of UV irradiation of the TiO$_2$-SiO$_2$ thin films on polycarbonate.

3.4.3.6 Abrasion resistance

The abrasion resistances of the thin films were examined by a felt-abrasion test followed by the measurement of the water contact angle and by the determination of the photonic efficiencies of the photocatalytic degradation of MB. The data are included in Table 3.7 and

Figure 3.52. It is obvious from Table 3.7 that the water contact angles of the samples usually increase by rubbing the surface with the felt but in all cases the superhydrophilic state with water contact angles <5° was reconstituted within 24 h by UV(A) irradiation of the film. The determination of the photonic efficiencies of the films after a felt abrasion test (cf. Figure 3.52) revealed that the photocatalytically active films prepared here as well as the TiO_2 layer of Pilkington Activ^{TM} are not stable against abrasion. In all cases, a significant decrease of the photonic efficiency was observed (Figure 3.52). Under the experimental conditions employed here the photonic efficiency of Pilkington Activ^{TM} decreased by more than 40% while the efficiency of the TiO_2-SiO_2(1:0.9) being the photocatalytically most active film immediately after preparation decreased by more than 60%. On the other hand, the incorporation of only small amounts of SiO_2 into the TiO_2 film resulted in a much lower decrease of the photonic efficiency (< 30%) indicating a stabilization of the surface against abrasion.
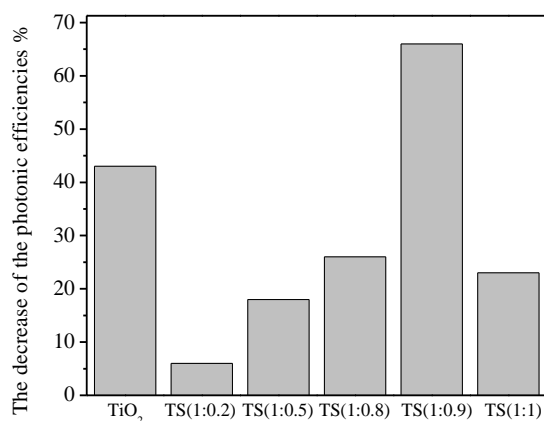
Figure 3.52: Decrease (in%) of the photonic efficiencies of the photocatalytic degradation of methylene blue (MB) after the stability test on TiO₂-SiO₂ thin films on polycarbonate (TiO₂-SiO₂ symbolized by TS).

4   Discussion

4.1   Modification of Polycarbonate and Deposition of SiO₂ Intermediate Layer

It is well known that metal oxide films attached directly onto a "clean" polycarbonate surface lead to destruction of the support [77]. Therefore, the polymer support and the photocatalytically active coating have to be separated by an inactive layer.

Hence, an intermediate SiO_2 layer was deposited on the surface of PC. To ensure a strong interaction between the polymer and the intermediate SiO_2 layer, covalent C–O–Si bonds are to be generated. For this reason the surface of the PC sheets was modified by irradiation with UV(C) light. Polycarbonate (PC) is known to undergo a photo-Fries reaction upon exposure to UV illumination yielding a hydroxylated and/or carboxylated surface.

The photo-Fries rearrangement of polycarbonate yielding phenylsalicylates and dihydroxybenzophenones is possibly activated by a chain scission at the carbonyl group [78]. As this chain scission proceeds, a reduction in the molecular weight of PC and an increase in the number of hydroxyl and carboxyl chain ends will be the result (Figure 4.1) [57].
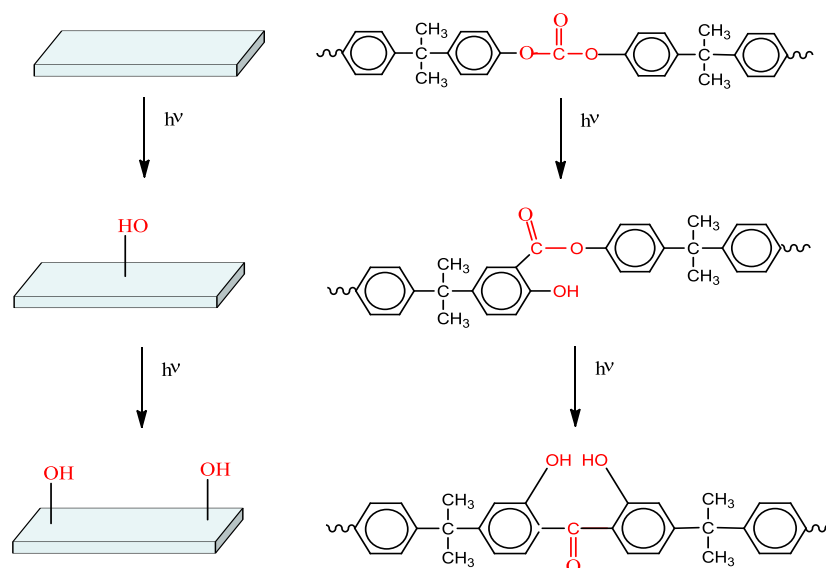
Figure 4.1: The photo-Fries reaction scheme for the polycarbonate surface modified upon UV(C) illumination.

The decrease in the water contact angle values of the irradiated polycarbonate surface from 81° to 68°, as well as the appearance of FTIR band at 3470 and 3660 cm^{-1} confirm the formation of hydroxyl groups on the PC surface upon its treatment with UV(C) light. The increase in the number of hydroxyl and carboxyl groups on the UV(C) illuminated PC leads to a strong adhesion of the subsequently deposited layers on the polycarbonate surface [60]. It is worth mentioning that the degradation reaction of the polycarbonate by UV light occurs on the surface. A region of extreme degradation was localized from the surface to a depth of 0.2 μm [79]. In particular, the rate of degradation is even more extreme in the region of 0–0.2 μm depth if the irradiation time proceeds for at least 72h [79].

Subsequently a silica layer was successfully deposited onto the UV(C) illuminated polycarbonate surface. A suitable silicate gel was synthesized by hydrolyzing tetraethylorthosilicate in the presence of the mineral acid (HCl). At the functional group level, three reactions are generally used to describe the following sol gel process [47].

Hydrolysis: $\equiv$SiOR + H$_2$O $\rightarrow$ $\equiv$SiOH + ROH   *Eq.4.1*

Condensation: $\equiv$SiOH + ROSi$\equiv$ $\rightarrow$ -SiOSi- + ROH   *Eq.4.2*

$\equiv$SiOH + HOSi$\equiv$ $\rightarrow$ -SiOSi- + H$_2$O   *Eq.4.3*
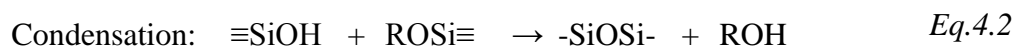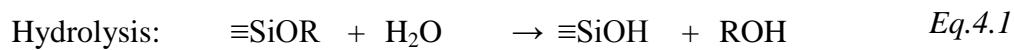
The role of the SiO$_2$ layer is not only to enhance the binding between the organic polymer PC and the inorganic TiO$_2$ layer but also to protect the PC from the TiO$_2$ layer, which otherwise may induce photocatalytic degradation of the PC resulting in an exfoliation of the photocatalytically active layer. This is why improvement is importing for the binding between the polymer and the photocatalytically active layer.

4.2 The photocatalytically Active Films

After the modification of the polycarbonate sheets and the deposition of the SiO$_2$ intermediate layer, either TiO$_2$-ZnO, TiO$_2$-SiO$_2$ or mesoporous TiO$_2$ thin films have been

successfully deposited by dip-coating. Hence, the SiO_2-protected polycarbonate surface has been successfully coated with a self-cleaning superhydrophilic and photocatalytically active surface layer. Thus, the obtained layers on the polycarbonate sheets can be schematically presented as shown in Figure 4.2.
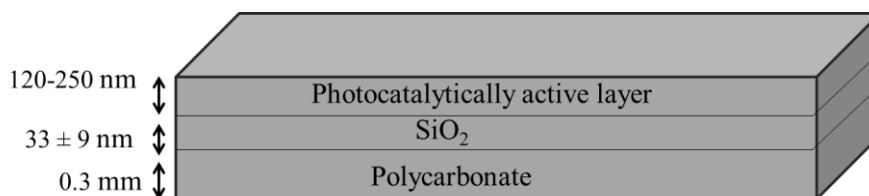
Figure 4.2: Schematic presentation of the deposition of different layers on the polycarbonate surface.

Table 4.1 presents an overview of the most interesting results obtained in this work. As can be seen from Table 4.1, all prepared films have thicknesses between 120 nm and 250 nm and all of them exhibit high adhesion strengths (except TiO_2-ZnO 1:0.2, see entry 8 in Table 4.1) and therefore sufficient mechanical stability.

4.2.1   Optical Properties

The optical properties of the prepared films were determined by recording the absorption spectra in the range 400-800 nm using a UV/Vis spectrophotometer. All photocatalytically active films coated PC prepared in this work are highly transparent showing an optical transmittance in the visible range of the spectrum, i.e., between 400 and 800 nm (Figure 3.3, Figure *3.28*, and Figure 3.43), which is only 3–6% lower than that of the uncoated polycarbonate substrate.

The drastic decrease of the transmission at wavelengths < 420 nm is due to the intrinsic absorption of the polycarbonate substrate. At wavelengths > 420 nm all samples show a high optical transmittance nearly achieving the values determined for the uncoated substrate, indicating that all of the resultant coatings were highly transparent.

Table 4.1: Physical and photocatalytic properties of thin films on polycarbonate sheets modified with UV(C) light and a SiO_2 intermediate layer.

Entry	Photocatalytic thin film	Thickness / nm	Transmission at 500 nm / %	BET surface area / m² g⁻¹	CA / 1°					ξ / %			Δξ / % for	Ranking for
					before irradiation	after storage in the dark for 326 h	after Irradiation / X h	after dipping in oleic acid		MB	MS	AA	MB after	UV resistance
								before irradiation /X h	After irradiation /X h				abrasion test	
1	Pilkington Activ™	n.d.	n.d.	n.d.	67 ± 2	26	<5°/ 48 h	34.54°	<5°/140 h	0.026	0.009	0.07	45	n.d
2	Meso-TiO₂	203 ± 4	95	234	48 ± 5	35°	<5°/ 96 h	63.01°	<5°/ 675 h	0.078	0.016	0.084	30	1
3	TiO₂	132 ± 10	98	124	<5°	40°	<5°/ 48 h	68.74°	<5°/140 h	0.009	0.011	0.02	43	0
4	TZ 1:0.025	248 ± 4	98	n.d	<5°	34°	<5°/ 24 h	67.52°	<5°/120 h	0.012	0.008	0.029	14	0
5	TZ 1:0.05	169 ± 15	96	131	<5°	24°	<5°/ 24 h	63.3°	<5°/70 h	0.023	0.006	0.084	14	0
6	TZ 1:0.075	221 ± 18	96	n.d	<5°	31°	<5°/ 24 h	58.26°	<5°/120 h	0.021	0.011	0.049	21	0
7	TZ 1:0.1	202 ± 4	97	n.d	<5°	39°	<5°/ 24 h	56.41°	<5°/180 h	0.013	0.006	0.049	45	0
8	TZ 1:0.2	213 ± 10	98	71	<5°	39°	<5°/ 72 h	61.04°	<5°/180 h	0.014	0.005	0.065	40	4
9	ZnO	210 ± 23	97	n.d	<5°	41°	<5°/ 24 h	37.56°	<5°/180 h	0.011	0.006	0.046	87	0
10	TiO₂ (Hombikat)	186 ± 19	95	270	54 ± 3	53	<5°/ 72 h	52.06°	<5°/ 675 h	0.028	0.026	).0108	43	1
11	TS (1:0.2)	222 ± 5	95	n.d.	55 ± 2	48	<5°/ 72 h	63.80°	<5°/ 675 h	0.032	0.057	0.119	6	1
12	TS (1:0.5)	216 ± 11	94	n.d.	51 ± 4	17	<5°/ 48 h	59.58°	<5°/ 675 h	0.039	0.037	0.058	18	1
13	TS (1:0.8)	170 ± 30	94	374	53 ± 6	36	<5°/ 48 h	51.09°	<5°/ 675 h	0.046	0.025	0.065	26	1
14	TS (1:0.9)	144 ± 13	96	428	52 ± 2	25	<5°/ 48 h	47.49°	<5°/ 675 h	0.064	0.023	0.181	66	1
15	TS (1:1)	148 ± 25	95	391	52 ± 1	31	<5°/ 72 h	50.14°	<5°/ 675 h	0.046	0.035	0.025	23	1

* TZ = TiO₂-ZnO

**TS = TiO₂- SiO₂

The high transmittance values of the thus obtained photocatalytically active films are most likely caused by their high porosity, the small particle size, and additionally in the case of the mesoporous TiO_2 film, by the surface uniformity. On the other hand, the high transmittance of TiO_2-SiO_2 films, which have been prepared in the absence of any template, can be attributed to a decrease of the light scattering of the surface by the addition of small SiO_2 particle. Such a phenomenon has been reported before by Guan et al. [80].

4.2.2   Hydrophilic Properties

The hydrophilic properties of the layers, determined by the measurement of the water contact angle, show that the TiO_2-ZnO films are superhydrophilic immediately after their preparation (cf. entries 4-8 in Table 4.1). It is worth mentioning here that these layers have already been pre-irradiated by UV(A) for about 24h in order to remove the residual organic template, i.e., Pluronic 123 employed to introduce porosity to the prepared layers.

The mesoporous TiO_2 and TiO_2-SiO_2 films were found to be only slightly wettable by water (cf. entries 2, 11-15 in Table 4.1), i.e., only slightly hydrophilic. However, under UV(A) irradiation the water contact angle of these films decreased to values $< 5°$ evincing the superhydrophilicity of all coatings (Table 4.1). Thus, to establish the fully developed superhydrophilic state all the prepared samples have to be irradiated for several days (cf. Figure 3.46). Shorter irradiation times (of less than 24 hours) have been reported to yield the superhydrophilic state of self-cleaning TiO_2 coatings [60]. However, it should be mentioned that usually films showing a fast decrease of the water contact angle unpon UV(A) irradiation have been treated at temperatures $> 100°C$ [60] resulting in a removal of most of the organic adsorbate remaining at the surface after the coating process. Under our experimental conditions samples have been dried at ambient temperature and treated at $80°C$, therefore, it is assumed that residual ethanol is still adsorbed at the surface and is slowly decomposed by the photocatalytic action of the TiO_2 present in these films. This assumption is supported by the

fact that the time required to establish the superhydrophilic state is significantly shorter for samples which have already been converted into a superhydrophilic state and afterwards stored in the dark (cf. Figure 3.49).

All prepared photocatalytically active films show a long lasting superhydrophilicity, i.e., water contact angles $< 5°$, during storage at ambient atmosphere in the dark. Even after 326 hours of dark storage, the films exhibit significantly lower water contact angles than directly after their preparation. This long lasting superhydrophilicity seems to be a characteristic feature of these films and is similar to that reported by several authors [30-32] although they have prepared their films at higher temperatures.
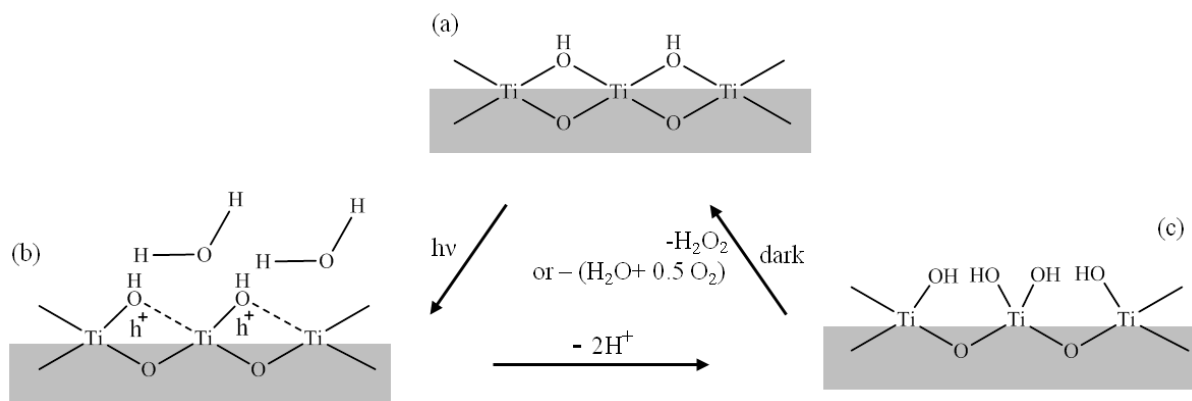
Figure 4.3: Changes in the O-H surface groups of a TiO$_2$ layer during UV(A) irradiation (a) Before irradiation, (b) (at the transition state) the photogenerated hole is trapped by lattice oxygen, and (c) (after UV irradiation) new OH groups are formed [81].

It has been postulated that the change of the wettability of a TiO$_2$ surface during UV(A) irradiation is due to the photoinduced reconstruction of Ti–OH bonds on the TiO$_2$ surface, i.e, it is due to an increase in the amount of surface OH groups [47]. Illumination of the TiO$_2$ surface with UV(A) light results in a lengthening of one of the Ti-O-Ti bonds on the surface via the trapping of a hole as shown in Figure 4.3. The adsorption of molecular water arouses the rupture of this weakened bond with a proton separation to mentain the charge equalization on the surface. Thus, a new OH group is formed. Long-term storage of TiO$_2$ surface resulted in reconversion of the surface wettability, which is attributed to the desorption of hydroxyl

groups from the surface in the form of H_2O_2 or H_2O and O_2. The desorption of these oxygen species was confirmed by XPS measurements by Sakai et al. [81].

It is also possible to build more than one layer of adsorbed water on the surface, or a porous wall in case of porous TiO_2, as has been explained by Wang et al. [82]. After the chemisorption of the first layer onto the available active sites of the TiO_2 surface as will be explained later, the next layer of water molecule is physisorbed through double hydrogen bonding on the two adjacent hydroxyl groups (Figure 4.4). The increasing thickness of the physisorbed water layers leads to a gradual filling of water molecules into the capillary pores, in the case of porous TiO_2, according to Kelvin's law [82].
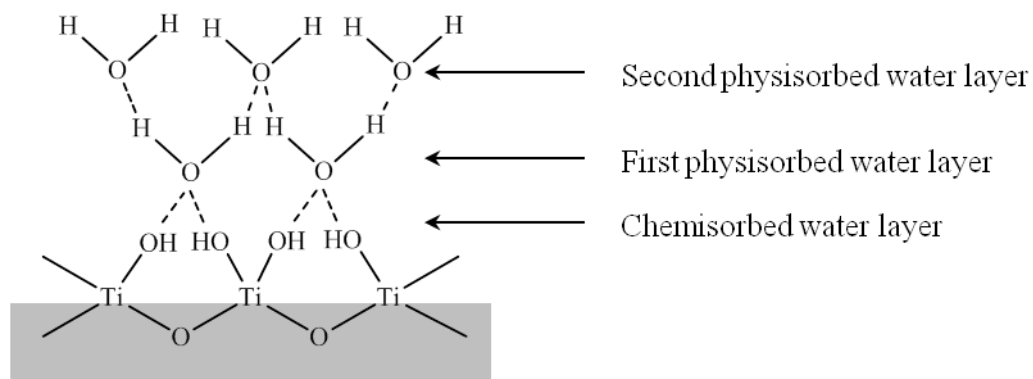
Figure 4.4: Schematic diagram of water chemi- and physi--adsorption on the surface of TiO_2 [82].

In the case of TiO_2-SiO_2 composite oxides, the hydrophilicity of TiO_2-SiO_2 thin films can be explained by the following reasons: (1) Surface roughness of the films leading to increased hydrophilicity. (2) Chemical or morphological changes of the surface structure resulting from the conversion of relevant Ti^{4+} sites to Ti^{3+} sites by trapping of conduction band electrons formed by excitation of the semiconducting TiO_2 have been suggested to be favorable for dissociative water adsorption. (3) Enhanced acidity of the Si–O–Ti bonds at the interfaces possibly inducing a greater amount of hydroxyl groups at the film surface.

It has been proposed by Tanabe et al. [83] that acid sites on binary metal oxides are formed

by an excess of negative or positive charges in the mixed oxides. For TiO_2-SiO_2 mixed oxides, where TiO_2 is the major component, Lewis acidity is assumed to appear, while in the case SiO_2 being the major component, Brønsted acidity is predicted. A recently published extension of Tanabe´s hypothesis predicts for TiO_2.-SiO_2 mixed oxides, where TiO_2 is the major component, the coexistence of Lewis acid sites and Brønsted acid sites at the surface of the mixed oxide with the Lewis acid sites being the major sites [84]. Consequently, the enhanced hydrophilicity of the TiO_2-SiO_2 composite films has been explained by several authors by this increase of the surface acidity [80, 85-87].

Actually the amount of –OH groups on TiO_2 films has a strong influence on their surface wettability, but it is not only the affecting factor. Factors such as porosity, pore size, morphology, and roughness of the films [88, 89] need to be taken into account as well. Furthermore, the water contact angle also strongly depends on the chemical composition and also on the morphology of the films [90].

4.2.3   Photoinduced Superhydrophilicity Conversion under Polluted Atmosphere

In the presence of pollutants, such as acetone or propan-2-ol, the effect of the atmosphere around the films on their hydrophilic properties was studied for the TiO_2-ZnO films. Exposure of the superhydrophilic films to an atmosphere containing a high concentration of one of these organic molecules (acetone or propan-2-ol) resulted in an increase of the water contact angle from values $<5°$ to values of $>30°$ within two hours of exposure (cf. Figure 3.38 and Figure 3.39).

When the films prepared here and Pilkington Activ^{TM} glass were stored in the dark in an atmosphere containing propan-2-ol, the TiO_2 and ZnO films maintained their superhydrophilicity for 1h while the TiO_2-ZnO film with a molar ratio 1:0.05 and Pilkington Avtiv^{TM} glass preserved their superhydrophilicity for 2h. After the increase of their water contact angles, all films were irradiated with UV light. As a consequence, the contact angles

of the prepared films decreased to values < 5° after 6h of UV(A) illumination whereas the contact angle of Pilkington Activ^{TM} glass became <5° after 12h irradiation (cf. Figure 3.38).

The effect of the addition of ZnO to TiO$_2$ on the photoinduced properties was less pronounced in the case of acetone being the gas phase pollutant. Figure 3.39 presents the time dependence of the change in water contact angle for TiO$_2$-ZnO films during the storage in the dark under an atmosphere of acetone and during subsequent UV(A) irradiation with 10 Wm^{-2}. The water contact angle of the TiO$_2$-ZnO (1:0.05) film increased after 1h of storage in the dark in an acetone containing atmosphere. After UV irradiation for 5h, its contact angle decreased again from 65° to <5°. The commercial Pilkington Activ^{TM} glass has stable superhydrophilic properties for 0.75h. After this time its water contact angle increased. Then its surface was irradiated by UV(A) light. Consequently, its water contact angle drops from 64° to <5° within 5h of UV irradiation.

The rate of conversion of a surface from a hydrophilic to a hydrophobic state depends on the adsorption of the hydrocarbons onto their surfaces which depends on their polarity as well as on the polarity of the adsorbent pollutant. The recovery of their hydrophilicity depends on their photocatalytic activity and their water adsorption ability. Acetone and propan-2-ol were used here as organic pollutants. The polarity index of acetone and propan-2-ol are 5.1 and 3.9, respectively. This means that acetone should be adsorbed more strongly on polar surfaces than propan-2-ol. Indeed, it can be observed by the comparison between Figure 3.38 and Figure 3.39 that acetone needs longer time than propan-2-ol to decompose on the surfaces and become superhydrophilic again (The calculated rates of conversions to superhydrophilic state for TiO$_2$-ZnO 1:0.05 and Pilkington Activ^{TM} are -9°/1h and -5°/1h respectively under 2-propanolic atmosphere and -13°/1h and -12°/1h respectively under acetonic atmosphere). Since acetone is proposed to be an intermediate in the photocatalytic oxidation of propan-2-ol, it is expected that the photocatalytic removal of acetone is faster than that of propan-2-ol. However, the

amount of acetone adsorbed on the TiO_2 surface, presents in saturated acetone atmosphere, will be higher than that of propan-2-ol adsorbed on the surface of TiO_2, presents in saturated propan-2-ol atmosphere, due to the high affinity of TiO_2 surface to acetone [91]. This explains the lower removal rate, expressed as the decreasing rate in the contact angle, of acetone in comparison with the removal rate of propan-2-ol in our case.
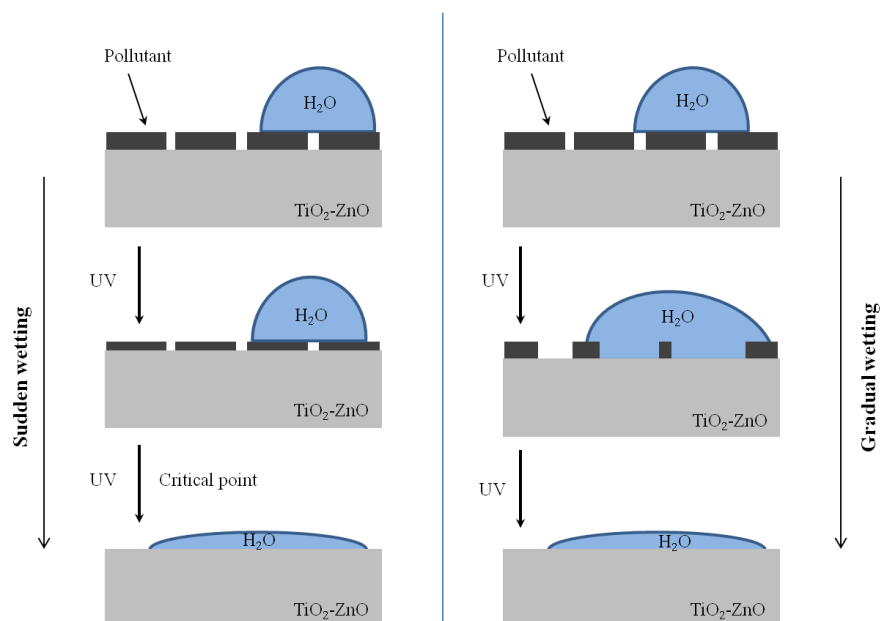
Figure 4.5: Dependence of the hydrophilicity of photocatalytically active surfaces in a polluted atmosphere on the photocatalytic process [92].

The proposed to explain mechanism for the UV-induced hydrophilicity of photocatalytically active surfaces exposed to a polluted atmosphere is based on the photocatalytic process [92]. Adsorbed organic contaminants will be oxidized photocatalytically, thus, the ''clean'' surface shows hydrophilic properties. The schemes in Figure 4.5 differentiate two different ways of pollutant removal, i.e. the layer by layer way (Figure 4.5, left) and the partial way (Figure 4.5, right). In the former one, the water droplet will not spread over the surface until the organic contaminants are totally decomposed by the photocatalytic effect. At this critical point the water droplet moves towards the clean surface and spreads completely. In the second case, the contamination decreases continuously at certain points on the surface under illumination with UV-light, which is followed by the

observed decrease of water contact angle. As the water contact angle on the prepared TiO_2-ZnO films exposed to a polluted atmosphere decreases gradually as a function of the irradiation time (cf. Figure 3.38 and Figure 3.39), the proposed ''partial'' way (Figure 4.5, right) appears to be more favorable mechanism here.

4.2.4   Photocatalytic Activity

All TiO_2-containing films prepared during this work were found to be photocatalytically active for methylene blue degradation test which is considered to be applicable to evaluate the specific self-cleaning activity of photocatalytic surfaces [67, 93].

Films obtained from already prepared powder

the films prepared from mesoporous TiO_2 and from Hombikat UV100 exhibit photonic efficiencies comparable or even outperforming that of commercial Pilkington Activ^{TM} glass, i.e., ξ = 0.026%, 0.009%, and 0.07% for MB, MS, and AA, respectively. The photonic efficiencies determined for the TiO_2- SiO_2 films indicate a promoting influence of the amount of SiO_2 incorporated into the TiO_2 film on the photocatalytic activity. This promoting effect of SiO_2 might be due to an increase of the roughness of the photocatalytically active thin film (Figure 3.47) resulting in an increase of the surface area (see entries 10, 13-15,Table 4.1) and/or to the capacity of SiO_2 to act as an adsorbent [71, 94]. The increase of surface area is known to facilitate the formation of more effective adsorption sites which might promote the photocatalytic activity by increasing the local concentration of contaminants, i.e., MB and AA, and of reaction intermediates near the TiO_2 surface [95]. The photocatalytic degradation efficiencies of mesoporous TiO_2 exceeds that of Hombikat UV-100 thin films for both MB and AA, although the Hombikat TiO_2 material is a highly crystalline anatase phase (100% anatase phase) and is, therefore, much more crystalline than the prepared mesoporous TiO_2 films here (c.f. Figure 3.16). This difference cannot be explained by different surface areas or crystallinity, both of which are even higher for the Hombikat material. The high photonic efficiencies of the

mesoporous TiO_2 films as compared with the Hombikat UV100 films can rather be attributed to different effects, such as a lower light scattering effect of the ordered mesopores, an accumulated local concentration of $^{\bullet}OH$, [96, 97] and/or a fast transport of the target molecules, i.e., MB and AA, to the active sites. The latter can be expected due to their facile diffusion through the ordered porous network, which for Hombikat UV100 is hindered by the heterogeneity existing in the bulk sample. Therefore, we conclude that the mesoporous TiO_2 supports the transport properties of all reactants involved in the photocatalytic process and, thus, enhances the overall photocatalytic activity. Hence, the photocatalytic $^{\bullet}OH$ production is expected to occur mainly on internal surfaces [98]. Furthermore, MB or AA adsorption onto mesoporous TiO_2 should take place mainly within the pores of this high surface area material. Therefore, it can be expected that the concentration of these molecules inside the pores will be higher in the mesoporous TiO_2 samples as compared with Hombikat UV100. Although the films prepared from mesoporous TiO_2 and from Hombikat UV100 have almost similar thickness (~200nm), the photonic efficiency of meso-TiO_2 is found to be three times higher than the photonic efficiency of the Hombikat UV100 film. This is attributed to the photonic efficiency being limited by the diffusion rate of these molecules to the photocatalytically active surface, as a result of the difference in the size and in the number of pores. It is worth noting that Hombikat UV100 has also some porosity as can be seen from Figure *3.17*. However, the absence of the hysteresis loop for the commercial photocatalyst Hombikat UV100 shows that the mesoporosity of this sample is lower than that of mesoporous TiO_2, i.e., the pores in UV100 can be regarded as irregular voids between TiO_2 particles [66].

Moreover, the porosity can enhance the photocatalytic activity of the prepared films via the so-called antenna effect [99]. In this case, the three-dimensional mesoporous TiO_2 network acts as an antenna system transferring the initially generated charged carriers from the location of light absorption to the point on which the organic pollutant is adsorbed.

Furthermore, the photocatalytic activity has been reported to increase with larger surface area and smaller pore size distribution [100].

On the other hand, the films prepared from Hombikat UV100 exhibit better photocatalytic activity for the MS degradation than the mesoporous TiO_2 films. This can be explained by the difference of their wettability. While methyl stearate has hydrophobic properties, TiO_2 has hydrophilic properties. Furthermore, as mentioned in the experimental part, mesoporous TiO_2 is prepared using Pluronic F127, which improves the wettability, whereas Hombikat UV100 is prepared without using any template. That means, spreading of methyl stearate on Hombikat UV100 surface is favorite rather than the mesoporous TiO_2 surface. Thus, the contact between methyl stearate and Hombikat UV100 should be better thus increasing the degradation efficiency of methyl stearate.

Effect of the addition of ZnO to TiO$_2$

Both pure TiO_2 and ZnO coatings show only rather small photocatalytic activities in the MB and AA degradation tests, whereas, the TiO_2-ZnO coatings exhibit higher photonic efficiencies in these tests, which, however, are not higher than Pilkington Activ^{TM} glass. The TiO_2-ZnO coating with a molar ratio of 1: 0.05 exhibits the highest photonic efficiency ($\xi_{MB} =$ 0.023%), which is only about 10% lower than the photonic efficiency determined for Pilkington Activ™ glass.

The modification of the electronic properties of the coupled materials with respect to the single ones is invoked to explain the increased activity of TiO_2-ZnO as compared with both pure materials. Thus, the electron transfers from the conduction band of ZnO to the conduction band of TiO_2 under illumination and, conversely, the hole transfers from the valence band of TiO_2 to the valence band of ZnO should result in a decrease of the rate of electron-hole recombination, i.e., to an increase of the lifetime of the charge carriers (see Figure 4.6). This modification increases the availability of the electron-hole pairs on the

surface of the photocatalysts and consequently improves the occurrence of redox processes [101]. It has also been reported that the surface recombination occurs more easily in ZnO [100] thus providing an explanation for the decreasing photonic efficiencies at high molar ratio of ZnO: TiO$_2$.
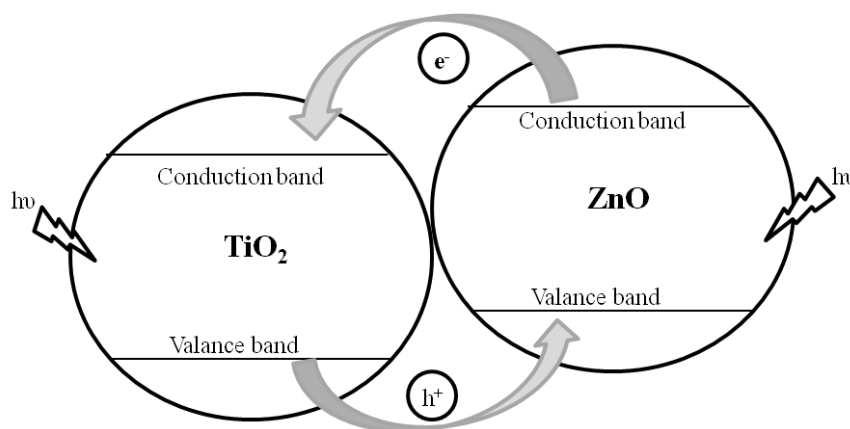
Figure 4.6: Energy diagram for a heterogeneous TiO$_2$-ZnO film [101].

The photonic efficiencies of the photocatalytic MS degradation on the surface of the TiO$_2$ and TiO$_2$-ZnO thin films have been found to be in the same range as those determined for Pilkington Activ™ glass (ξ_{MS} = (0.009 $\pm$ 0.002)%). The TiO$_2$-ZnO coating on the polycarbonate substrate with a molar ratio of 1: 0.05 exhibits a photonic efficiency of (0.006 $\pm$ 0.0015)% which is comparable with the value of Pilkington Activ™. This is attributes to the similar wettability of TiO$_2$ and ZnO.

4.2.5   Self-Cleaning Performance

The self-cleaning performance was tested according to the ISO 27448 method [69]. After applying oleic acid to the surfaces of the prepared films, the surfaces are converted to hydrophobic state (with different water contact angle values depending on the nature of these surfaces) due to the hydrophobic property of oleic acid adsorbed on the surfaces. During UV(A) irradiation of the oleic acid coated films, oleic acid adsorbed on the surface is decomposed by the photocatalytic oxidation as well as the prepared films themselves (meso-TiO$_2$, Hombikat UV100,TiO$_2$- SiO$_2$, TiO$_2$, ZnO, and TiO$_2$-ZnO) which in turn become

hydrophilic simultaneously (see Table 4.1). The main products of photocatalytic degradation

of oleic acid are nonanal and 9- oxononanoic acid [102]. Therefore, the nonanal will produce

azelaic acid and/or octanoic acid. On the other hand, oxononanoic acid will be degraded

photocatalytically yielding nonanoic acid (cf. Figure 4.7).
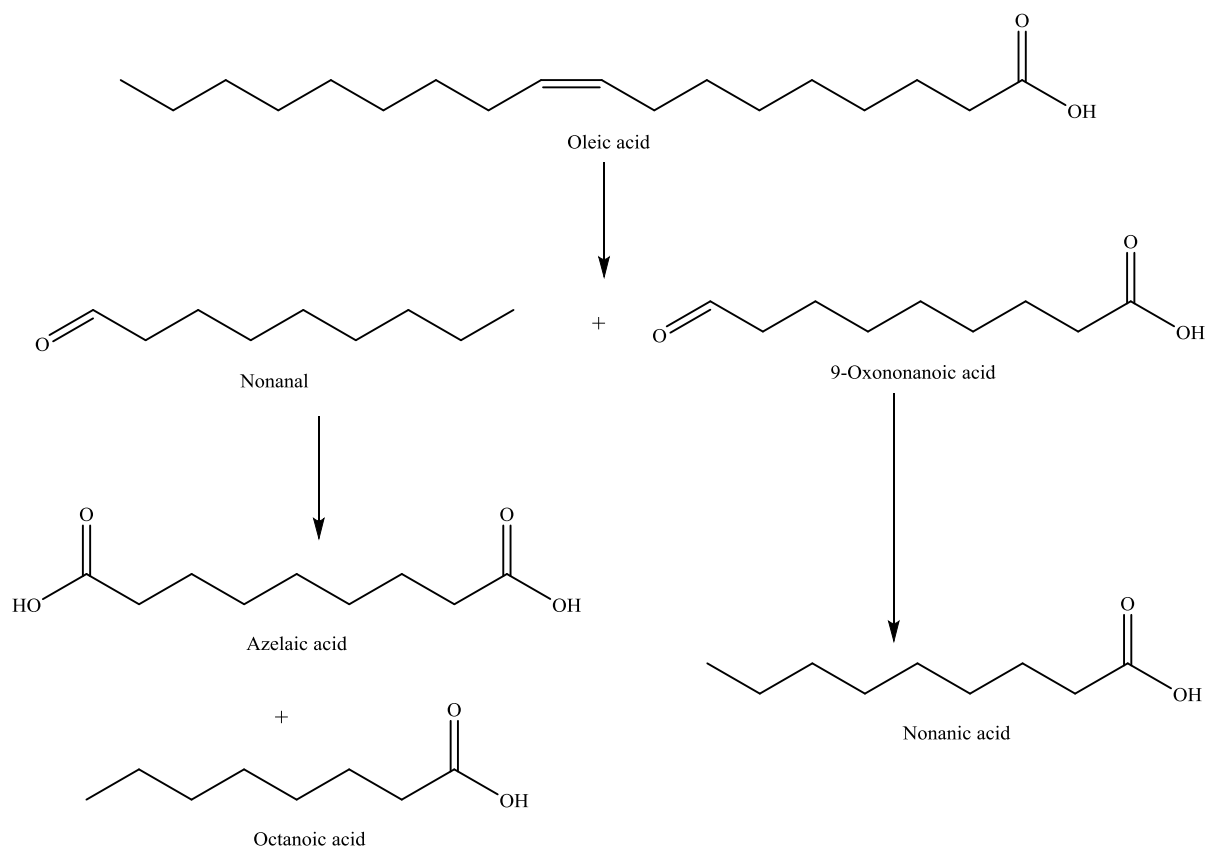
Figure 4.7: The main products of the photocatalytic degradation of oleic acid.

It is well known that 9-oxononanoic acid is much more hydrophilic than nonanal. The

formation of 9-oxononanoic acid as the main product of the photocatalytic degradation of

oleic acid leads to a faster decrease of the water contact angle than the case of the formation

of nonanl. On the other hand, the products of the photocatalytic degradation of nonanal are

more hydrophilic than the product of the photocatalytic degradation of 9-oxononanoic acid.

That brings us to assume that on the surface of the Hombikat UV100 and TiO_2 films, 9-

oxononanoic acid is mainly could be produce whereas the nonanal is mainly might be produce

on the surface of meso-TiO_2, ZnO, and TiO_2-SiO_2 (1:0.2) films. In the case of the TiO_2-ZnO

and TiO_2-SiO_2 (except the molar ratio 1:0.2) films, nonanal and 9-oxononanoic acid may be produce in different ratio depending on the molar ratio of TiO_2 to ZnO or Hombikat to SiO_2.

As result, in the comparison between all the prepared films, TiO_2-ZnO with molar ratio (1:0.05) shows the best self-cleaning performance.

The mechanism for the UV- induced superhydrophilicity in the case of the oleic acid degradation can be described according to ref [1]. In their mechanism the authors combined the three individual mechanisms (i.e., the generation of surface vacancies, the photo-induced reconstruction of Ti-OH bonds and the photocatalytic decomposition of organic adsorbents). If a surface is contaminated with organic compounds, these compounds will be photocatalytically decomposed by UV irradiation until a "clean" surface is reached. After that, the UV-generated electron-hole pairs are consumed to form oxygen vacancies. Meanwhile, water molecules may coordinate into the oxygen vacancy sites ($\square$) leading to the dissociative adsorption of the water molecules on the surface. This process gives rise to increased water adsorption on the illuminated surfaces [1]. By the adsorption of molecular water, new OH groups are built at the surface and the surface energy is then increased due to an increasing number of hydrogen bonds, consequently, hydrophilic conversion is achieved. In the absence of UV light, the newly built hydroxyl groups desorbed and the initial state appears again [1].

4.2.6   Mechanical Stability and Adhesion Strength

Abraiding the prepared photocatalytically active films with a felt prior to the methylene blue degradation test resulted in significantly lower photonic efficiencies. The photonic efficiencies after stability test of all TiO_2-ZnO and Hombikat UV100-SiO_2 films are generally higher than the photonic efficiencies of the pure materials. Thus means that the addition of ZnO or SiO_2 improves the stabilisation of the surface against abrasion which depends on the type of binding which can be formed between the film and the substrate [103]. Furthermore,

the SiO_2 interlayer plays an important role in improving the adhesion strength between the films and polycarbonate substrate. It forms covalent bonds between the polycarbonate substrate on one side and the photocatalytically active layer on the other side [104].

Moreover, an increase of the water contact angle was observed after applying a felt abrasion test. However, this effect was found to be reversible under UV(A) irradiation indicating rather a contamination of the surface by photocatalytically degradable organic compounds than a deterioration of the functional surface.

On the other hand, the prepared films exhibit good adhesion qualities as defined quantitatively by cross-cut tests according to ISO 2409 standard (cf. Figure 3.24, Figure 3.41, and Figure 3.51) The results revealed that all prepared films (except TiO_2-ZnO 1:0.2) were quite stable and adhesive and that the SiO_2 interlayer actually performs its task as a protecting layer against damage initiated by photocatalytically generated oxidizing species such as hydroxyl radicals.

5   Conclusions

- In this work, polycarbonate was successfully coated with stable photocatalytic and superhydrophilic thin films employing a dip coating sol-gel method with respective adhesion strength, mechanical stability, and self-cleaning properties.

- The binding between the polycarbonate and the photocatalytically active layer has been improved through the light modification (UV(C)) of polycarbonate's surface and the addition of the SiO_2 intermediate layer.

- A systematic work has been performed to study how the coatings on the polycarbonate surface affect the adhesion strength, the mechanical stability, the wettability, and the photocatalytic activity. The coated surfaces displayed considerable photocatalytic activity and superhydrophylicity after exposure to UV(A) light. The results revealed that the mesoporous TiO_2 film has the highest

photonic efficiency for MB degradation. However, its activity decreases by 45% after the felt abrasion test. The addition of SiO_2 resulted in an improvement of the optical properties by a decrease of the light scattering, and to an increase of the photocatalytic activity of the TiO_2 film reaching the highest value at a molar ratio TiO_2-SiO_2 equal to 1:0.9 and at 1:0.2 for methyl stearate degradation. In spite of the high photocatalytic activities of these films, rather long illumination times are requierd to reach the superhydrophilic state. On the other hand, the superhydrophilic coating with a molar TiO_2-ZnO ratio of 1: 0.05 exhibits the best results of the photonic efficiency combined with a good mechanical stability and a very good stability against UV irradiation.

6   References

1.   Zhang, L., Dillert, R., Bahnemann, D., Vormoor, M.; *Photo-induced hydrophilicity and self-cleaning: models and reality*; **Energy Environ. Sci**., **2012**, 5, 7491-7507.

2.   Gould, P.; *Smart clean surfaces*; **Mater. today**, **2003**, 6, 44-48.

3.   Mills, A., Lepre, A., Elliott, N., Bhopal, S., Parkin, I.P., Neill, S.A.O.; *Characterisation of the photocatalyst Pilkington Activ™: a reference film photocatalyst?*; **J. Photochem. Photobio. A**, **2003**, 160, 213-224.

4.   Adams, M.R., Gartonl, A.; *Surface modification of bisphenol-A-polycarbonate by far-UV radiation. Part II: In air*; **Polym. Degrad. Stab**., **1993**, 42, 145-151.

5.   Polycarbonate Market Forecasts and Growth Trends to 2015 - Increased Growth in Electronic Applications Driving the Market. GBI Research; Online available at www.marketresearch.com/vendors/viewvendor.asp?vendorid=3759.

6.   PC/BPA group Plastics Europe, Applications of BPSA, August 2007.

7.   Schnell, H.; *Herstellung und Eigenschaften aromatischer Polyester der Kohlensäure*; **Angew. Chem. Int. Ed**., **1956**, 68, 633-640.

8.   *Polycarbonate: A major contributor to Europe's economy and quality of life*, 2007, www.bisphenol-a-europe.org].

9.   Houmard, M., Riassetto, D., Roussel, F., Bourgeois, A., Berthome,G., Joud, J.C., Langlet, M.; *Morphology and Natural Wettability Properties of Sol–Gel Derived TiO$_2$–SiO$_2$ Composite Thin Films*; **Appl. Surf. Sci.**, **2007**, 254, 1405–1414.

10.   Yu, J., Zhao, X., Yu, J.C., Zhong, G., Han, J., Zhao, Q.; *The Grain Size and Surface Hydroxyl Content of Super-hydrophilic TiO$_2$/SiO$_2$ Composite Nanometer Thin Films*; **J. Mater. Sci. Letters**, **2001**, 20, 1745 – 1748.

11.   Fateh, R.; Ismail, A.A.; Dillert R.; Bahnemann, D.; *Highly Active Crystalline Mesoporous TiO$_2$ Films Coated onto Polycarbonate Substrates for Self-Cleaning Applications*; ***J. Phys. Chem. C***, **2011**, 115, 10405-10411.

12.   Niehimoto, S., Bhushan, B.; *Bioinspired self-cleaning surfaces with superhydrophobicity, superoleophobicity, and superhydrophilicity*; ***RSC Adv.***, **2013**, 3, 671-690.

13.   Parkin, I.P., Palgrave, R.G.; *Self-cleaning coatings*; ***J. Mater. Chem***., **2005**, 15, 1689-1695.

14.   Irie, H., Hashimoto, K.; *Photocatalytic active surfaces and photoinduced high hydrophilicity/ high hydrophobicity*; ***Hdb Env Chem***, **2005**, 2, 425.

15.   Goddard, J.M., Hotchkiss, J.H.; *Polymer surface modification for the attachment of bioactive compounds*; ***Prog. Polym. Sci***., **2007**, 32, 698-725.

16.   Ryan, B.J., Poduska, K.M.; *Roughness effects on contact angle measurements*; ***Am. J. Phys***., **2008**, 76, 1074-1077.

17.   Feng, X., Jiang, L.; *Design and creation of superwetting/ antiwetting surfaces*; ***Adv. Mater***., **2006**, 18, 3063-3078.

18.   Morris, R.E.; *The Sol-Gel Process: Uniformity, Polymers and Applications*; ***Nova Science Pub***., **2011**.

19.   Hoffmann, M.R., Martin, S.T., Choi, W., Bahnemann, D.W.; *Environmental Applications of Semi-conductor Photocatalysis*; ***Chemical Reviews***, **1995**, 95, 69-96.

20.   Arimitsu, N., Nakajima, A. Katsumata, K.I., Shiota, T., Watanabe, T., Yoshida, N., Kameshima, Y., Okada, K.; *Photoinduced surface roughness variation in polycrystalline TiO$_2$ thin films under different atmospheres*; ***J. Photochem. Photobiol. A***, **2007**, 190, 53-57.

21.   Wang, R., Sakai, N., Fujishima, A., Watanabe, T., Hashimoto, K.; *Studies of Surface Wettability Conversion on TiO$_2$ Single-Crystal Surfaces; J. Phys. Chem. B*, **1999**, 103, 2188-2194.

22.   Liu, Z., Zhang, X., Murakami, T., Fujishima, A.; *Sol–gel SiO$_2$/TiO$_2$ bilayer films with self-cleaning and antireflection properties*; ***Sol. Energy Mater. Sol. Cells***, **2008**, 92, 1434-1438.

23.   Carp, O., Huisman, C.L., Reller, A.; *Photoinduced reactivity of titanium dioxide*; ***Prog. Solid State Chem***., **2004**, 32, 33-177.

24.   Corma, A.; *From Microporous to Mesoporous Molecular Sieve Materials and Their Use in Catalysis*; ***Chem Rev***., **1997**, 97, 2373-2420.

25.   W.-S. Chae, S.-W. Lee and Y.-R. Kim, *Templating Route to Mesoporous Nanocrystalline Titania Nanofibers* ; ***Chem. Mater***., **2005**, 17, 3072–3074.

26.   Inumaru, K., Yasui, M., Kasahara, T., Yamaguchi, K., Akira Yasuda, A., Yamanaka, S; *Nanocomposites of crystalline TiO$_2$ particles and mesoporous silica: molecular selective photocatalysis tuned by controlling pore size and structure; **J. Mater. Chem**.*, **2011**, 21, 12117- 12125.

27.   Suwanchawalit, C., Wongnawa, S.; *Triblock copolymer-templated synthesis of porous TiO$_2$ and its photocatalytic activity*; ***J. Nanopart. Res***., **2010**, 12, 2895-2906.

28.   Ismail, A. A., Bahnemann, D. W.; *Mesoporous titania photocatalysts: preparation, characterization and reaction mechanisms*; ***J. Mater. Chem***., **2011**, 21, 11686- 11707.

29.   Fu , X., Clark , L.A., Yang , Q., Anderson, M.A.; *Enhanced Photocatalytic Performance of Titania-Based Binary Metal Oxides: TiO$_2$/SiO$_2$ and TiO$_2$/ZrO$_2$*; ***Environ. Sci. Technol***., **1996**, *30*, 647–653.

30.   Cetinkaya, T., Neuwirthová, L., Kutláková, K. M., Tomásek, V., Akbulut, H.; *Synthesis of nanostructured TiO$_2$/SiO$_2$ as an effective photocatalyst for degradation of acid orange*; ***Appl. Surf. Sci.***, **2013**, 279, 384-390.

31.   Gnatyuk, Y.; Smirnova, N.; Eremenko, A.; *Design and photocatalytic activity of mesoporous TiO₂/ZrO₂ thin films*; ***Adsorp. Sci. Technol***., **2005**, 23, 497-508.

32.   Ennaoui, A., Sankapal B.R., Skryshevsky V. Lux-Steiner M.C.; *TiO₂ and TiO₂-SiO₂ Thin Films and Powders by One-step Soft Solution Method: Synthesis and Characterizations*; ***Sol. Energ. Mater. Sol. Cells***; **2006**, 90, 1533-1541.

33.   Zhou L., Yan S., Tian B., Zhang J. Anpo M.; *Preparation of TiO₂-SiO₂ film with High Photocatalytic Activity on PET Substrate*; ***Mater. Lett***., ***2006***, 60, 396-399.

34.   Cheng, P., Zheng, M., Jin, Y., Huang, Q., Gu, M.; *Preparation and Characterization of Silica Doped Titania Photocatalyst Through Sol-Gel Method*; ***Mater. Lett***., **2003**, 57, 2989-2994.

35.   Abd Aziz, R., Asyikin, N., Sopyan, I.; *Synthesis of TiO₂-SiO₂ powder photocatalyst via sol – gel method: effects of titanium precursor type on powder properties*; ***J. Inst. Eng. Malay.,*** **2009**, 70, 34-40.

36.   Liao, S., Donggen, H., Yu, D., Su, Y., Yuan, G.; *Preparation and characterization of ZnO/TiO₂, SO₄²⁻/ZnO/TiO₂ photocatalyst and their photocatalysis*; ***J. Photochem. Photobiol. A***, **2004**, 168, 7-13.

37.   Mills, A., Matthew, C.; *A study of factors that change the wetability of titania films*; ***Inter. J. Photoenergy***, **2008**, (Article Number: 470670).

38.   Nakajima, A., Koizumi, S., Watanabe, T., Hashimoto, K.*; Effect of repeated photo-illumination on the wettability conversion of titanium dioxide*; ***J. Photochem. Photobiol., A***, **2001**, 146, 129-132.

39.   White, J. M., Szanyi, J., Henderson, M. A.; *The Photon-Driven Hydrophilicity of Titania: A Model Study Using TiO₂(110) and Adsorbed Trimethyl Acetate***; J. Phys. Chem. B**, **2003**, 107, 9029- 9033.

40.   Sakai, N., Fujishima, A., Watanabe T., Hashimoto, K.; *Quantitative Evaluation of the Photoinduced Hydrophilic Conversion Properties of TiO₂ Thin Film Surfaces by the Reciprocal of Contact Angle*; **J. Phys.Chem. B**, *2003*, 107, 1028 -1035.

41.   Takeuchi, M., Sakamoto, K., Martra, G., Coluccia, S., Anpo, M.; *Mechanism of Photoinduced Superhydrophilicity on the TiO₂ Photocatalyst Surface*; **J. Phys. Chem. B**, **2005**, 109, 15422- 15428.

42.   Sun, R-D., nakajima, A., Fujishima. A., Watanabe. T., Hashimoto, K.; *Photoinduced surface wettability conversion of ZnO and TiO₂ thin films*; **J. Phys. Chem. B**, 2001, 105, 1984-1990.

43.   Hennessy, D. C., Pierce, M., Chang, K.C., Takakusagi, S., You, H., Uosaki, K.; *Hydrophilicity transition of the clean rutile TiO₂ (1 1 0) surface*; **Electrochim. Acta**, **2008**, 53, 6173- 6177.

44.   Mackenzie, J.D., Bescher, E.; *Some Factors Governing the Coating of Organic Polymers by Sol-Gel Derived Hybrid Materials*, **J. Sol-Gel Sci. Technol**., **2003**, 27, 7-14.

45.   Langlet, M., Kim, A., Audier, M., Guillar, C., Herrmann, J.M.; *Transparent photocatalytic films deposited on polymer substrates from sol–gel processed titania sols*; **Thin Solid Films**, **2003**, 429, 13–21.

46.   Schmidt, H.; *Chemistry of material preparation by the sol-gel process*; **J. Non-Cryst. Solids**, **1988**, 100, 51-64.

47.   Brinker, C.J., Scherer, G.W., *Sol- Gel Science*, **Academic Press**, **2002**.

48.   Beling, S., "Nasschemische Abscheidung und Charakterisierung Charakterisierung von TiO₂-Schichten den Sensoreinsatz beim Gasnitrieren ". **2002**.

49.   Sahu, N., Parija, B., Panigrahi, S.; *Fundamental understanding and modeling of spin coating process: A review*; **Indian J. Phys**., **2009**, 83, 493-502.

50. Faure, B., Salazar-Alvarez, G., Ahniyaz, A., Villaluenga, I., Berriozabal, V., Miguel, Y. R. D., Bergstr̈om, L.; *Dispersion and surface functionalization of oxide nanoparticles for transparent photocatalytic and UV-protecting coatings and sunscreens*; **Sci. Technol. Adv. Mater.**, **2013**, 14**,** 23001-23024.

51. Diepens, M., Gijsman, P.; *Photo-oxidative degradation of bisphenol A polycarbonate and its possible initiation processes*; **Polym. Degrad. Stab**., **2008**, 93, 1383-1388.

52. Diepens, M., Gijsman, P.; *Photodegradation of bisphenol A polycarbonate*; **Polym. Degrad. Stab.**, **2007**, 92, 397-406.

53. Fujishima, A.Z., Zhang, X., Tryk, D.A.; *TiO$_2$ photocatalysis and related surface phenomena*; **Surf. Sci. Rep**., **2008**, 63, 515-582.

54. Ganesh, V. A., Raut, H. K., Nair A.S., Ramakrishna, S.; *A review on self-cleaning coatings; **J. Mater. Chem**., **2011**, 21, 16304-163022.

55. Nakata, K.F., Fujishima, A.; *TiO$_2$ photocatalysis: Design and applications*; **J. Photochem. Photobiol. C**, 2012, 13, 169-189.

56. Çamurlu, H.E., Kesmez, Ö., Burunkaya, E., Kiraz, N., Yeşil, Z., Asiltürk, M., Arpaç, E.; *Sol-gel thin films with anti-reflective and self-cleaning properties*; **Chem. Pap**., 2012, 66, 461-471.

57. Langlet, M.; Kim, A.; Audier, M.; Herrmann, J. M.; *Sol-Gel Preparation of Photocatalytic TiO$_2$ Films on Polymer Substrates*; **J. Sol-Gel Sci. Technol**., **2002**, 25, 223-234.

58. Langlet, M. Kim, A., Audier, M., Guillard, C., Herrmann, J.M.; *Liquid phase processing and thin film deposition of titania nanocrystallites for photocatalytic applications on thermally sensitive substrates*; **J. Mater. Sci**., **2003**, 38, 3945-3953.

59. Kwon, C.H.; Shin, H.M.; Kim, J.H.; Choi, W.S.; Yoon, K.H.; *Degradation of methylene blue via photocatalysis of titanium dioxide*; **Mater. Chem. Phys**., **2004**, 86, 78-82.

60.   Lam, S-W, Soetanto, A., Amal, R.; *Self-cleaning performance of polycarbonate surfaces coated with titania nanoparticles*; ***J. Nanopart. Res***., **2009**, 11, 1971-1979.

61.   Yaghoubi, H.; Taghavinia, N.; Alamdari, E.K.; *Self-cleaning TiO₂ coating on polycarbonate: Surface treatment, photocatalytic and nanomechanical properties*; ***Surf. Coat. Technol.***, **2010**, 204, 1562-1568.

62.   Matsuda, A.; Matoda, T.; Kotani, Y.; Kogure, T.; Tatsumisago, M.; Minami, T.; *Evaluation of Photocatalytic Activity of Transparent Anatase Nanocrystals-Dispersed Silica Films Prepared by the Sol-Gel Process with Hot Water Treatment*; ***J. Sol-Gel Sci. Technol***., **2003**, 26, 517-521.

63.   Horiuchi, Y., Ura, H., Kamegawa, T., Kohsuke Mori, K., Yamashita, H.; *Low-temperature synthesis of highly hydrophilic Ti-containing mesoporous silica thin films on polymer substrates by photocatalytic removal of structure-directing agents*; ***J. Mater. Chem***., **2011**, 21, 236-241.

64.   Rivaton, A., Mailhot, B., Soulestin, J., Varghese, H., Gardette, J.-L.; *Influence of the chemical structure of polycarbonates on the contribution of crosslinking and chain scissions to the photothermal ageing*; ***Europ. Poly. J***., **2002**, 38, 1349–1363.

65.   Aslan, K., Holleya, P., Geddes, C. D.; *Metal-enhanced fluorescence from silver nanoparticle-deposited polycarbonate substrates*; ***J. Mater. Chem***., **2006**, 16, 2846–2852.

66.   Ismail, A.A., Bahnemann, D.W., Robben, L., Yarovyi, V., Wark, M.; *Palladium Doped Porous Titania Photocatalysts: Impact of Mesoporous Order and Crystallinity*; ***Chem. Mater***., **2010**, 22, 108-116.

67.   DIN *52980, Photokatalytic activity of surfaces – Determination of photocatalytic activity in aqueous medium by degradation of methylene blue*, ***Der Normenausschusses Materialprüfung***, www.nmp.din.de.

68.   22197-2:2011, I., "Fine ceramics (advanced ceramics, advanced technical ceramics) --
        Test method for air-purification performance of semiconducting photocatalytic
        materials -- Part 2: Removal of acetaldehyde". **2011**.

69.   ISO 27448, *Test method for self-cleaning performance of semiconducting
        photocatalytic materials*, **2009**

70.   ISO 2409, *Cross - cut test*, **2007**.

71.   Gude, K., Gun'ko, V. M., Blitz, J. P.; *Adsorption and photocatalytic decomposition
        of methylene blue on surface modified silica and silica-titania*; ***Colloids Surf. A***, **2008**,
        325, 17-20.

72.   Patil, S.R., Akpan, U.G., Hameed, B.H., Samdarshi, S.K.; *A comparative study of the
        photocatalytic efficiency of Degussa P25, Qualigens, and Hombikat UV-100 in the
        degradation kinetic of congo red dye*; ***Desalin Water Treat***, **2012**, 46, 188-195.

73.   Tian, J., Chen, L., Dai, J.,Wang, X., Yin, Y., Wu, P.; *Preparation and
        characterization of TiO$_2$, ZnO, and TiO$_2$/ZnO nanofilms via sol–gel process*; ***Ceram.
        Int***., **2009**, 35, 2261-2270.

74.   Kaneko, K.; *Determination of pore size and pore size distribution: 1. Adsorbents and
        catalysts*; ***J. Mem. Sci***., **1994**, 96, 59-89.

75.   Lim, C.S., Ryu, H., Kim,D.H., Cho, S.Y., Oh, W.C.; *Reaction morphology and the
        effect of pH on the preparation of TiO$_2$ nanoparticles by a sol-gel method*; ***J. Ceram.
        Process. Res.,*** **2010**, 11, 736-741.

76.   Musat, V., Fortunato, E., Petrescu, S., Botelho do Rego, A.M.; *ZnO/SiO$_2$
        nanocomposite thin films by sol–gel method*; ***Phys. Status Solidi A***, **2008**, 205, 2075-
        2079.

77.   Ohko, Y.; Ando, I.; Niwa, C.; Tatsuma, T.; Yamamura, T.; Nakashima, T.; Kubota,
        Y.; Fujishima, A.; *Degradation of Bisphenol A in Water by TiO$_2$ Photocatalyst*;
        Environ. Sci. Technol., **2001**, 35, 2365-2368.

78.   Claude, B.; Gonon, L.; Duchet, J.; Verney, V.; Gardette, J.L.; *Surface cross-linking of polycarbonate under irradiation at long wavelengths*; ***Polym. Degrad. Stab***., **2004**, 83, 237-240.

79.   Nagai, N., Okumura, H., Imai, T., Nishiyama, I.; *Depth profile analysis of the photochemical degradation of polycarbonate by infrared spectroscopy*; ***Polym. Degrad. Stab***., **2003**, 81, 491-496.

80.   Guan. K, Lu. B, Yin. Y; *enhanced effect and mechanism of SiO_2 addition in super-hydrophilic property of TiO_2 films**; surf. coat. technol.**, **2003**, 173, 219-223.

81.   Sakai, N., Fujishima, A.,Watanabe, T.,Hashimoto, K.; *Quantitative Evaluation of the Photoinduced Hydrophilic Conversion Properties of TiO_2 Thin Film Surfaces by the Reciprocal of Contact Angle*; ***J. Phys.Chem. B***, **2003**,107, 1028-1035.

82.   Wang, Z., Shi, L., Wu, F., Shuai Yuan, S., Zhao, Y., Zhan, M.; *The sol-gel template synthesis of porous TiO_2 for a high performance humidity sensor*; ***Nanotechnol.***, **2011**, 22, 275502-275510.

83.   Tanabe, K., Sumizoshi, T., Shibata, K., Krzoura, T., Kitagawa, J.; *A New Hypothesis Regarding the Surface Acidity of Binary Metal Oxides*, ***Bull. Chem. Soc. Jap.,*** **1974**, 47, 1064-1066.

84.   Shen, Y.; *A new hypothesis of micro-region acid sites regarding the surface acidity of binary oxides*; ***RSC Adv***., **2012**, 2, 5957-5960.

85.   Eshagi, A.D., Dashti, A., Eshaghi, A., Mozaffarinia, R.; *Photo-induced superhydrophilicity of nanocomposite TiO_2-SiO_2 thin film*; ***Mater. Sci. Poland***, **2011**, 29, 22-28.

86.   Guan, K.H.; *Relationship between Photocatalytic Activity, Hydrophilicity and Self-Cleaning effect of TiO_2/SiO_2 Films*, ***Surf. Coat. Technol***., **2005**, 191, 149-407.

87. Liu, Y., Qian, L.Q, Guo, C., Jia, X., Wang, J.W., Tang, W.H.; *Natural superhydrophilic TiO2/SiO2 composite thin films deposited by radio frequency magnetron sputtering*; *J. Alloys Comp*., **2009**, 479, 532-535.

88. Kubiak, K.j., Wilson, M.C.T., Mathia, T.G., Carval, Ph.; *Wettability versus roughness of engineering surfaces*; *Wear*, **2011**, 523.

89. Yu, J.C., Yu, J., Ho, W., Zhao, J.; *Light-induced super-hydrophilicity and photocatalytic activity of mesoporous TiO2 thin films*; *J. Photochem. Photobio. A*, **2002**, 148, 331-339.

90. Kuo, C-S., Tseng, Y-H., Li, Y-Y.; *Wettability and superhydrophilic TiO2 film formed by chemical vapor deposition*; *Chem. Letters*, **2006**, 35, 356.

91. Barakat, C., Gravejat, P., Guaitella, O., Thevenet, F., Rousseau, A.; *Oxidation of isopropanol and acetone adsorbed on TiO2under plasmagenerated ozone flow: Gas phase and adsorbed species monitoring*; *Appl. Catal. B*, **2014**,147, 302- 313

92. Zubkov, T., Stahl, D., Thompson, T.L., Panayotov, D., Diwald, O., John T. Yates, Jr, J.T.; *Ultraviolet Light-Induced Hydrophilicity Effect on TiO2(110)(1×1). Dominant Role of the Photooxidation of Adsorbed Hydrocarbons Causing Wetting by Water Droplets*; *J. Phys. Chem. B*, **2005**, 109, 15454-15462.

93. Simonsen, M.E., Sørensen, M.B., Søgaard, E.G.; *Comparison of methods for evaluation of activity of photocatalytic films*; *Environ. Sci. Pollut. Res*., **2012**, 19, 3772-3781.

94. Gun'ko, V. M., Yurchenko, G.R., Turov, V.V., Goncharuk, E.V., Zarko, V.I., Zabuga, A.G., Matkovsky, A.K., Oranska, O.I., Leboda, R., Zięba, J.S., Janusz, W., Phillips, G.J., Mikhalovsky, S.V.; *Adsorption of polar and nonpolar compounds onto complex nanooxides with silica, alumina, and titania*; *J. Colloid Interface Sci*., **2010**, 348, 546-558.

95.   Qi, K., Chen, X., Liu, Y., Xin, J.H., Makb, C.L., Daoud,W.A.; *Facile Preparation of Anatase/SiO2 Spherical Nanocomposites and their Application in Self-Cleaning Textiles*; ***J. Mater. Chem***., **2007**, 17, 3504-3508.

96.   Lawless, D., Serpone, N., Meisel, D.; *Role of hydroxyl radicals and trapped holes in photocatalysis. A pulse radiolysis study*; ***J. Phys. Chem***., **1991**, 95, 5166-5170.

97.   Tojo, S., Tachikawa, T., Fujitsuka, M., Majima, T.; *Oxidation processes of aromatic sulfides by hydroxyl radicals in colloidal solution of TiO_2 during pulse radiolysis*; ***Chem. Phys. Lett.***, **2004**, 384, 312-316.

98.   Kamat, P.V.; *Photochemistry on nonreactive and reactive (semiconductor) surfaces*; ***Chem. Rev***., **1993**, 93, 267-300.

99.   Ismail, A.A.; Bahnemann, D.W.; Bannat, I.; Wark, M.; *Gold Nanoparticles on Mesoporous Interparticle Networks of Titanium Dioxide Nanocrystals for Enhanced Photonic Efficiencies*; ***J. Phys. Chem. C*** , **2009**, 113, 7429.

100. Kim, D.W.; Lee, S.; Jung, H.S.; Kim, J.Y.; Shin, H.; Hong, K.S.; *Synthesis and photocatalytic activity of mesoporous TiO_2 with the surface area, crystallite size, and pore size*; ***Int. J. Hydrogen Energy***, **2007**, 32, 3137-3140.

101. Marci, G.; Augugliaro, V.; Lopez-Munoz, M.J.; Martin, C.; Palmisano, L.; Rives, V.; Schiavello, M.; Tilley, R.J.D.; Venezia, A.M.; *Preparation Characterization and Photocatalytic Activity of Polycrystalline ZnO/TiO_2 Systems. 2. Surface, Bulk Characterization, and 4-Nitrophenol Photodegradation in Liquid-Solid Regim*e; ***J. Phys. Chem. B***, **2001**, 105, 1033-1040.

102. Rathousky, J.; Kalousek, V.; Kolar, M.; Jirkovsky, J.; Bartak, P.; *A study into the self-cleaning surface properties - The photocatalytic decomposition of oleic acid*; ***Catal. Today***, **2011**, 161, 202-208.

103. Pulker, H.K.; *Characterization of optical thin films*; ***Applied Optics***, **1979**, 18, 1969-1977.

104. D. Bahnemann, R.D., ; M. Königs,; R. Fateh, Erhöhung der aktiven und passiven Sicherheit von Fahrzeugen durch neuartige multifunktionelle Nanobeschichtungen - NanoSafe: Abschlußbericht zum BMBF-Verbundvorhaben (Increase of the active and passive safety of automobiles through novel multi-funtional nano-coatings -Nanosafe: Final Report of a BMBF-Project) 03 × 2510H. Hannover: 2009 [Available online: http://edok01.tib.uni-hannover.de/edoks/e01fb10/ 61786439X.pdf].

Publication

- R. Fateh, R. Dillert, D. Bahnemann, "*Self-Cleaning Properties, Mechanical Stability, and Adhesion Strength of Transparent Photocatalytic TiO$_2$-ZnO Coatings on Polycarbonate*", Applied materials and interfaces, 2014, DOI: 10.1021/am4051876.

- R. Fateh, R. Dillert, D. Bahnemann, "*Preparation and Characterization of Transparent Hydrophilic Photocatalytic TiO$_2$/SiO$_2$Thin Films on Polycarbonate*", Langmuir, 2013, 29, 3730−3739.

- R. Fateh, A.A. Ismail, R.Dillert, D. W. Bahnemann, "*Highly Active Crystalline Mesoporous TiO$_2$ Films Coated onto Polycarbonate Substrates for Self-Cleaning Applications*", The Journal of Physical Chemistry C, 2011, 115, 10405-10411.

- D. Bahnemann,; R. Dillert,; M. Königs,; R. Fateh, Erhöhung der aktiven und passiven Sicherheit von Fahrzeugen durch neuartige multifunktionelle Nanobeschichtungen - NanoSafe: Abschlußbericht zum BMBF-Verbundvorhaben (Increase of the active and passive safety of automobiles through novel multi-funtional nano-coatings -Nanosafe: Final Report of a BMBF-Project) 03 × 2510H. Hannover: 2009 [Available online: http://edok01.tib.uni-hannover.de/edoks/e01fb10/ 61786439X.pdf].

- R. Fateh, R. Dillert, D. Bahnemann, "*Transparent hydrophilic photocatalytic thin films on polycarbonate substrates prepared by a sol-gel process*", <u>In</u>: *Recent Advances in Materials Science [Proc. 1st WSEAS Int. Conf. on Materials Science]*. WSEAS Press: 2008, 95-100

Oral Presentations

- R. Fateh, R. Dillert, D. Bahnemann, "*Self-Cleaning Properties, Mechanical Stability, and Adhesion Strength of Transparent Photocatalytic TiO$_2$-ZnO Coatings on Polycarbonate*", Europmat, Montpelier, 12 − 15 September 2011.

- R. Fateh, R. Dillert, D. Bahnemann, "*Transparent Photocatalytic TiO2-ZnO Coatings on polycarbonate*", 2nd European Conference on Environmental Applications of Advanced Oxidation Processes- EAAOP2, Nicosia, Cyprus, 9 -11 September 2009.

- R. Fateh, R. Dillert, D. Bahnemann, "*Transparent Hydrophilic Photocatalytic Thin Film on Polycarbonate Substrate by Sol Gel Process*", 1st WSEAS International

Conference on Material science (MATERIALS'08), Bucharest, Romania, November 7-9, 2008.

Poster Presentations

- R. Fateh, R. Dillert, D. Bahnemann,"*Transparent Photocatalytic TiO$_2$-ZnO Coatings on Polycarbonate*", NanoDay, Universität Hannover, 27 September 2012.

- R. Fateh, Adel A. Ismai, R. Dillert, D. Bahnemann *"Preparation and Characterization of Highly Active Crystalline Mesoporous TiO$_2$ Coatings on Polycarbonate"*, JEP, Bordeaux, 29-30 September 2011.

- R. Fateh, R. Dillert, D. Bahnemann, *"Polycarbonate surfaces modified by transparent self-cleaning coatings",* 1st conference of chemistry, Damascus, 10 October 2010.

- R. Fateh, Adel A. Ismai, R. Dillert, D. Bahnemann *"Highly Active Crystalline Mesoporous TiO$_2$ Films for Self-Cleaning Applications"*, 6th European meeting on Solar Chemistry and Photocatalysis: Environmental Applications (SPEA6), Prague, 13-16 June 2010.

- R. Fateh, R. Dillert, D. Bahnemann,"*Transparent Photocatalytic TiO$_2$-ZnO Coatings on Polycarbonate*", NanoDay, Universität Hannover, 30 September 2009.

- R. Fateh, R. Dillert, D. Bahnemann, *"Photocatalytic activity of TiO$_2$/ZnO thin film on polycarbonate substrates"*. Photocatalytic Products and Technologies Conference - PPTC'09. Guimarães, Portugal, May 11-13, 2009.

- R. Fateh, R. Dillert, D. Bahnemann, *"Self-cleaning polymer surfaces modified by transparent photoactive TiO$_2$/ZnO coating"*. NanoDay, Universität Hannover, 25 September 2008.

Curriculum Vitae

Personal information

First name / Surname	**Razan Fateh**
Nationality	Syrian
Date of birth	26.03.1978
Gender	Female

Education and training

Dates	2008-2014
Title of qualification awarded	PhD Chemistry
Principal subjects/occupational skills covered	Thesis Title*: "Transparent Self Cleaning Coatings on Polycarbonate Surfaces "*
Name and type of organization providing education and training	Institut of technical chemistry, Hannover university, Germany
Level in national or international classification	ISCED 6
Dates	2002-2004
Title of qualification awarded	MSc Chemistry
Principal subjects/occupational skills covered	Thesis Title*: "Synthesis of active carbon from natural wastes and its applications",* Determine the surface area by nitrogen gas BET adsorption technique at ($77°$ K).
Name and type of organization providing education and training	Faculty of sciences, Damascus university, Syria
Level in national or international classification	ISCED 5
Dates	2001-2003
Title of qualification awarded	Special Diploma in educational skills
Principal subjects/occupational skills covered	Overall view about psychology and practical training of teaching
Name and type of organization providing education and training	Faculty of Education, Damascus University, Syria
Level in national or international classification	ISCED 5

Dates	1999-2000
Title of qualification awarded	High Diploma in Chemistry
Principal subjects/occupational skills covered	Thesis Title*: "Kinetic Study of Autoxidation of Cyclohexane Using Molecular Oxygen",* Using column chromatography, thin-layer chromatography, GC, and FTIR.
Name and type of organization providing education and training	Faculty of sciences, Damascus university, Syria
Level in national or international classification	ISCED 5

Dates	1995-1999
Title of qualification awarded	BSc, Applied Chemistry
Principal subjects/occupational skills covered	Final year project title: *"Extraction and Separation of Menthol from mint"*, Using column chromatography, thin-layer chromatography, HPLC, and FTIR.
Name and type of organization providing education and training	Faculty of sciences, Damascus university, Syria
Level in national or international classification	ISCED 5

Work experience

Dates	2004-2006
Occupation or position held	Assistant in the laboratory
Main activities and responsibilities	Teaching organic industries and inorganic industries
Name and address of employer	Department of chemistry, faculty of sciences in Damascus university, Syria
Type of business or sector	Education

Dates	2000-2004
Occupation or position held	Assistant in the laboratory
Main activities and responsibilities	Teaching analytical chemistry and physical chemistry
Name and address of employer	Department of chemistry, faculty of pharmacy in Damascus university, Syria
Type of business or sector	Education

Dates	1999-2003
Occupation or position held	Supervised the practical lessons as an assistant in

	the laboratory of chemistry
Main activities and responsibilities	Teaching analytical chemistry and organic chemistry
Name and address of employer	Institute of chemical industries, Damascus, Syria
Type of business or sector	Education